

Metabolic consequences of neuronal mitochondrial fission ablation

Inauguraldissertation

zur

Erlangung der Würde eines Doktors der Philosophie
vorgelegt der
Philosophisch-Naturwissenschaftlichen Fakultät
der Universität Basel

von

Lisa Michelle Restelli

aus Italien

Basel, 2016

Genehmigt von der Philosophisch-Naturwissenschaftlichen Fakultät
auf Antrag von

Fakultätsverantwortlicher: Prof. Christoph Handschin

Dissertationsleiter: Prof. Dr. Stephan Frank

Koreferent: Prof. Anne Spang

Basel, den 23.02.2016

Unterschrift des Fakultätsverantwortlichen

Prof. Dr. Jörg Schibler
(Dekan)

Preface

The following dissertation was written by the author. The “Manuscript” section consists of a published manuscript (Oettinghaus, Schulz, Restelli et al, 2016), which the author significantly contributed to write. The results section is the result of a collaborative work. Please refer to the Authors’ contribution section for further details.

Acknowledgements

My most heartfelt thanks go to my boss, Prof. Stephan Frank, for his patient mentoring and his endless support.

I am grateful to Dr. Björn Oettinghaus for sharing his project and his kind guidance, and for the nice cooperation of the past three years.

Many thanks to our valuable collaborators, Luca Scorrano, Albert Neutzner, Josef Bischofberger, Alex Schmidt, David Lasar, Christian Wolfrum, Jamal Bouitbir, Götz Schlotterbeck, Jürgen Hench, Markus Tolnay, for helpful discussions and technical support.

I also thank colleagues and technicians at the Institute of Pathology, for helpful discussions and practical support with sample preparation. Special thanks go out to the staff at the ZLF animal facility for their constant excellent support.

This work was supported by Swiss National Science Foundation grant 31003A_127308, the Novartis Foundation for Medical-Biological Research and the Desirée und Niels YDE Stiftung.

Abstract

Dynamin-related protein 1 (Drp1), the main mammalian mediator of mitochondrial fission, has an especially important role in neuronal development, such that its deletion gives rise to pre- or perinatal lethality. However, less is known about the need for Drp1 in adult neurons; this is relevant because inhibition of Drp1 could prevent pre-apoptotic mitochondrial fragmentation, and therefore be neuroprotective.

In our mouse model, inducible Drp1 ablation in the forebrain of adult mice leads to swollen, perinuclearly aggregated mitochondria and to impaired synaptic transmission. Of note, ablated mice also develop a complex and ultimately lethal catabolic phenotype, marked by weight loss, increased lipolysis and elevated corticosterone. We traced this back to the activation of the integrated stress response in Drp1-ablated brain regions, culminating in the ectopic induction of metabolic cytokine Fgf21. Fgf21 is normally produced in liver, fat and muscle tissue in response to fasting or exercise, and no reports exist of it being produced in the brain. This “mitokine” increases insulin sensitivity and stimulates corticosterone production via receptors in the hypothalamus, thus explaining essential aspects of the catabolic phenotype.

This work has implications not only for mitochondrial biology but also for the understanding of the central regulation of systemic metabolism.

Index

PREFACE	III
ACKNOWLEDGEMENTS	V
ABSTRACT	VII
INDEX	IX
1. INTRODUCTION	15
1.1. Mitochondria	15
1.1.1. Structure	15
1.1.2. Dynamics	16
1.1.2.1. Mitochondrial fission	19
1.1.2.2. Mitochondrial fusion	22
1.1.2.3. Cristae remodeling	23
1.1.3. Integration of mitochondrial dynamics in cellular functions	24
1.1.3.1. Apoptosis	24
1.1.3.2. Mitochondrial quality control and the response to stress	25
1.1.3.3. Interaction with other organelles	27
Mitochondria and the endoplasmic reticulum	28
Mitochondria and lysosomes	32
Mitochondria and peroxisomes	32
Mitochondria and lipid droplets	33
1.1.3.4. Mitochondrial motility	34
1.1.4. Mitochondrial dynamics in neurodegeneration	35
1.1.4.1. Mitochondrial dynamics in sporadic and familial neurodegenerative diseases	36
Alzheimer's disease	36
Parkinson's Disease	37
Huntington's Disease	38
Amyotrophic lateral sclerosis	39
Other diseases	39

1.1.4.2. Primary disorders of mitochondrial dynamics	40
Autosomal dominant optic atrophy	40
Charcot-Marie-Tooth Disease	41
1.2. Central regulation of systemic metabolism	42
1.2.1. Systemic regulation of energy metabolism	42
1.2.1.1. Hypothalamic circuits regulating feeding behavior	42
Adiposity signals	44
Gastrointestinal signals	44
Nutrient signals	46
1.2.1.2. Energy expenditure	46
Basal metabolic rate	47
Thermogenesis and brown adipose tissue	47
Shivering thermogenesis and exercise	48
1.2.1.3. Pituitary adrenal axis and corticosterone influence on metabolism	48
1.2.1.4. Fgf21 and the “mitokine” concept	49
Signaling	49
Regulation of glucose metabolism	51
Adaptation to caloric restriction and starvation	51
Thermogenesis and effects on adipose tissue	51
Neuroendocrine effects of Fgf21	52
Non-canonical mechanisms of Fgf21 induction	53
1.2.1.5. Cellular nutrient sensing	54
Indicators and sensors of nutrient deficiency	55
Cellular measures to cope with nutrient stress	56
Mitochondrial dynamics in cellular metabolism	57
2. AIMS OF THE WORK	60
3. MANUSCRIPT	62
3.1. Summary	63
3.3. Introduction	64
3.4. Results	65
3.4.1. Inducible <i>Drp1</i> ablation in the adult mouse forebrain.	66
3.4.2. <i>Drp1</i> ablation causes progressive changes in mitochondrial morphology.	66
3.4.3. Synaptic transmission is impaired in <i>Drp1</i> -deficient CA1 pyramidal neurons.	67
3.4.4. Adult forebrain neurons do not degenerate within 10 weeks of <i>Drp1</i> ablation.	68

3.5. Discussion	70
3.6. Materials and Methods	72
3.6.1. Mice	72
3.6.2. Histology	73
3.6.3. Transmission electron microscopy	73
3.6.4. Electrophysiology	74
3.6.5. Behavioral analyses	74
3.6.6. Western Blot	74
3.6.7. Tissue culture	74
3.6.8. Quantitative proteomics	75
3.6.9. Oxygen consumption and ATP levels	76
3.7. Acknowledgements	76
3.7.1. Authors' Contributions	77
3.8. References	77
3.9. Figure legends	84
4. EXPERIMENTAL PROCEDURES	105
4.1. Mouse lines	105
4.2. Mitochondrial membrane potential measurement	105
4.3. Oxygraph measurements	105
4.4. ER morphology evaluation	106
4.5. Metabolic Measurements	106
4.6. Western blot	107
4.7. ELISA	107
4.8. Quantitative real-time PCR	108
4.9. Pharmacological treatments	108
4.10. BAT sympathectomy	108
5. RESULTS	110

5.1. Drp1 ablation in adult mouse forebrain impairs mitochondrial structure and respiratory activity	110
5.2. Drp1-ablated mice develop a catabolic phenotype	110
5.3. Metabolic pathways that regulate fuel choice in Drp1^{flx/flx} Cre⁺ mice	111
5.4. Drp1-ablated brain regions secrete metabolic cytokine Fgf21 in an eIF2α-ATF4-mediated fashion	112
5.5. Drp1 ablation in neurons causes ER stress	114
5.6. Pharmacological inhibition of ER stress does not prevent Fgf21 expression	114
5.7. Lack of mtUPR activation and evidence for amino acid deprivation and iron handling alterations in Drp1^{flx/flx} Cre⁺ mice	115
5.8. Genetic rescue	118
5.9. Figures	119
Figure 5.1 Mitochondrial morphology and function in Drp1-ablated neurons	120
Figure 5.2 Macroscopic metabolic alterations in Drp1 ^{flx/flx} Cre ⁺ mice	122
Figure 5.3 Clinical chemistry and hormones in Drp1 ^{flx/flx} Cre ⁺ mice	124
Figure 5.4 Production of Fgf21 in Drp1 ^{flx/flx} Cre ⁺ mice	126
Figure 5.5 ER stress in Drp1 ^{flx/flx} Cre ⁺ mice	128
Figure 5.6 Pharmacological ER stress rescue	130
Figure 5.7 Integrated stress response in Drp1 ^{flx/flx} Cre ⁺ mice	132
Figure 5.8 Genetic rescue	134
6. DISCUSSION	136
6.1. Drp1 deletion in forebrain neurons activates the integrated stress response	137
6.2. Ectopic Fgf21 expression in Drp1^{flx/flx} Cre⁺ brains causes a systemic catabolic phenotype	141
6.3. Conclusion and perspectives	147
7. REFERENCES	149
8. ABBREVIATIONS	168

9. AUTHORS' CONTRIBUTIONS	171
10. CURRICULUM VITAE	170

1. Introduction

1.1. Mitochondria

Mitochondria are the result of the engulfment, over 1.5 billion years ago, of an α -proteobacterial ancestor by a larger host cell. This initiated a process of endosymbiosis (Margulis, 1975), whereby mitochondria provided the host cell with energy and metabolites, and in exchange surrendered control of their replication and morphology to the host. This was achieved via the transfer of most of the mitochondrion's genetic material to the nucleus, leaving only a 16-kilobase-long circular chromosome within the organelle. The mitochondrial genome (mtDNA) codes for a total of 37 genes, of which 13 are protein subunits of the respiratory chain, 22 are mitochondria-specific transfer RNAs (tRNAs) and 2 are ribosomal RNAs (rRNAs). The remainder of the estimated 1000 proteins that constitute the mitochondrial proteome (Calvo et al., 2016; Pagliarini et al., 2008) is nuclear-encoded and imported post-translationally into the mitochondria.

1.1.1. Structure

The standard depiction of a mitochondrion is that of a bean-shaped organelle, ranging in size from 0.5 to 10 μm , bound by two membranes.

The **outer mitochondrial membrane** (OMM) envelops the **inner mitochondrial membrane** (IMM), which folds to form membrane invaginations termed **cristae**. The two membranes define two distinct compartments: the **intermembrane space** (IMS) between OMM and IMM; and the **matrix**, within the IMM.

The OMM serves as both a barrier – albeit a poorly selective one – for solutes, metabolites and larger molecules, as well as a hub for interorganelle communication, mediating contacts between mitochondria and other cellular compartments (i.e. the endoplasmic reticulum, lysosomes, peroxisomes, ribosomes; see 1.1.3.3).

The IMM can further be subdivided in three specialized zones: the inner boundary membrane (IBM), the cristae junctions (CJ) and the cristae.

The IBM is the portion of the IMM that is closely apposed to the OMM; it mainly contains protein complexes that are responsible for polypeptide import. It has also been implicated in matrix-cytosol energy transfer, lipid transfer and in the relaying of apoptotic signals (Reichert and Neupert, 2002; Tatsuta et al., 2014).

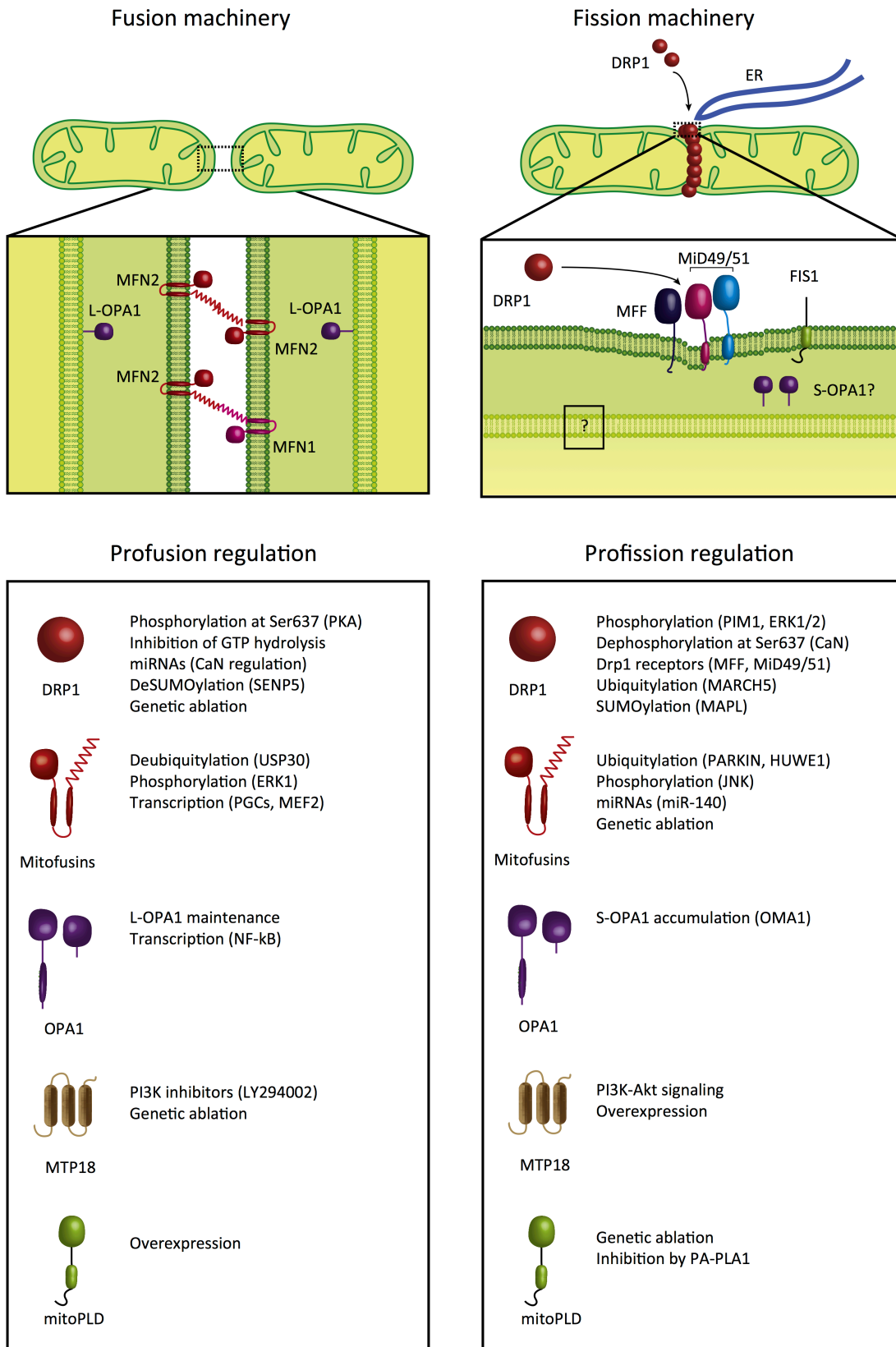
The IMM attachment to the OMM is interrupted by the cristae, deep IMM invaginations protruding into the matrix space. The cristae are enriched in proteins and protein complexes that carry out biosynthetic and bioenergetic roles within mitochondria, foremost among them respiratory complexes and supercomplexes (Cogliati et al., 2013).

The cristae compartment is physically separated from the rest of the intermembrane space and the IMM by a 20-50 nm-wide tightening at the base of the cristae, termed cristae junction (CJ). The architecture of the CJs is controlled by the **MICOS complex** (mitochondrial contact site and cristae organizing system), a protein network on the IMS side of the IMM composed of six different subunits. Of these six, two (Mitofilin and Mio10) are essential to maintain cristae morphology, such that their absence leads to massive cristae rearrangement and IMM stacking. The remaining four subunits (Aim5, Aim13, Aim37, Mio27) are important for mtDNA inheritance, suggesting that they interact with nucleoids (van der Laan et al., 2012). The MICOS complex interacts with both the protein import machinery and the ER-tethering machinery (discussed in 1.1.3.3), as well as with other structural IMM proteins like prohibitins (van der Laan et al., 2012).

1.1.2. Dynamics

This classical textbook presentation of mitochondria as static organelles stems primarily from electron microscopy (EM) observations on fixed tissues (Palade, 1953); nevertheless, as early as 1914, studies on live cells had revealed that mitochondria are, in fact, a dynamic network that is able to fuse and divide in response to intra- and extracellular cues (Lewis and Lewis, 1914). The processes of mitochondrial fusion and fission and of cristae remodeling are collectively termed **mitochondrial dynamics**, and they provide the mitochondrial network with the flexibility to adapt to the cell's metabolic and biosynthetic requirements.

Mitochondrial dynamics are controlled by a family of large GTPases termed dynamin-related proteins (DRPs), which have the ability to remodel biological membranes via self-assembly and GTP hydrolysis. **Dynamin-related protein 1** (Drp1) is the main effector of mitochondrial fission, while fusion is accomplished by the coordinated action of OMM **Mitofusin 1 and 2** (Mfn1, Mfn2) and IMM **Optic Atrophy 1** (OPA1). Of note, Drp1 also plays a role in peroxisomal fragmentation (Koch et al., 2003; Li and Gould, 2003).



Trends in Endocrinology & Metabolism

Figure 1.1 Regulators of mitochondrial morphology. Summary of the proteins required for mitochondrial fusion and fission, and the corresponding translational and posttranslational modifications (Wai and Langer, 2016).

1.1.2.1. Mitochondrial fission

The generation of two daughter mitochondria by constriction of a single mitochondrial tubule is termed mitochondrial fission, and its main mediator is Dynamin-Related Protein 1 (Drp1, also known as Dnm1l).

Drp1 structural studies have revealed 4 functional domains:

1. A GTPase domain at the N-terminus, harboring the enzymatic activity.
2. A middle domain.
3. A variable domain, which undergoes alternative splicing and harbors sites of posttranslational modification.
4. A GTPase effector domain at the C-terminus, which can interact with the GTPase domain.

The middle domain and the GTPase effector domain harbor α -helix-containing stalk domains which mediate Drp1 dimerization (Faelber et al., 2011; Ford et al., 2011).

Given that most of a cell's Drp1 pool is cytosolic, recruitment mechanisms are in place to activate it and to direct it to mitochondria in order to mediate fission (Labrousse et al., 1999; Smirnova et al., 2001). Mitochondrial fission articulates in three steps: (I) the selection and marking of a prospective fission site; (II) the assembly of the division complex around the mitochondrial tubule; (III) the GTP-driven constriction that causes the severing of the mitochondrial unit into two daughters.

The marking of the fission site initiates the division process by ensuring that the mitochondrial tubule, normally 300-500 nm in diameter, constrict to an extent compatible with the 120-nm Drp1 helix. This is accomplished by the ER wrapping around prospective fission sites on mitochondria (Friedman et al., 2011) in a process termed **ER-associated mitochondrial division** (ERMD). Additional support for mitochondrial tubule constriction comes from actin polymerization by the inverted formin INF2, followed by Myosin II recruitment (Hatch et al., 2014; Korobova et al., 2013); this is further supported by reports that actin destabilization prevents mitochondrial fission (Korobova et al., 2013, 2014). Other proteins located at contact sites between the ER and mitochondria are able to further

facilitate fission: such is the case for the ancient SNARE Syn17, which in fed cells localizes to the ER-mitochondria contact sites and facilitates mitochondrial division (Arasaki et al., 2015).

Given that Drp1 does not harbor membrane-interaction domains, it needs to bind protein adaptors on the OMM in order to exert its effects on mitochondria. In yeast, Drp1 recruitment to mitochondria is accomplished by C-terminal-anchored OMM protein **Fis1** and adaptor protein Mdv1, which does not have a mammalian ortholog. In mammals, four Drp1-recruiting proteins have been identified so far: mitochondrial fission factor (**Mff**), mitochondrial dynamics proteins of 49 and 51 kDa (**MiD49** and **MiD51**, also known as Mief1), and Fis1. Of note, Fis1 is not strictly required for fission, but its knockdown causes mitochondrial elongation and its overexpression fragments mitochondria (Gomes and Scorrano, 2008; James et al., 2003; Koirala et al., 2013; Losón et al., 2013; Shen et al., 2014). Mff is the main Drp1 recruiter in basal condition, and it functions independently of Fis1 (Gandre-Babbe and van der Bliek, 2008; Losón et al., 2013; Otera et al., 2010). MiD49 and MiD51 are both able to bind Drp1, but they can either sequester it in an inactive form or promote its nucleation, depending on the availability of co-factors. For instance, MiD51 stimulates Drp1 assembly only in the presence of ADP, when respiration is disrupted (Palmer et al., 2011; Zhao et al., 2011; Richter et al., 2014). A similar mechanism is hypothesized, but has not yet been identified, for MiD49 (Pernas and Scorrano, 2015).

Parallel to its recruitment to the OMM, posttranslational modifications are able to regulate the fission capacity of Drp1: namely, Drp1 can undergo phosphorylation, S-nitrosylation, ubiquitylation and SUMOylation (SUMO, small ubiquitin-like modifier) (Oettinghaus et al., 2012; Wilson et al., 2013).

Two serine residues, both located in the GTPase effector domain, can undergo phosphorylation.

Protein Kinase A (PKA), when activated by high levels of cyclic adenosine monophosphate (cAMP), phosphorylates Drp1 on Ser637, resulting in the inhibition of its fission activity (Chang and Blackstone, 2007; Cribbs and Strack, 2007), possibly by interfering with helix assembly (Cereghetti et al., 2008). The same residue can also be phosphorylated by **calcium/calmodulin-dependent kinase I** (CaMKI; (Han et al., 2008)). Conversely,

phosphorylated Ser637 can be targeted by phosphatase **calcineurin**, resulting in an enhancement of Drp1 fission activity (Cereghetti et al., 2008). In neurons, **protein phosphatase 2A** (PP2A) is also able to dephosphorylate Ser637 (Dickey and Strack, 2011).

Phosphorylation of Drp1 in Ser616 by the **Cdk1/CyclinB** complex exerts the opposite effect of Ser637, promoting rather than inhibiting mitochondrial fission (Taguchi et al., 2007).

Protein Kinase C δ (PKC δ) has also been reported to target Ser616 for phosphorylation in neurons (Qi et al., 2011), though the relevance of this process for physiological contexts has not been proved (Wilson et al., 2013). Nevertheless, it may be significant in pathological conditions, such as Alzheimer's disease (Wang et al., 2009) and in the presence of oxidative stress (Qi et al., 2011).

These two cases exemplify how the cell is able to coordinate mitochondrial fission to adapt to the cell's needs. In the case of Ser637, mitochondrial fission is inhibited via PKA-mediated phosphorylation when the cell undergoes starvation; this causes mitochondrial network hyperfusion, which protects mitochondria from macroautophagy in order to preserve the cell's ATP-producing abilities (Gomes et al., 2011); on the other hand, elimination of the defective portions of the mitochondrial network may be achieved via AMPK-mediated phosphorylation of Mff (Toyama et al., 2016). In the case of Ser616, mitochondrial fission is coordinated with cell division allowing for even partitioning of smaller mitochondrial units into the two daughter cells (Taguchi et al., 2007).

Drp1 can also undergo **S-nitrosylation** on a conserved cysteine residue in the GTPase effector domain (Barsoum et al., 2006; Cho et al., 2009). This leads to an increase in mitochondrial fission, possibly by enhancing the effects of Drp1-activating phosphorylation (Bossy et al., 2010).

In addition, ubiquitylation can modulate Drp1 function. Ubiquitin E3 ligase **MARCH5** (also known as MITOL) can ubiquitylate Drp1 and MiD49, modulating mitochondrial morphology in a pro- or anti-fusion fashion in a manner that is still controversial (Fang et al., 2013; Nagashima et al., 2014; Xu et al., 2016). Likewise, it is not yet confirmed whether Drp1 is a direct target of E3 ligase parkin (Wilson et al., 2013) or whether more complex mechanisms linking parkin activity and mitochondrial morphology are in place (Buhlman et al., 2014).

Finally, **SUMO** can be covalently attached to Drp1, rendering it more stable at the OMM (Harder et al., 2004). MAPL (also known as MULAN), Ubc9 and SUMO1 have all been

implicated in Drp1 SUMOylation (Braschi et al., 2009; Figueroa-Romero et al., 2009; Harder et al., 2004), while the removal of the SUMO moieties is performed by SUMO protease SenP5 (Zunino et al., 2007). Of note, Drp1 stabilization by MAPL-mediated SUMOylation has recently been implicated as an apoptosis-promoting mechanism downstream of Bax/Bak activation, stabilizing ER-mitochondria contacts that generate mitochondrial constriction and cytochrome c release ((Prudent et al., 2015); see paragraph 1.1.3.1).

Following recruitment to the OMM, Drp1 self-assembles in a GTP-dependent manner into helical structures that wrap around ER-marked mitochondrial tubules; together with actin and the ER, the assembly of the Drp1 helix further constricts the mitochondrion (Lackner et al., 2009). Finally, following GTP hydrolysis, the Drp1 helix further constricts causing membrane severing and organelle division. Of note, incorporation of a hydrolysis-deficient Drp1 mutant (K38A, (Naylor et al., 2006)) into the helix acts in a dominant-negative manner, allowing for helix assembly but preventing membrane scission.

While Drp1 is the primary actor of mitochondrial division, there have been reports of Drp1-independent mitochondrial fragmentation during apoptosis, bacterial infection or with specific mutations of α -synuclein (Guardia-Laguarta et al., 2014; Ishihara et al., 2009; Stavru et al., 2013); furthermore, Drp1-deficient mouse embryonic fibroblasts (MEFs) are still able to partition their mitochondria during cell division (Pernas and Scorrano, 2015). This suggests that alternative mechanisms may be able to mediate mitochondrial fission, but none has been identified to date.

1.1.2.2. Mitochondrial fusion

Mitochondrial fusion is essential to maintain the overall health of the mitochondrial network; indeed, fusion allows for the dilution of toxic species such as oxygen radicals, and for complementation of mtDNA and mitochondrial membrane potential (Chan, 2012). Unlike mitochondrial fission, which exerts its effects on the OMM and IMM at the same time, mitochondrial fusion involves two separate mechanisms for OMM and IMM fusion.

OMM fusion is accomplished thanks to dynamin-related GTPases **Mitofusin 1 and 2** (Mfn1 and Mfn2; (Legros et al., 2002; Santel and Fuller, 2001; Santel et al., 2003)). Mfn1 and Mfn2 have 64% amino acid identity: both possess a GTPase domain at the N-terminus, a transmembrane domain, and two predicted heptad repeats that are postulated to mediate tethering between adjacent mitochondria (Pernas and Scorrano, 2015). However, their function is only partially redundant, as Mfn2 in particular possesses some specialized roles in ER-mitochondria tethering and mitochondria motility (Labbé et al., 2014); this is also reflected by the differences in tissue-specific expression of the two genes, and by the fact that Mfn1, but not Mfn2, can complement certain pathogenic mutations in Mfn2 (Detmer and Chan, 2007).

They form homo- or heterodimers in trans to tether mitochondrial membranes and bring them into close proximity. The exact mechanisms of membrane fusion have not yet been elucidated, but they are postulated to involve lipid mixing: one candidate for this process in mammals is **MitoPLD**, which converts cardiolipin to phosphatidic acid (Choi et al., 2006).

The fusion of the IMM is controlled by **Opa1**, which undergoes alternative splicing and proteolytic cleavage resulting in long (l-Opa1) and short (s-Opa1) isoforms, with the latter increasing during cellular stress (processing explained in cristae remodeling section, 1.1.2.3). L-Opa1 is N-terminally anchored to the IMM and it is sufficient to induce IMM fusion and to restore fusion in an Opa1-deficient cell (Song et al., 2009; Tondera et al., 2009). On the other hand, there are reports that the s-Opa1 isoform, which is produced under stress conditions, mediates mitochondrial fragmentation (Anand et al., 2014).

1.1.2.3. Cristae remodeling

Cristae can display different morphologies with regards to both number and size. For instance, treating cells with a non-glycolytic substrate causes an increase in the number of mitochondrial cristae, which is paralleled by increased **supercomplexes** assembly and respiratory capacity (Cogliati et al., 2013; Rossignol et al., 2004). In parallel, during starvation, cristae width decreases to facilitate supercomplex assembly and increase respiratory efficiency (Cogliati et al., 2013).

In addition to its role in regulating IMM fission, Opa1 controls cristae morphology and remodeling (Wong et al., 2000). The two processes are actually independent, as interfering with OMM fusion does not affect cristae shape (Frezza et al., 2006). The *Opa1* gene can be alternatively spliced to generate 8 different isoforms, which are then proteolytically processed by two groups of mitochondrial proteases: AAA proteases **AFG3L2** and **paraplegin**, and metalloprotease **YME1L**; the resulting l-Opa1 cleavage products can be further processed by **OMA1** or rhomboid-like protease **PARL** to generate soluble s-Opa1 (Cipolat et al., 2006). The current model for cristae structure and maintenance holds that oligomers of l-Opa1 line the length of cristae, where they tether opposite-facing membranes. Cleavage of l-Opa1 results in a disruption of cristae structure and in a widening of the cristae junction, which can cause the release of proteins from the intracristae space (see apoptosis, (Pernas and Scorrano, 2015)). S-Opa1 forms are believed to be less important for cristae structure at the steady state, and more relevant for dynamic remodeling of cristae morphology following stressor challenges (Pernas and Scorrano, 2015).

1.1.3. Integration of mitochondrial dynamics in cellular functions

1.1.3.1. Apoptosis

Apoptosis is a form of cell death that can be triggered by external or intracellular stimuli (Kroemer et al., 2009). The death stimuli converge on the OMM, where homo-oligomers of Bcl2 proteins **BAX** and **BAK** cause OMM permeabilization via the formation of pores (Antignani and Youle, 2006). The combination of cristae remodeling and OMM permeabilization leads to the release of cytochrome c into the cytosol, where they form the apoptosome with APAF1 and caspase 9; this initiates the apoptotic cascade (Li et al., 1997).

Mitochondrial fragmentation is a mechanistically important step in the apoptotic cascade. Indeed, increased resistance to apoptosis has been observed in cells deficient in mitochondrial fission (Frank et al., 2001); a similar phenotype is present in Fis1-knockout or in Mfn1-overexpressing cells (Cassidy-Stone et al., 2008; Estaquier and Arnoult, 2007; Lee et al., 2004), as well as in MAPL-KO cells (Prudent et al., 2015). Conversely, mitochondrial

fragmentation by excessive fission or decreased fusion increases sensitivity to apoptotic stimuli (Leboucher et al., 2012; Lee et al., 2004). While this does not hold true for all cell types and apoptotic stimuli, the general consensus is that the membrane topology generated by Drp1 wrapping favors BAX insertion into the OMM (Montessuit et al., 2010). Given that most of a mitochondrion's cytochrome c resides in the cristae compartment, its release is contingent upon a widening of the cristae junctions. This is achieved via proteolytic cleavage of l-Opa1 isoforms either directly by pro-apoptotic proteins (e.g. truncated Bid, (Scorrano et al., 2002)) or by stress-activated proteases (i.e. PARL, (Cipolat et al., 2006; Frezza et al., 2006)). Conversely, upregulation of Opa1 protects cells against apoptotic insults by preventing cytochrome c release (Civiletto et al., 2015; Cogliati et al., 2013; Varanita et al., 2015).

1.1.3.2. Mitochondrial quality control and the response to stress

The mitochondrial proteome is composed of both nuclear- and mitochondria-derived proteins, which need to be perfectly coordinated in order to yield productive respiratory and biosynthetic complexes. Thus, quality control pathways are in place to monitor respiratory efficiency and the eventual presence of misfolded proteins (Friedman and Nunnari, 2014). The main readout for any mitochondrial imbalance is disruption of the **electrochemical potential** across the IMM, which is the direct outcome of an effective electron transport chain.

Alternative processing of Opa1 is one of the switches that signal mitochondrial stress. Constitutive Opa1 processing involves cleavage by YME1L, which generates both l- and s-Opa1 isoforms, in a regulated proportion. Alternative processing by OMA1 is also possible, but OMA1 undergoes constitutive degradation upon mitochondrial import in healthy organelles (Ehse et al., 2009; Head et al., 2009). A decrease in mitochondrial membrane potential allows OMA1 to accumulate and to convert l-Opa1 isoforms into s-Opa1, resulting in mitochondrial fragmentation (Anand et al., 2014). Depending on the type of stress, a contrary response of mitochondrial hyperfusion can be observed; this is hypothesized to

dilute the oxygen radicals as well as to protect mitochondria from degradation (Gomes et al., 2011; Tondera et al., 2009).

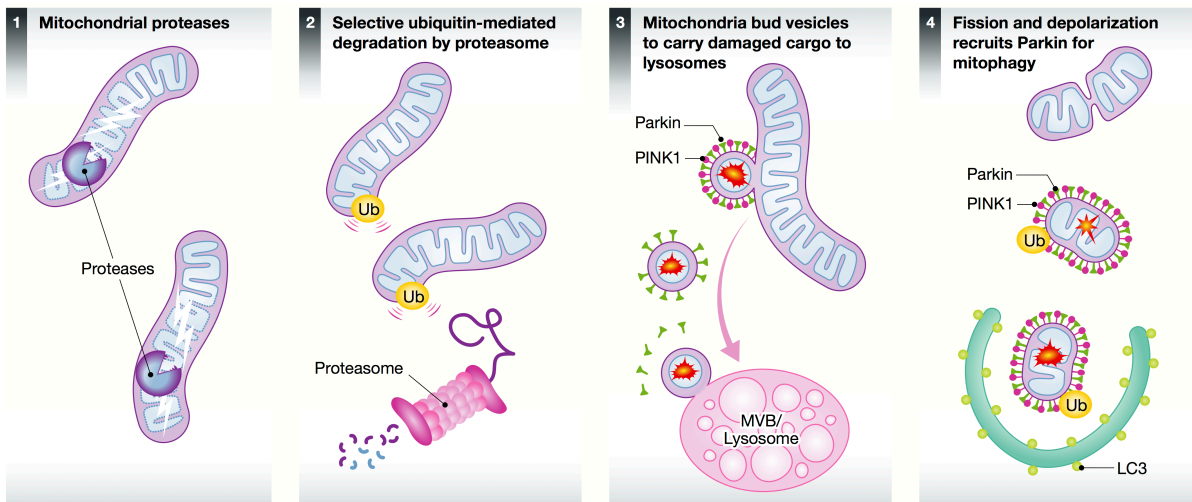


Figure 1.2 Pathways and degrees of mitochondrial quality control. Moderate or localized stress is first sensed and coped with by mitochondrial proteases and by the mtUPR (1); specific damaged proteins can be ubiquitylated and retrotranslocated to the cytosol, where they are degraded by the proteasome (2); patches of mitochondrial damage can be selectively removed and targeted to lysosomes (3); only in the presence of high levels of stress, entire mitochondria are targeted for degradation via mitophagy (4) (Sugiura et al., 2014).

One recently discovered line of defense against mitochondrial stress induced by protein imbalance is the **mitochondrial unfolded protein response (mtUPR)**. Originally identified in the nematode *C. elegans*, mtUPR exploits impaired protein import into mitochondria as a switch to target transcription factor ATFS1 to the nucleus, where it upregulates mitochondrial chaperones and proteases (namely, Hsp60, Hsp10, ClpP and mtDNAJ; (Yoneda et al., 2004; Zhao et al., 2002). This form of mtUPR has since been extensively studied in *C. elegans* and in *Drosophila* (Mottis et al., 2014; Zhao et al., 2002). Nevertheless, a mammalian version of the mtUPR has been reported in cultured cells; it relies on the activation of transcription factor **CHOP**, which also has parallel roles in ER-specific unfolded protein response (see next section). Additionally, oxidized OMM proteins can be ubiquitylated and retrotranslocated to be targeted for degradation in a process termed OMMAD (outer mitochondrial membrane-associated degradation); this process depends on p97 and the 26S proteasome (Hemion et al., 2014).

Intermediate, or localized, forms of stress will elicit the formation of **mitochondria-derived vesicles** (MDVs, (Sugiura et al., 2014)), which isolate selected damaged cargo and convey it to lysosomes or peroxisomes for degradation (discussed in detail in the following section).

Sustained or aggressive forms of stress will instead trigger a more terminal response, in the form of **mitophagy**, which is the selective targeting of damaged mitochondria for degradation and recycling (Youle and Narendra, 2011). Mitophagy triggering also depends on the $\Delta\Psi_m$, and in particular on the reliance of the protein import machinery on an intact membrane potential. In healthy organelles, kinase **PINK1** (PTEN-induced putative kinase 1) is imported into mitochondria, where it is cleaved by mitochondrial processing peptidase MPP and PARL, and then degraded via the N-end rule pathway (Yamano and Youle, 2013). When mitochondrial protein import is impaired, PINK1 evades degradation and accumulates on the OMM, where it interacts with the TOM import machinery. There, it homodimerizes and autophosphorylates, becoming fully active (Eiyama and Okamoto, 2015)c.

Parkin is an E3 ubiquitin ligase which is activated by the combination of phosphorylation by PINK1 and by binding of S65-phosphorylated ubiquitin (also performed by PINK1; (Kane et al., 2014; Kazlauskaitė et al., 2014; Koyano et al., 2014). The targets of Parkin ubiquitylation include Mfn1, Mfn2, and Miro, which is a mitochondria transport factor ((Chan et al., 2011; Tanaka et al., 2010; Wang et al., 2011b) see 1.1.3.4). This inhibits mitochondrial fusion and transport at the same time, facilitating the segregation of the damaged mitochondrion (Chan, 2012). Of note, Drp1-mediated mitochondrial fission, in parallel with the inhibition of fusion, is essential for the successful completion of mitophagy (Twig et al., 2008).

1.1.3.3. Interaction with other organelles

Most cellular functions are compartmentalized into membrane-bound organelles; however, it is increasingly acknowledged that a complex interplay among cellular organelles exists. Mitochondria are a fundamental hub in organellar interaction, establishing physical and functional connections with the ER, lysosomes, peroxisomes and lipid droplets (Schrader et al., 2015).

Mitochondria and the endoplasmic reticulum

The mitochondria-ER contact first became apparent in the 1960s, with the first EM images showing that certain subdomains of the ER, termed the **MAMs** (mitochondria-associated membranes) were linked to mitochondria (Copeland and Dalton, 1959); however, hints at the actual structure of the tether have only been found in recent years. In yeast, a tethering structure termed **ERMES** (ER-mitochondria encounter structure) has been described, with important roles in mitochondrial fission and lipid transfer (Kornmann et al., 2009). Also in yeast, the EMC (ER membrane protein complex) has been found to participate in lipid transport (Lahiri et al., 2014). Finally, small GTPase Arf1, which is canonically responsible for coatamer assembly at the Golgi apparatus, is important for mitochondria-ER contacts, as its deficiency results in mitochondrial dysfunction and protein aggregation (Ackema et al., 2014; Spang, 2015). Direct homologs of these complexes have not yet been identified in higher eukaryotes; nevertheless, other tethering units have been surfacing in the past few years. Mfn2 can reside in the MAM and form homo- or heterodimers with Mfn1, tethering the MAMs to mitochondria (de Brito and Scorrano, 2008). A second tethering pair is composed of VAPB and PTPIP51, residing respectively at the MAM and OMM (Stoica et al., 2014). Finally, mitochondrial fission adaptor Fis1 can interact with MAM protein Bap31 in the course of the apoptotic signaling cascade (Breckenridge et al., 2003; Iwasawa et al., 2011).

The MAM is the preferential site of a number of enzymatic and cellular activities linking the ER and mitochondria: (I) phospholipid synthesis and transfer; (II) calcium signaling; (III) ER stress response; (IV) mitochondrial fission; (V) mitophagy; (VI) apoptosis regulation; (VII) antiviral response. For the sake of this work, the first three are the most significant.

(I) Phospholipid synthesis and transfer

The role for the MAMs in lipid metabolism was the first to be elucidated (Vance, 1990). Unlike other cellular compartments, in which lipid transfer occurs via vesicular transport, the ER and mitochondria are able to directly exchange phospholipid species and precursors. As a result, phosphatidylserine (PS) produced in the ER is transferred to mitochondria, where it is converted to phosphatidylethanolamine (PE) via the PS decarboxylation pathway (Shiao

et al., 1995). PE can then be transferred back to the ER or further processed to generate phosphatidylcholine (PC) or cardiolipin (CL) within the IMM (Raturi and Simmen, 2013).

(II) Calcium signaling

Calcium ions are highly concentrated in the extracellular space and within the ER, while their concentration is 4 orders of magnitude lower in the cytosol (de la Fuente et al., 2013). Within mitochondria, calcium is important to regulate the enzymatic functions of the TCA cycle, and mitochondrial motility (Giacomello et al., 2007; Rowland and Voeltz, 2012). Exchanges of calcium between the two organelles are facilitated by the **MCU** (mitochondrial calcium uniporter), which has a relatively low affinity for calcium (Baughman et al., 2011; De Stefani et al., 2011). This is overcome by close juxtaposition between the MAMs, enriched in IP3R (inositol-1,4,5-tris-phosphate-sensitive receptor) calcium channels, and the mitochondria, which allows for the ER calcium efflux to be channeled into the MCU (Baughman et al., 2011; De Stefani et al., 2011).

(III) ER stress response

The endoplasmic reticulum is the subcellular compartment where most secreted and transmembrane proteins fold and mature, acquiring the necessary post-translational modifications to perform their cellular functions. However, the total amount of polypeptides within the ER can change rapidly as a response to cellular signals, potentially resulting in an imbalance between ER folding capacity and protein load, which is termed **ER stress** (Ron and Walter, 2007). In order to prevent ER stress from permanently damaging the cell, three different responses are in place to regulate the balance between ER folding capacity and polypeptide load; collectively, they are termed the **UPR** (unfolded protein response). By a vast generalization, the UPR is initially a rectifying response, tuning protein synthesis and chaperone production to restore correct protein folding; if, however, the stress signal is prolonged, then the same pathways can induce cell death (Hetz et al., 2015). All three arms of the UPR rely on ER-resident transmembrane proteins that act as relays: with their ER-luminal domain, they sense unfolded polypeptides and chaperone (i.e. BiP/GRP78) depletion; this causes them to undergo conformational or post-translational changes that activate their different downstream functions. These relays, for which the three arms are

named, are **PERK** (protein kinase RNA-like endoplasmic reticulum kinase), **IRE1** (endoribonuclease inositol-requiring enzyme 1-alpha) and **ATF6** (activating transcription factor 6).

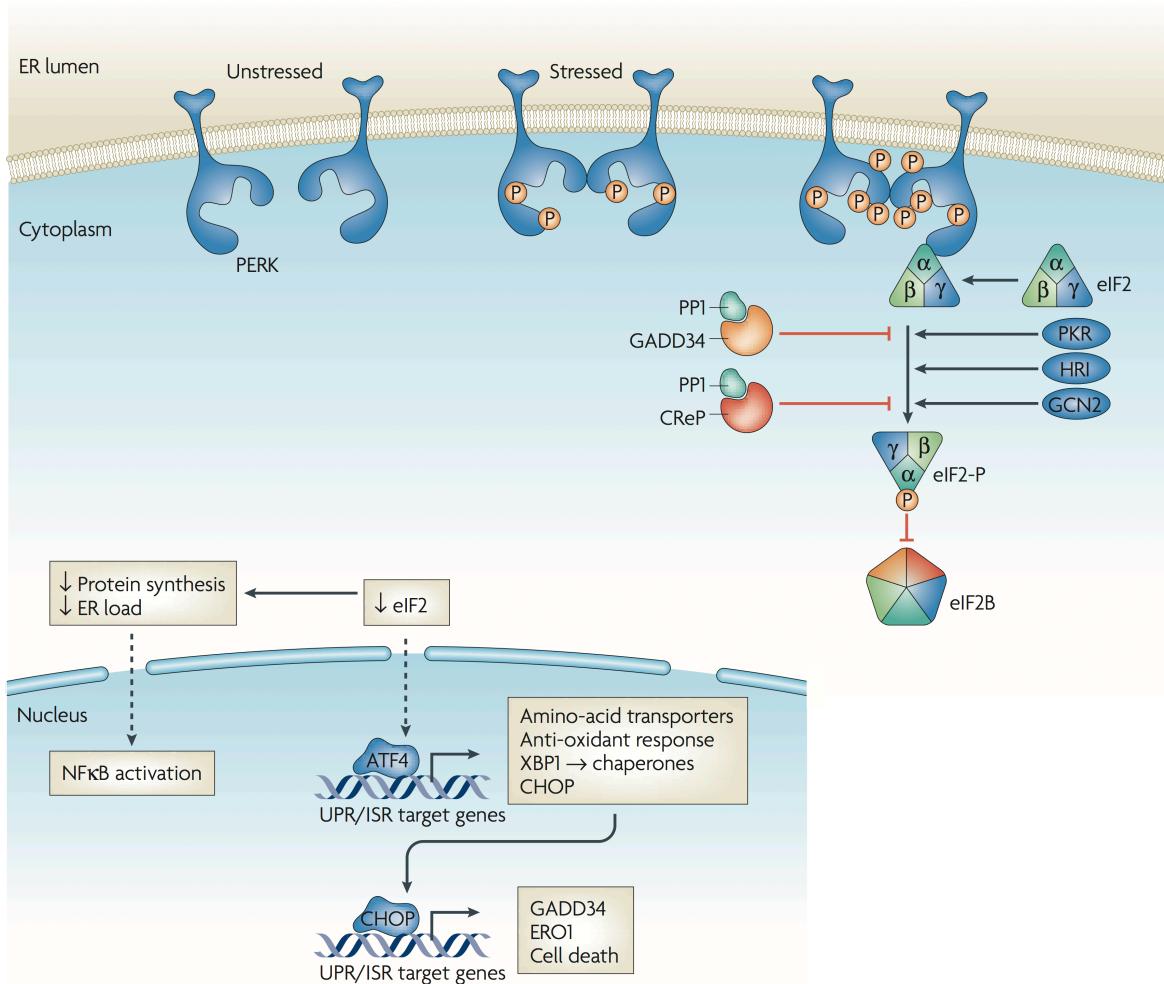


Figure 1.3 ER stress intersection with the integrated stress response. In response to ER stress, transmembrane kinase PERK oligomerizes and auto-phosphorylates, becoming active. P-PERK then phosphorylates eIF2 α on Ser51; the same phosphorylation can be performed by GCN2, PKR or HRI. Phosphorylated eIF2 α prevents recycling of eIF2 to its active form, thus blocking translation. ATF4 translation is increased when eIF2 α is phosphorylated, and it translocates to the nucleus, where it transcribes chaperones, amino acid transporters, antioxidant genes and CHOP (Ron and Walter, 2007).

The activation of **PERK**, which is generally believed to be the first-line response to ER stress, occurs via oligomerization and auto-phosphorylation; active PERK then phosphorylates the α subunit of **eukaryotic translation initiation factor 2 α** (eIF2 α) at serine 51. This decreases the overall activity of the eIF2 translational initiation complex, leading to a global translational repression, with the immediate effect of decreasing protein load on the ER. The mRNA encoding for **ATF4** (activating transcription factor 4) contains two inhibitory upstream

open reading frames (uORFs) that normally block its translation; however, upon eIF2 α phosphorylation, the ribosome skips these uORFs, leading to translation of the ATF4 ORF. ATF4 is a cAMP response element binding protein and acts as a transcription factor, leading to the expression of both anti- or pro-apoptotic genes (including CHOP, GADD34 and ATF3). Notably, other stimuli, like amino acid deficiency, double-stranded RNAs or heme deficiency, can also lead to eIF2 α phosphorylation and ATF4 activation, which are collectively termed the **integrated stress response** (Donnelly et al., 2013; Wek et al., 2006).

ATF6 exists as an inactive precursor in the ER membrane; upon ER stress induction, it is translocated from the ER to the Golgi apparatus, where specific resident proteases cleave it twice, releasing it from the membrane. This ATF6f (fragment) can then translocate to the nucleus, where it transcribes UPR target genes (which are mainly responsible for protein folding and posttranslational modifications).

IRE1 (inositol-requiring protein-1) is also activated by trans-phosphorylation following oligomerization. Its activation gives it the ability to specifically cleave one particular mRNA (coding for XBP-1, X-box-binding protein 1), excising an intron and leading to the translation of the mature and more stable form of the protein. XBP-1 is a transcription factor that positively regulates the expression of genes related to protein folding, lipid synthesis and ER-associated protein degradation.

While the short-term response induced by the ER stress is a general repression of protein synthesis, the UPR is generally believed to be a broader program aimed at restoring the cell's secretion capacity; for this reason, lipid-synthesizing pathways are also upregulated by the UPR, with the aim of increasing ER volume in parallel with its folding capacity (Ron and Walter, 2007).

Another aspect of the UPR is the increase in ER-mitochondria contact sites; the resulting increase in mitochondrial calcium concentrations boosts the TCA cycle and makes more ATP available for chaperone-mediated folding (Bravo et al., 2012), to assist during the rectifying phase of the UPR. Nevertheless, sustained unfolded protein stress will result in excessive mitochondrial calcium accumulation, which triggers apoptosis (Chami et al., 2008).

Conversely, disrupting mitochondrial morphology and ER-mitochondria contacts by ablating Mfn2 causes ER stress (Debattisti et al., 2014; Diaz et al., 2015; Muñoz et al., 2013; Ngho et al., 2012; Schneeberger et al., 2013), underlining that, in the case of ER and mitochondria,

distress in one organelle is effectively transduced to the other to coordinate cellular responses.

Mitochondria and lysosomes

Lysosomes are single-membrane organelles with lytic function (Novikoff et al., 1956). They constitute the final step of the endocytic pathway and of **autophagy**, in which cytosolic elements or entire organelles are engulfed by a phagophore, fused to endosomes and then conveyed to lysosomes for degradation (Noda and Inagaki, 2015). The selective autophagic degradation of mitochondria is **mitophagy**, and it has been addressed in paragraph 1.1.3.2. Mitochondria are also liable to undergo non-selective autophagy in the case of nutrient starvation; in the initial phases of the response, hyperfusion of the mitochondrial network can prevent their autophagic degradation ((Gomes et al., 2011) and see paragraph 1.1.2.1).

A more recent form of communication between mitochondria and lysosomes (and also peroxisomes, see next paragraph) is the formation of **mitochondria-derived vesicles** (MDVs), cargo-selective single- or double-membrane vesicles that bud off the OMM and are targeted for degradation to different organelles (Sugiura et al., 2014). Lysosome-targeted MDVs are TOM20-positive and enriched in oxidized proteins; their formation is PINK1/parkin-dependent and Drp1-independent (McLelland et al., 2014; Soubannier et al., 2012). They are postulated to act as a first line of defense against localized oxidative insults, eliminating small aggregated oxidized proteins before the terminal process of mitophagy can be initiated (Sugiura et al., 2014).

Mitochondria and peroxisomes

Peroxisomes are single-membrane organelles responsible for fatty acid β -oxidation, paired with the degradation of hydrogen peroxide (Smith and Aitchison, 2013). For both these functions, peroxisomes have a close relationship with mitochondria, which generate reactive oxygen species (ROS) and initiate the breakdown of fatty acids (Schrader et al., 2015).

Notably, mitochondria and peroxisomes also share their fission machinery (Koch et al., 2003; Li and Gould, 2003).

In yeast, subpopulations of peroxisomes localize to sites of ER-mitochondria interaction in response to certain metabolic conditions (i.e. in the presence of glucose; (Cohen et al., 2014)). Interactions between mitochondria and peroxisomes are also important for the inheritance of both organelles in yeast (Jourdain et al., 2008). Finally, again in yeast, mitochondria have been suggested to take part in peroxisome fission, much in the same way the ER aids mitochondrial constriction (Mao et al., 2014).

While in mammals less is known about the nature and the functions of physical interactions between mitochondria and peroxisomes, it is clear that a close functional coupling exists in the context of **lipids and ROS handling** (Schrader et al., 2015). Indeed, altered lipid and ROS metabolism in peroxisomes reflects on the redox balance within the mitochondria (Walton and Pizzitelli, 2012). Conversely, mitochondria generate MDVs that are specifically targeted to peroxisomes in a MAPL- and Vps35-dependent manner (Braschi et al., 2010; Neuspiel et al., 2008). Vps35 belongs to the retromer complex, and mutations in this gene have been associated to Alzheimer's (AD) and Parkinson's (PD) disease (Vilariño-Güell et al., 2011; Zimprich et al., 2011); of note, PD-derived mutations in Vps35 in dopaminergic neurons have important consequences on mitochondrial morphology (Tang et al., 2015), suggesting that its role in quality control may have effects also on mitochondrial dynamics.

Mitochondria and lipid droplets

Lipid droplets are dynamic organelles that store neutral lipids (e.g. triacylglycerols) and sterol esters within cells (Schrader et al., 2015). They associate, and exchange lipids with, most cellular organelles (Dugail, 2014).

Mitochondria physically interact with lipid droplets, possibly by means of perilipin 5 (Wang et al., 2011a), and they draw in fatty acids to use in β -oxidation. Of note, it has been recently reported that lipid droplet-localized fatty acids are transported into mitochondria under starvation conditions; within mitochondria, they are oxidized in a manner that is dependent on mitochondrial fusion (specifically, on Mfn1). In starved Mfn1-knockout cells, fatty acids

fail to distribute throughout mitochondria and are ultimately released from the cell (Rambold et al., 2015).

Also of note is the recent observation that defects in neuronal mitochondrial metabolism (i.e. ROS challenge and Ndufs4 mutation) result in the accumulation of lipid droplets rich in oxidized lipids in the surrounding glial cells, which then leads to neurodegeneration (Liu et al., 2015b).

1.1.3.4. Mitochondrial motility

Aside from continuously changing its morphology, the mitochondrial network needs to be localized to different areas of the cells in order to accomplish some of its functions; neuronal mitochondria are particularly affected by this requirement, due to neurons being very large (up to 1 m long) and having high energy requirements in specific cellular compartments (i.e. pre- and post-synaptic sites). Furthermore, mitochondria that are stationed close to synapses are important for local calcium buffering (Lin and Sheng, 2015).

Mitochondria in neurons are transported over long distances on microtubule tracks, with the aid of specific **motor proteins** that exploit the polarity of microtubules (Lin and Sheng, 2015). Live cell imaging has revealed that mitochondria can undergo both anterograde and retrograde transport, with occasional stalling, and they can be tethered close to a synapse (MacAskill and Kittler, 2010).

Anterograde mitochondrial transport depends on the **KIF5** family of kinesins, which all feature an ATPase motor domain at the N-terminus and a cargo-binding C-terminal domain (Hirokawa et al., 1991). Retrograde transport is driven by **dynein**, in association with **dynactin** (Pilling et al., 2006).

Mitochondria associate to both motor complexes via adaptor proteins and OMM proteins. In mammals, **TRAK1** and **TRAK2** (homologous to *Drosophila* Milton) are adaptor proteins bridging OMM proteins **Miro1** and **Miro2** and the molecular motors (Koutsopoulos et al., 2010). Specifically, TRAK1 can interact with both kinesin and dynein, while TRAK2 predominantly binds the dynein/dynactin complex (Lin and Sheng, 2015). Miro is an OMM GTPase with two EF-hand calcium-binding domains (Fransson et al., 2006). Other adaptor proteins have been identified, such as syntabulin, which specifically links mitochondria to

kinesin motors (Cai et al., 2005; Su et al., 2004), and FEZ1, which mediates anterograde transport of mitochondria during NGF-induced neurite outgrowth *in vitro* (Fujita et al., 2007).

Mitochondrial localization within the neuritic compartment is activity-dependent: high synaptic activity causes a sustained calcium entry, which is sensed by the EF-hand domains of Miro1 and Miro2; this causes the disassembly (or the inactivation) of the Miro/TRAK/molecular motor complexes, arresting mitochondria at sites where synapses are active (Lin and Sheng, 2015). In addition, **syntaphilin** is a mitochondria-docking protein that immobilizes mitochondria in axons in instances of sustained neuronal activity (Chen and Sheng, 2013).

Of note, Miro proteins have also been shown to regulate mitochondrial morphology in response to calcium increases: at resting calcium concentrations, Miro favors fusion by inhibiting Drp1 activity; conversely, when calcium levels rise, Drp1-mediated mitochondrial fragmentation is initiated (Saotome et al., 2008). Accordingly, our own previous work and that of others have shown that Drp1 ablation in neurons affects synaptic mitochondrial distribution *in vivo* (Oettinghaus et al., 2016; Shields et al., 2015; Verstreken et al., 2005).

1.1.4. Mitochondrial dynamics in neurodegeneration

Given its high energy demand and low cell turnover rate, the brain is especially sensitive to disruptions in mitochondrial function (Schon and Przedborski, 2011). Indeed, even for those diseases that occur primarily in a sporadic form, studying the fewer familial cases has highlighted that mitochondria and related pathways may be common nodes in the pathogenesis ((Schon and Przedborski, 2011) and references therein).

In addition to their role in cellular bioenergetics, which accounts for a fraction of disease-causing mutations in brain, mitochondria in a neuron are crucially integrated in the cell's physiology by means of their network dynamics:

- (I) Long, polarized neurons require that mitochondria be efficiently transported to pre- and post-synaptic sites to produce ATP and to buffer calcium;
- (II) ER-mitochondria interaction is crucial in neurons to handle calcium waves and lipid biosynthesis, among others

- (III) Mitochondrial quality control not only ensures a functioning ATP-producing system, but also prevents the accumulation of damage, which is more difficult for postmitotic cells to cope with (Schon and Przedborski, 2011).

These functions, or often a combination thereof, are affected in a number of neurodegenerative conditions with very different etiologies. This is in addition to the observation that *in vitro* models of neurodegenerative diseases present with a very fragmented mitochondrial network (Cho et al., 2010; Costa et al., 2010; Lutz et al., 2009; Shirendeb et al., 2012; Song et al., 2011; Wang et al., 2009).

On the other hand, mutations or deletion of genes important for mitochondrial morphology often result in a primarily neurodegenerative disease, indicating that the brain is the tissue where mitochondrial dynamics are most crucial – or where cells possess the least plasticity to cope with damage (Burté et al., 2015).

1.1.4.1. Mitochondrial dynamics in sporadic and familial neurodegenerative diseases

Alzheimer's disease

Alzheimer's disease (AD), the most common form of dementia, is characterized by cerebral cortex atrophy and the deposition of intracellular aggregates of hyperphosphorylated **Tau** protein (neurofibrillary tangles) and of extracellular plaques of **amyloid- β** peptide (A β ; (Vinters, 2015)). The pathogenic mechanism is far from understood, with some investigators bringing into question neuronal metabolism and deeming protein aggregates just an epiphenomenon (Demetrius et al., 2014). Nevertheless, the study of both the sporadic and the familial forms of the diseases, together with animal models, has highlighted alterations of mitochondrial dynamics at different levels.

In autaptic samples from patients with sporadic AD, as well as in familial AD mouse models, defects in mitochondrial trafficking, in the form of accumulated mitochondria and multilamellar bodies in axons, were detected (Du et al., 2010; Pigino et al., 2009; Stokin et al., 2005). This is paralleled by altered levels of mitochondria-shaping proteins together with fragmented or perinuclearly aggregated mitochondria (Kopeikina et al., 2011; Manczak et al., 2011; Wang et al., 2009).

A β , one of the possible toxicity-mediating peptides, can mislocalize to mitochondria, where its aggregation causes oxidative stress (Lustbader et al., 2004; Pagani and Eckert, 2011). Of note, AD-associated genes Presenilin1 and 2, which belong to a multiprotein complex that cleaves the A β precursor protein APP, are highly enriched in the MAM (Area-Gomez et al., 2009).

Tau toxicity derives from a combination of its hyperphosphorylation and its C-terminal cleavage, which result in its aggregation. Depending on its posttranslational modifications and on the co-expression of A β , Tau leads to mitochondrial fragmentation or hyperelongation (DuBoff et al., 2012). Of note, both in *Drosophila* and in mouse neurons, mutant human Tau expression disrupts cytoskeletal dynamics by stabilizing F-actin (stable, fibrillar actin). As a result, Drp1 association to the mitochondria and the subsequent fission are impaired, leading to a hyperelongated mitochondrial network; inhibition of mitochondrial fusion restored neuronal health in these models (DuBoff et al., 2012).

Parkinson's Disease

Parkinson's disease (PD) is a neurodegenerative disease characterized by tremors and difficulties of movement, due to loss of dopaminergic neurons in the substantia nigra pars compacta. Neuropathological aspects include intracellular deposition of **Lewy bodies**, composed of α -synuclein and other co-aggregating proteins (Haelterman et al., 2014).

Historically, PD has been linked to a deficiency in mitochondrial complex I activity, due to the fact that exposure to 1-methyl-4-phenyl-1,2,3,6-tetrahydropyridine (MPTP) caused PD-mimicking syndromes in drug users (Langston and Ballard, 1983; Langston et al., 1983). Nevertheless, studies have revealed a number of different mitochondria-related genes to be mutated in the familial forms of PD. Among them, most are related to mitochondrial quality control, though some also affect mitochondrial motility; therefore, PD is now largely regarded as a disease of mitochondrial quality control (Schon and Przedborski, 2011).

Parkin and **PINK1** can both be mutated in recessive forms of familial PD, leading to symptoms that are very similar to those of sporadic cases – though with an earlier age of onset and possibly a different neuropathological appearance of the Lewy bodies (Pickrell and Youle, 2015). However, mouse models deficient in Parkin display a much milder phenotype

than the human disease, sometimes only when challenged with additional stresses (Pickrell and Youle 2015, Sterky 2011). On the other hand, the PINK1-deficient mouse model presents with complex I defects, impaired DOPA release and synaptic plasticity (Kitada et al., 2007; Morais et al., 2009). Remarkably, neurotoxicity in this model is attenuated by inhibition of mitochondrial fission, highlighting the important role for Drp1 in mitochondrial quality control pathways (Rappold et al., 2014).

Another PD-causing gene is ***α-synuclein***, which when mutated gives rise to an autosomal dominant form of the disease; despite extensive studies, its physiological role is still unclear (Schon and Przedborski, 2011). In addition to its aggregation phenotype, a role for α -synuclein in the MAMs has recently been proposed (Guardia-Laguarta et al., 2014, 2015). Indeed, a fraction of wild-type α -synuclein resides in the MAMs; mutant forms of α -synuclein are strongly recruited to the MAMs, which results in a decrease in MAM-related activities, a decrease in ER-mitochondria contacts, and in mitochondrial fragmentation (Guardia-Laguarta et al., 2014).

DJ-1 is another PD-associated gene with implications for mitochondrial quality control: it harbors antioxidant enzymatic activity and it modulates mitochondrial dynamics in a ROS-dependent fashion (Irrcher et al., 2010). Furthermore, its deletion modulates mitochondrial membrane potential by reducing the expression of uncoupling proteins Ucp4 and Ucp5, reducing the physiological state of “mild uncoupling” that would attenuate mitochondrial ROS production (Guzman et al., 2010; Kwok et al., 2010; Ramsden et al., 2012), again underlining a role in mitochondrial quality control.

Finally, kinase **LRRK2** can be mutated in dominant forms of PD. It has been shown to interact with the fusion and fission machinery, modulating mitochondrial morphology towards a fragmented phenotype. Furthermore, mutant LRRK2 also upregulates uncoupling proteins Ucp2 and Ucp4 *in vitro* (Ryan et al., 2015).

Huntington's Disease

Huntington's disease is an autosomal dominant disease caused by a CAG trinucleotide expansion in the coding region of the **huntingtin** (HTT) gene, which gives rise to a polyglutamine stretch that makes the protein both dysfunctional and aggregation-prone (Orr and

Zoghbi, 2007). It presents with personality changes compounded with choreic movements of the face and arms, culminating in dementia. On the neuropathological level, the primary finding is the loss of medium-size spiny neurons in the striatopallidal and striatonigral pathways, together with caudate nucleus and putamen atrophy.

Expression of mutant HTT impairs mitochondrial transport *in vitro* (Chang et al., 2006) as well as in mouse models (Trushina et al., 2004); one hypothesis is that TRAK1 interacts with both HTT and dynactin due to its close homology with a native HTT interactor (Stowers et al., 2002); this would then impair mitochondrial transport.

Furthermore, though the significance of this finding is not clear, HTT interacts with IP3Rs at the MAMs (Tang et al., 2003).

Above all, mutated HTT impinges on mitochondrial morphology by causing mitochondrial fragmentation and cristae remodeling, in a manner that is partially due to direct interaction of HTT with Drp1 (Costa et al., 2010; Shirendeb et al., 2012; Song et al., 2011).

Amyotrophic lateral sclerosis

Amyotrophic lateral sclerosis (ALS) is a disease of muscle wasting due to the loss of cortical and spinal motor neurons; this is usually due to the formation of protein-based inclusions within the neurons of the corticospinal tract (Kiernan et al., 2011). It is mostly sporadic, with a minority of familial-transmission cases.

Motor neurons being as long as 1 meter, it comes as no surprise that mitochondrial defects manifest with trafficking impairments in this disease. In fact, both anterograde and retrograde transport are reduced in mouse models of ALS caused by mutant **superoxide dismutase 1** (SOD1, one of the few known causative genes; (De Vos et al., 2007; Shi et al., 2010)). Likewise, ALS-related genes *alsin* and **TAR DNA binding protein 43** (TDP-43) also impaired mitochondrial transport (Millecamps et al., 2005; Shan et al., 2010).

Other diseases

There are a number of families of genetic diseases for which a role for mitochondrial dynamics has been hypothesized or demonstrated. Most of them are umbrella terms for a plethora of different entities with similar phenotypes and a broad range of genetic causes.

Foremost among them are Charcot-Marie-Tooth disease, Hereditary Spastic Paraplegias, Spinocerebellar Ataxias and Optic Atrophies. A detailed discussion of the individual altered processes in these diseases is beyond the scope of this work. The most notable entities, which are due to mutations in formal mitochondrial morphology-regulating proteins, will be addressed separately in the following paragraph.

1.1.4.2. Primary disorders of mitochondrial dynamics

In addition to diseases in which mitochondrial dynamics are affected, some genetic conditions are directly due to loss or mutation of mitochondria-shaping proteins. Depending on the affected process and the level of redundancy of the pathway, these conditions can manifest with a broad range of symptoms and affect different tissues (Burté et al., 2015).

Autosomal dominant optic atrophy

Autosomal dominant optic atrophy (DOA) is the most common genetic disease of the optic nerve (Burté et al., 2015). It causes loss of retinal ganglion cells, which then leads to optic nerve degeneration and blindness (Yu-Wai-Man et al., 2011).

More than half of the cases are due to missense mutations or premature termination within the **OPA1** gene (Alexander et al., 2000). The disease has autosomal dominant transmission, despite the mutations being loss of function, due to the effect of haploinsufficiency, i.e. one gene copy of Opa1 is not sufficient to cope with the requirements of the cell. It is interesting to note that Opa1 expression is ubiquitous, but the phenotype is almost exclusively affecting the eye; some variant cases, termed DOA+, can manifest with extraocular symptoms such as ataxia, peripheral neuropathy and myopathy (Burté et al., 2015). The variability of clinical presentations is partially attributed to defects in Opa1 affecting mtDNA integrity, which can result in the emergence of somatic mtDNA mutations and additional biochemical defects in a sporadic manner in some tissues (Burté et al., 2015).

One specific form of optic atrophy, which is alternatively termed Costeff optic atrophy syndrome or type III 3-methylglutaconic aciduria, is due to mutations in IMM protein **OPA3** (Anikster et al., 2001; Babbar and Sheikh, 2013). OPA3 mediates mitochondrial fission via a yet unidentified mechanism (Ryu et al., 2010). In a mouse model carrying the disease mutation, defects in systemic lipid metabolism were also identified, in the form of impairment in non-shivering thermogenesis and BAT lipid accumulation (Wells et al., 2012).

Charcot-Marie-Tooth Disease

Charcot-Marie-Tooth Disease (CMT) encompasses a broad spectrum of inherited peripheral neuropathies; they are characterized by progressive degeneration of the peripheral nerves, which can be due to demyelination (CMT1 and CMT4 subtypes) or to axonal (CMT2 subtype) pathology. This results in distal muscle weakness and in sensory loss, with highly variable rates of progression depending on the underlying genetic cause (Burté et al., 2015; Hoyle et al., 2015).

One severe form of axonal CMT, **CMT2A**, is due to mutations in the **Mfn2** gene (Bradbury, 2004; Züchner, 1993), which causes a peripheral motor neuropathy, sometimes accompanied by proprioceptive loss; other rarer symptoms include optic atrophy and subacute visual failure (Burté et al., 2015).

Another form of CMT, **CMT4A**, is due to loss-of-function mutations in **ganglioside-induced differentiation-associated protein 1** (GDAP1), which is involved in mitochondrial fission (Niemann et al., 2005; Pedrola et al., 2005; Züchner and Vance, 1993). It causes a neuropathy with both demyelination and axonal pathology (Detmer and Chan, 2007; Huber et al., 2013). Mouse studies have highlighted that calcium homeostasis and store-operated calcium release are disrupted in peripheral GDAP1-KO neurons (Barneo-Muñoz et al., 2015).

1.2. Central regulation of systemic metabolism

An overview of the regulation of systemic metabolism by the central nervous system is given below. Particular emphasis is given to circulating metabolism-altering factors that are relevant to this work.

In addition, some aspects of intracellular nutrient sensing are addressed.

1.2.1. Systemic regulation of energy metabolism

The maintenance of a generally constant body mass is achieved through a finely regulated balance between food intake and energy expenditure. Food intake is regulated mostly at the hypothalamic level, while energy expenditure occurs throughout the body via different mechanisms.

1.2.1.1. Hypothalamic circuits regulating feeding behavior

The hypothalamus is composed of distinct nuclei regulating different aspects of body homeostasis, from sleep/arousal to feeding and thermoregulation. The two areas that control appetite and feeding are:

- (I) The **ventromedial hypothalamus** (VMH), which is orexigenic;
- (II) The **ventrolateral hypothalamus** (VLH), which is anorexigenic (Anand and Brobeck, 1951, 1951)

The opposing activities of the VMH and the VLH are coordinated by two subpopulations of neurons in the arcuate nucleus of the hypothalamus (ARC) (Horvath et al., 1992):

- (I) **AgRP/NPY neurons** produce neurotransmitters Agouti-Related Peptide (AgRP) and Neuropeptide Y (NPY), as well as γ -aminobutyric acid (GABA), and their stimulation is orexigenic;
- (II) **POMC** neurons produce precursor peptide proopiomelanocortin, which is then processed to α -Melanocyte-Stimulating Hormone (α -MSH), and they are

anorexigenic (Aponte et al., 2011; Betley et al., 2013; Krashes et al., 2011; Zhan et al., 2013).

Neurons in the ARC sense the body's overall energy in the form of circulating hormones and metabolites that inform on the different aspects of feeding and on the condition of stored reserves (Sandoval et al., 2008). Additional layers of control, such as stress signals, conscious control and the hedonic aspect of feeding are in place, and they are integrated through a complex crosstalk between the autonomic nervous system, the prefrontal cortex and brain stem nuclei (Sandoval et al., 2008).

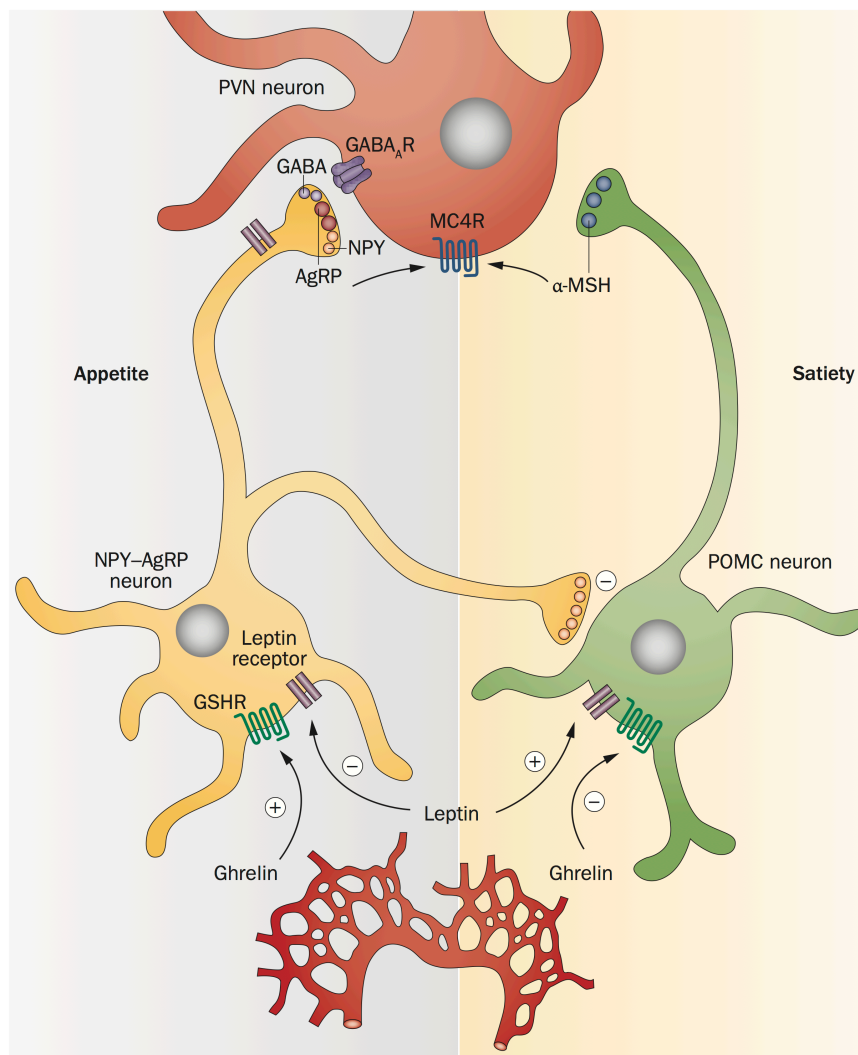


Figure 1.4 Melanocortin system in the arcuate nucleus of the hypothalamus. Orexigenic NPY-AgRP neurons and anorexigenic POMC neurons send projections to the paraventricular nucleus. NPY-AgRP neurons also inhibit neighboring POMC cells. Leptin activates POMC neurons to secrete α -MSH, which binds to MC4R and promotes satiety. Leptin inhibits AgRP neurons, which are activated by ghrelin, promoting feeding and silences firing of POMC neurons. (Nasrallah and Horvath, 2014)

Adiposity signals

The CNS is informed on the state of fat depots thanks to **leptin** and **insulin**, which circulate in concentrations that are proportional to the body's fat mass (Sandoval et al., 2008). Both are able to cross the blood-brain barrier (BBB) and reach their receptors in the ARC, where they stimulate anorexigenic POMC neurons and inhibit AgRP/NPY neurons, causing a decrease in feeding and an increase in energy expenditure (Cowley et al., 2001). Accordingly, leptin KO mice display an obese phenotype attributable to hyperphagia and decreased energy expenditure (Thenen and Mayer, 1976).

Gastrointestinal signals

Another important element in the control of feeding is information on recently ingested nutrients. This is conveyed to the brain by circulating factors released from the gastrointestinal tract during and after a meal (Sandoval et al., 2008).

Ghrelin is produced by specialized cells in the stomach mucosa in response to fasting, and it stimulates feeding via receptors in the ARC (Tschöp et al., 2000).

On the other hand, other signals from the gastrointestinal tract, like cholecystokinin, amylin, peptide YY and glucagon-like peptide-1 (GLP1) are satiety signals and therefore anorexigenic. Together with gastrointestinal distension, these signals are conveyed via the vagus nerve to the Nucleus Tractus Solitarius (NTS), which induces a short-term decrease in food intake (Morton et al., 2014).

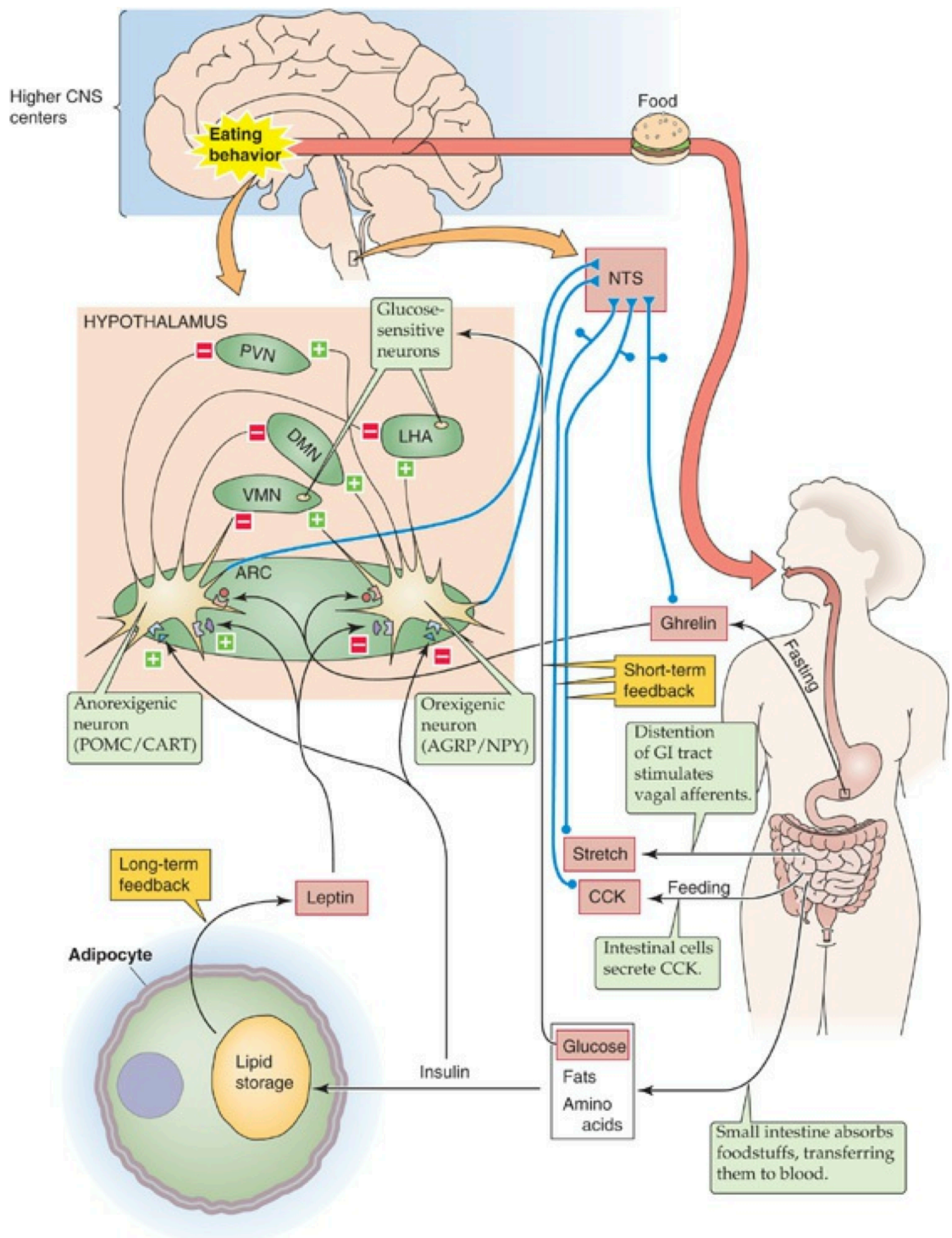


Figure 1.5 Central regulation of appetite. The arcuate nucleus of the hypothalamus receives input in the form of circulating hormones (leptin, ghrelin, insulin) and circulating nutrients (amino acids, glucose, lipids). It then integrates the signals and communicates with higher nuclei and with the nucleus tractus solitarius, which also receives input from the gastrointestinal system. (Boron and Boulpaep, 2009)

Nutrient signals

Circulating metabolites are also important for the CNS to assess the body's energy state.

For instance, circulating **glucose** levels affect the excitability of neural populations in the ARC, inhibiting NPY neurons and activating POMC neurons; as a result, high blood glycemia promotes the activation of anorexigenic POMC neurons and decreases appetite (Muroya et al., 1999).

Fatty acids are sensed by specific subpopulations of anorexigenic neurons, because of the accumulation of their breakdown metabolites malonyl-CoA or of the CoA-bound form of long-chain fatty acids (Sandoval et al., 2008).

Furthermore, circulating **amino acids**, foremost among them branched-chain amino acid leucine, decrease the activity of AgRP neurons in the ARC, resulting in increased food intake (Sandoval et al., 2008).

1.2.1.2. Energy expenditure

Energy expenditure depends on a number of internal and external factors, as it is geared to shape energy balance in response to variations in temperature, physical activity, feeding and hormonal conditions (Münzberg et al., 2015). A body's total energy expenditure can be subdivided in:

- (I) **Basal metabolic rate**, which undergoes minimal variations, as it depends on basal ATP production and proton leaks making the process more or less efficient (Brand et al., 1999)
- (II) Adaptive **thermogenesis**, which functions by actively uncoupling ATP production and the proton-motive force, generating energy dispersion as heat.
- (III) Physical **activity**, which includes both voluntary activity and involuntary muscle shivering as a short-term response to cold, but normally has no global impact on long-term metabolism.

Basal metabolic rate

The basal metabolic rate includes cells' intrinsic ATP-producing ability and fuel preference, indicated by the **respiratory exchange ratio** (RER: carbohydrate versus fat oxidation; (Bouchard and Tremblay, 1990)). It can be modified by thyroid-derived T3 and T4, which act throughout the body on nuclear TXR receptors to exert their effects on metabolism. For instance, in liver, thyroid hormone action increases gluconeogenesis; in muscle, proteolysis is induced to provide amino acids for gluconeogenesis in the liver; in adipose tissue, lipolysis is induced to mobilize free fatty acids, which are then taken up by the liver to support gluconeogenesis. Overall, this is an energy-consuming effort that increases the basal metabolic rate (Boron and Boulpaep, 2009). In addition, thyroid hormones increase the production and the activity of the sodium/potassium pump, which consumes high amounts of ATP. Finally, they exert a positive modulation on the effects of thermogenic stimuli (see below) (Boron and Boulpaep, 2009).

Thermogenesis and brown adipose tissue

Brown adipose tissue (BAT) is a heat-generating tissue where adaptive thermogenesis takes place (Rothwell and Stock, 1979). It differs from white adipose tissue (WAT), which is mainly a reservoir for fat, in its mitochondria content, to which it owes its "brown" color. Of note, brown adipocytes can also develop within WAT depots in a process known as "beiging" ((Wu et al., 2013b); further discussed in 1.2.1.4). In rodents, the main BAT depot is the intrascapular, while in humans smaller depots exist in the supraclavicular, paraspinal, and neck region (Cypess et al., 2009; Zingaretti et al., 2009).

Noradrenergic sympathetic innervation is the main activator of BAT thermogenesis; brown adipocytes express the β 3-adrenoreceptor, which is a G-protein-coupled receptor associated with $G_{\alpha s}$ activity and adenylate cyclase; its activation causes an intracellular rise in cAMP and the activation of PKA. This directly activates lipolysis and proliferation, and in addition boosts BAT gene expression in order to sustain the thermogenic process (i.e. mitochondrial biogenesis, Ucp1 expression; (Cannon and Nedergaard, 2004)). The net result of increased

Ucp1 function is heat production, which is due to the mitochondrial membrane potential being dissipated across the IMM (Cannon and Nedergaard, 2004). Of note, both glucose, taken up from the circulation, and fatty acids derived from lipolysis, sustain BAT thermogenesis (Cannon and Nedergaard, 2004; Labbé et al., 2014).

Shivering thermogenesis and exercise

Mammals are also able to react to sudden drops in external temperature through shivering thermogenesis, which expends energy by hyper-activating muscles in a largely involuntary manner (Sandoval et al., 2008).

1.2.1.3. Pituitary adrenal axis and corticosterone influence on metabolism

Stress, relayed by the hypothalamus/pituitary/adrenal axis, can also affect systemic metabolism, mostly through its final circulating product cortisol (in rodents, the predominant glucocorticoid is cortisol's precursor, corticosterone, which differs from it by an hydroxyl group).

The axis is controlled by the **paraventricular nucleus** (PVN) of the hypothalamus, which releases corticotropin-releasing hormone (CRH) according to daily circadian rhythm or as a stress response (i.e. the fight or flight behavior) overseen by the amygdala. CRH stimulates the release of ACTH (adrenocorticotrophic hormone), another cleavage product of POMC, from the anterior portion of the pituitary gland. ACTH has receptors in the fasciculata and reticularis layers of the **adrenal glands**, which secrete cortisol into the bloodstream. Circulating cortisol, and to a smaller extent also ACTH, exert negative feedback on both CRH and ACTH synthesis in the hypothalamus and pituitary (Boron and Boulpaep, 2009).

The metabolic effects of circulating cortisol include an increase in gluconeogenesis in the liver, proteolysis in the muscle to provide amino acids for hepatic glucose synthesis, and fat mobilization. This results in a net increase in circulating glucose, which is available to face the challenge that prompted the onset of the "**fight or flight**" response (Boron and Boulpaep, 2009).

1.2.1.4. Fgf21 and the “mitokine” concept

Fgf21 (Fibroblast growth factor) is a recent addition (Kharitononkov et al., 2005) to the array of circulating metabolic regulators. It belongs to the subfamily of hormonal FGFs, which also includes Fgf19, Fgf15 and Fgf23. Of note, Fgf21 does not affect food intake, but it does exert a powerful and multifaceted effect on energy expenditure.

Signaling

Unlike other FGFs, hormonal FGFs require an obligate coreceptor for signaling; in the case of Fgf21, the coreceptor is **β -Klotho (KLB)**, in preferential complex with Fgf receptor FGFR1c, and with a lower affinity with FGFR2c, FGFR3c and FGFR4 (Ding et al., 2012; Fisher and Maratos-Flier, 2015). As a result, KLB is the main determinant of the tissue specificity of Fgf21 action. In mice, KLB is expressed in WAT and BAT, liver, both exocrine and endocrine pancreas, and the suprachiasmatic and paraventricular nuclei (SCN; PVN) of the hypothalamus (Bookout et al., 2013; Johnson et al., 2009; Wente et al., 2006; Xu et al., 2009). Upon Fgf21 binding, the KLB-FGFR1 complex dimerizes and auto-phosphorylates, creating a docking site for FGFR substrate 2 α (FRS2 α), which transduces the signal via MAPK/ERK cascades and via PI3K. The outcome of Fgf21 signaling is tissue- and cell-specific.

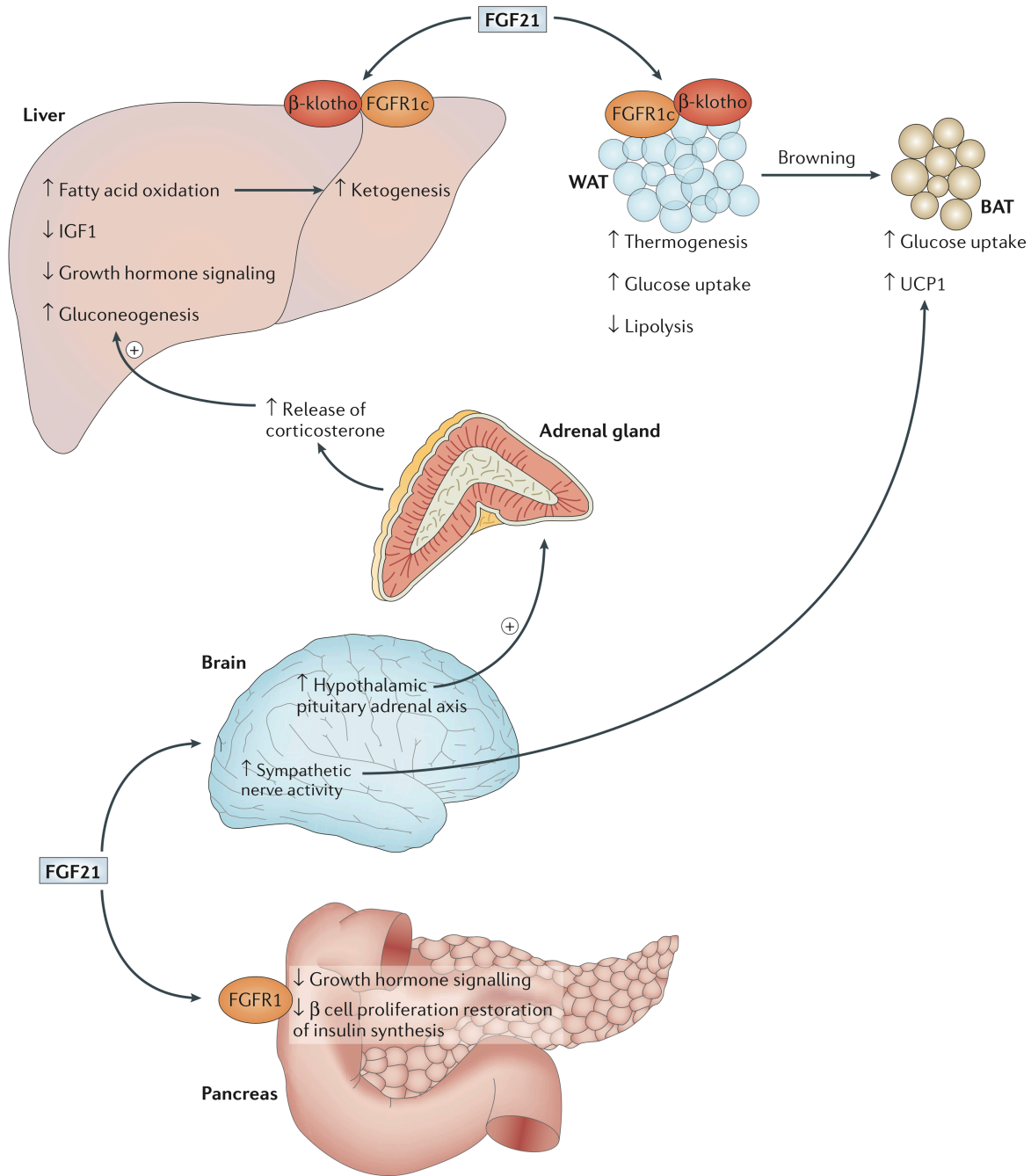


Figure 1.6 Pleiotropic metabolic actions of Fgf21. Fgf21 has both central and peripheral receptors. In the brain, Fgf21 signaling stimulates the activation of the hypothalamic-pituitary-adrenal axis via CRH, resulting in corticosterone release and liver gluconeogenesis. In the liver, Fgf21 stimulates ketogenesis. In BAT, Fgf21 stimulates glucose uptake and lipolysis, in coordination with brain Fgf21-mediated activation of the sympathetic nervous system, and it triggers WAT browning. In pancreas, Fgf21 protects β cells and restores insulin synthesis. (Degirolamo et al., 2016)

Regulation of glucose metabolism

The paradigm of Fgf21 induction is its hepatic upregulation upon prolonged fasting, which acts in an autocrine manner on the liver stimulating fatty acid oxidation, ketogenesis and gluconeogenesis via PGC1 α (Potthoff et al., 2009). A similar response is observed under different kinds of nutritional stress, such as amino acid-deficient, methionine-choline-deficient, or ketogenic diet (Badman et al., 2007; Fisher and Maratos-Flier, 2015).

On the other end of the spectrum, Fgf21 is also synthesized by the liver during refeeding or overfeeding; accordingly, it is increased in obese animals and humans. In this context, it acts as an insulin sensitizer to enhance glucose clearance from the bloodstream in a manner that is independent of hepatic insulin receptors but dependent on BAT and on WAT browning (Inagaki et al., 2007).

Finally, Fgf21 improves glucose homeostasis by virtue of the protective effect it exerts on pancreatic β -cells (Kharitonkov et al., 2007).

Adaptation to caloric restriction and starvation

In addition to the response to a short-term fast, Fgf21 also regulates body metabolism in case of longer stretches of caloric restriction (Degirolamo et al., 2016). Besides the aforementioned effects on lipolysis and ketogenesis, Fgf21 can also lead to a hibernation-like torpor in rodents, accompanied by a 10°C drop in body temperature (Inagaki et al., 2007). Accordingly, Fgf21-overexpressing mice display a lean phenotype, a smaller body size – which is due to Fgf21-mediated growth hormone resistance – and an **increased lifespan**, comparable to that obtained by caloric restriction (Zhang et al., 2012).

Thermogenesis and effects on adipose tissue

Both circulating and locally-produced Fgf21 can act on WAT and BAT, both of which express KLB and FGFR1c.

In WAT, Fgf21 induces genes involved in all aspects of lipid metabolism, from glucose uptake to lipogenesis and lipolysis (Owen et al., 2015). Its signaling in WAT is dependent on its induction of **adiponectin**, and some aspects of Fgf21 biology are lacking in adiponectin knockout animals (Lin et al., 2013). Furthermore, Fgf21 in WAT acts in a feed-forward loop with **PPAR γ** , whereby PPAR γ activation (for instance, by a pharmacological agonist of the thiazolidinedione family) stimulates Fgf21 production in WAT, and in turn Fgf21 stabilizes PPAR γ by preventing its SUMOylation and inactivation (Dutchak et al., 2012). Finally, Fgf21 signaling induces browning of WAT by upregulating Ucp1 (Fisher et al., 2012), though recent work has shown that this aspect of Fgf21 biology is not necessary for its weight loss and glucose homeostasis improvement (Samms et al., 2015; Véniant et al., 2015).

In BAT, Fgf21 induces Ucp1 expression and thermogenesis by activating PGC1 α , STAT3 and CREB, which cooperate to match the increased energy consumption with increased mitochondrial biogenesis and respiration (Labbé et al., 2015). Additional effects of Fgf21 on BAT are exerted via its receptors in the CNS (addressed below).

Neuroendocrine effects of Fgf21

Early evidence of the importance of the CNS Fgf21 receptors came from the observation that intracerebroventricular Fgf21 administration was sufficient to induce weight loss in obese mice (Sarruf et al., 2010). Indeed, Fgf21 crosses the blood-brain barrier and exerts CNS-specific actions that further substantiate its role as a systemic mediator of the starvation response.

- (I) It alters the **circadian rhythms** and physical activity patterns in mice (Bookout et al., 2013);
- (II) It causes temporary female **infertility** by suppressing vasopressin-kisspeptin signaling in the hypothalamus (Owen et al., 2013);
- (III) It activates the **hypothalamus-pituitary-adrenal** axis by upregulating CRH, leading to an increase in circulating corticosterone; in turn, corticosterone increases hepatic Fgf21 production in a feed-forward loop (Bookout et al., 2013; Patel et al., 2015);

(IV) Also via CRH, it activates the sympathetic branch of the **autonomic nervous system**, which mediates some of its effects on BAT – namely, Ucp1 increase and lipolysis (Owen et al., 2014).

Of note, all the above functions are lost upon conditional KLB knockout in the suprachiasmatic nucleus of the hypothalamus and in the dorsal vagal complex of the hindbrain (Bookout et al., 2013; Owen et al., 2013, 2014; Patel et al., 2015).

Non-canonical mechanisms of Fgf21 induction

In addition to diet alterations, other physiological conditions have been shown to increase circulating Fgf21, such as cold exposure and acute or chronic exercise (Cuevas-Ramos et al., 2012; Fisher et al., 2012). Fgf21 is also upregulated in systemic metabolic disorders, such as **diabetes** associated with obesity and liver disease (Kim and Lee, 2015). However, the remarkable aspect of Fgf21 biology is that it is also induced in seemingly unrelated pathological conditions and in specific experimental models.

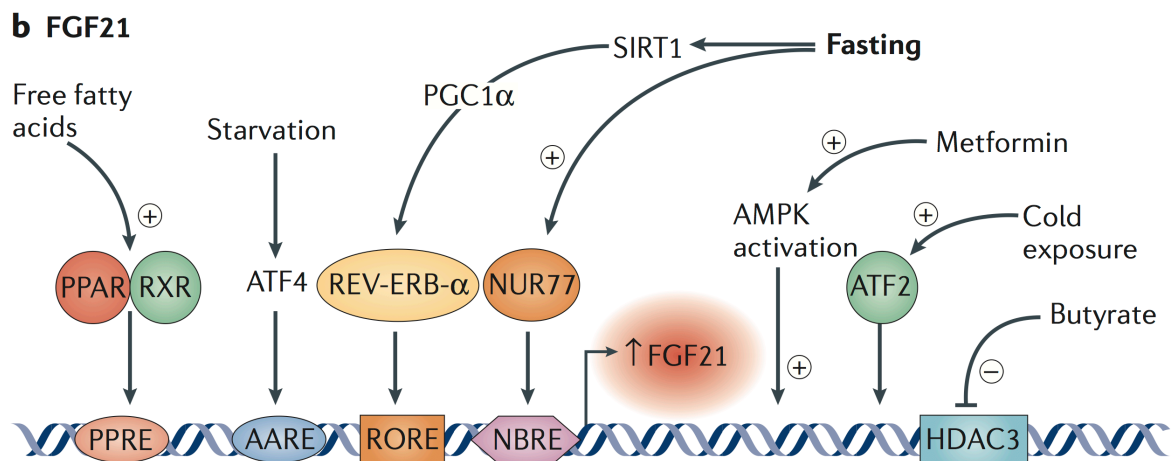


Figure 1.7 Transcriptional regulation of Fgf21. Fgf21 transcription is controlled by PPARs, which sense free fatty acids, ATF4, SIRT1 and PGC1 α , which monitor nutritional status, and drugs (metformin). In adipose tissue, ATF2 also transcribes Fgf21. (Degirolamo et al., 2016)

For instance, muscle myopathies caused by primary mitochondrial defects significantly upregulate Fgf21 via an Akt1- and/or an ATF4-mediated pathway (Crooks et al., 2014;

Suomalainen et al., 2011; Tynismaa et al., 2010). Indeed, Fgf21 is now being proposed as a **biomarker** for mitochondrial myopathies (Suomalainen et al., 2011).

Autophagy is also a sensitive target in skeletal muscle, such that its impairment causes Fgf21 expression. For instance, disrupting autophagy by ablating Atg7 (which is critical for autophagosome completion) in either skeletal muscle or liver resulted in Fgf21 production via PERK-eIF2 α -ATF4 pathway (Kim et al., 2013). Likewise, mice with a skeletal muscle-specific constitutive activation of mTORC1, which prevents autophagy, express Fgf21 in a PERK-dependent manner (Guridi et al., 2015). A similar effect is obtained when systemically ablating LAMP1, a lysosomal protein which mediates the final stages of autophagy (Yasuda-Yamahara et al., 2015).

It is now believed that many forms of **mitochondrial disruption** in muscle yield Fgf21 production. Drp1 overexpression, for instance, activates the PKR branch of the integrated stress response via the mitochondrial UPR, resulting in Fgf21 synthesis (Touvier et al., 2015). Mitochondrial uncoupling via Ucp1 overexpression in skeletal muscle exerts a similar effect, via a non-specified branch of the ISR (Keipert et al., 2014), as does ablation of one specific mitochondrial aminoacyl-tRNA synthetase (for aspartate, DARS2; (Dogan et al., 2014)).

Thus, it is now speculated that mitochondrial stress in skeletal muscle is a signal for generalized nutrient deficiency, and is conveyed systemically via Fgf21; this phenomenon has led to Fgf21 being referred to as a “**mitokine**” (Kim et al., 2013). Whether Fgf21 is an adaptive factor in this response, or just an epiphenomenon, has not yet been conclusively addressed (Kim and Lee, 2015; Lee, 2015).

1.2.1.5. Cellular nutrient sensing

Cells are able to fine-tune their growth and metabolic rate according to nutrient availability; this is fundamental for each individual cell's survival, and also has implications for the survival of whole organisms, which rely on cells in specialized tissues sensing bioenergetic needs and availability. Given the wide range of metabolic processes that take place within a

cell, different types of nutrients are sensed by different, integrated systems (Yuan et al., 2013).

Indicators and sensors of nutrient deficiency

The sensor for cellular energy is the **ATP:ADP/AMP ratio**, which controls the activation of **AMP-activated protein kinase** (AMPK; (Carling, 2004)). AMPK is a heterotrimer composed of a catalytic α subunit and two regulatory β and γ subunits. It monitors energy levels by direct binding to ATP, ADP and AMP, with different outcomes: ADP and AMP, the latter with a stronger effect, activate the kinase when bound; conversely, ATP keeps it inactive. Additional layers of regulation come from phosphorylation by liver kinase B1 (LKB1) and Calcium-calmodulin-activated protein kinase kinase β (CaMKK2 β ; Yuan 2013). AMPK can also be activated in response to general cellular stresses that impact energy production, such as oxygen or glucose starvation, metabolic poisons, antidiabetic drugs and xenobiotics (Hardie et al., 2012).

Another form of nutrient stress that cells can undergo is **amino acid deficiency**; the relevance of amino acids for the cell's metabolism is due to their role as building blocks not only for proteins, but also as precursors for nucleic acids and ATP (Yuan et al., 2013). In mammals, **mammalian Target of Rapamycin** (mTOR) is regulated by amino acids and in turn is a master regulator of cell growth. It exists in two distinct complexes, mTORC1 and 2, which contain accessory proteins Raptor and Rictor, respectively; of these, mTORC1 alone is amino acid-sensitive (Sancak et al., 2008). mTORC1 is activated at the lysosomes by the combined presence of amino acids and growth factors (relayed respectively by Rag/Rheb proteins and TSC1/TSC2).

General control non-derepressible (GCN2) is also a sensor for amino acid deprivation, and it becomes phosphorylated and thus activated upon binding to uncharged tRNAs; when active, it phosphorylates eIF2 α , activating one branch of the integrated stress response.

Cellular measures to cope with nutrient stress

The activation of AMPK shifts the cell's **metabolism** in different ways:

- (I) It increases substrate availability by promoting glucose uptake (i.e. by upregulating its transporter GLUT4) and fatty acids uptake;
- (II) It promotes glycolysis by phosphorylating and activating 6-phosphofructo-2-kinase, which synthesizes the allosteric activator of glycolysis rate-limiting enzyme 6-phosphofructo-1-kinase (Marsin et al., 2000);
- (III) It promotes mitochondrial biogenesis (see below);
- (IV) It inhibits anabolic pathways, including gluconeogenesis, fatty acid synthesis, protein synthesis and ribosomal RNA biogenesis (Hardie et al., 2012);
- (V) It reduces glycogen synthesis by phosphorylating and inhibiting glycogen synthase (Yuan et al., 2013).

AMPK also inhibits mTORC1, by phosphorylating both Raptor and TSC2, favoring catabolic over anabolic processes.

mTORC1 and GCN2 cooperate to **decrease global translation** in amino acid-deficient cells. Active mTORC1 – in amino acid-rich states – phosphorylates eukaryotic translation initiation factor 4E (eIF4E)-binding protein 1 (4E-BP1) and S6K1, which are respectively a translational repressor, inactivated by the phosphorylation, and a translational activator, activated by the phosphorylation (Ma and Blenis, 2009); as a result, translation is active in growth factor- and amino acid-rich conditions. Conversely, the translational blocks are in place when mTORC1 is not active in the absence of amino acids and growth factors. Given that protein synthesis is a major consumer of ATP, also in this context active AMPK inhibits mTORC1 to decrease translation (Yuan et al., 2013). Additionally, AMPK directly inhibits translation by acting on eukaryotic Elongation Factor 2 (eEF2; (Browne et al., 2004)).

In parallel, GCN2 activation of eIF2 α causes a global translational repression by inhibiting translation initiation ((Wek et al., 2006); see also paragraph 1.1.3.3).

Given that both cell growth and energy production rely on mitochondrial activity, mitochondrial biogenesis is induced by both AMPK and mTORC1 through **PGC1 α**

(peroxisome proliferator-activated receptor- γ co-activator 1 α); specifically, AMPK phosphorylates and activates PGC1 α , while mTORC1 promotes its transcriptional activity (Hardie et al., 2012; Yuan et al., 2013).

Under conditions of extreme or prolonged nutrient deprivation, when inhibiting biosynthetic pathways is not sufficient, **autophagy** is activated to provide recycled macromolecules for cell survival (Yuan et al., 2013). The process of autophagy entails the formation of a phagophore, which is controlled by the ULK1 complex regulating class III phosphatidylinositol 3-kinase complex (including Beclin 1, Atg14(L)/barkor, Vps15, Vps34, and Ambra1) at the ER; The Atg12–Atg5–Atg16L1 complex subsequently conjugates LC3 to PE on the phagophore, favoring its elongation and closure (Mizushima and Komatsu, 2011). mTORC1 inhibition relieves the block on autophagy imposed by mTOR-mediated ULK1 phosphorylation. Additionally, AMPK activation directly activates ULK1 and other autophagy mediators (Galluzzi et al., 2014), in addition to its inhibitory action on mTORC1. GCN2 activation is also important for autophagy, likely through some transcriptional targets of ATF4, though the mechanisms have not yet been identified (Galluzzi et al., 2014; Tallóczy et al., 2002). Of note, AMPK activation also promotes mitochondrial fragmentation by acting on MFF, possibly to favor mitophagic elimination of dysfunctional mitochondria – though how the fusion/fission balance is regulated based on the health of mitochondria is not yet clear (Toyama et al., 2016).

Mitochondrial dynamics in cellular metabolism

An important role for mitochondrial dynamics is emerging in the context of cellular nutrient sensing and in the ensuing metabolic response. As a general principle, starvation results in hyperelongation of the mitochondrial network to maximize energy production efficiency; nutrient excess, on the other hand, has been reported to cause mitochondrial fragmentation as a response to the ROS production that occurs during respiration (Cogliati et al., 2013; Gomes et al., 2011; Liesa and Shirihai, 2013; Molina et al., 2009; Twig et al., 2008).

Pancreatic β -cells gauge systemic nutrient availability by precisely coupling nutrient oxidation to nutrient availability; as a result, excess nutrients are oxidized to produce ATP, leading to insulin secretion (Rutter, 2001); however, they also lead to increased NADH production and oxidative stress. Indeed, in cultured pancreatic β cells, the presence of excessive nutrients triggers mitochondrial fragmentation, which in turn renders ATP production less efficient. In addition, mitochondrial fragmentation prevents the spreading of ROS generated from the respiratory chain (Liesa and Shirihai, 2013; Molina et al., 2009).

This process is also relevant in BAT, where the excess nutrients derived from lipolysis are converted to heat through futile energy cycling. On the other hand, muscle is equipped to produce ATP with high efficiency, and therefore undergoes significant oxidative stress upon large increases in nutrient availability (specifically, fatty acids) (Liesa and Shirihai, 2013). Accordingly, muscle-specific calcineurin ablation, which causes mitochondrial hyperelongation by inhibiting Drp1 activity, resulted in protection from diet-induced obesity in mice; however, it also reduced muscle performance under exercise conditions, underlining the tradeoff between ATP production and excess nutrient handling (Pfluger et al., 2015).

Conversely, in starvation conditions, ATP production must become more efficient; this is achieved through mitochondrial network fusion and cristae remodeling, which favors the dimerization of ATP synthase (Cogliati et al., 2013; Gomes et al., 2011).

While it is clear that bioenergetics affect mitochondrial dynamics, and mechanisms have been hypothesized to explain the morphological changes occurring upon a metabolic switch, the opposite (i.e. that mitochondrial dynamics directly affect bioenergetics) has not yet been convincingly proved. Nevertheless, numerous attempts at manipulating mitochondrial morphology to elicit changes in bioenergetics have highlighted that the **plasticity** of mitochondrial dynamics is crucial to the successful completion of this metabolic response. For instance, muscle Mfn2 ablation, which should mimic the response to excess nutrients, actually exacerbates this response, indicating that some residual Mfn2 activity is essential for cell survival upon nutrient overload (Sebastián et al., 2012). The current view now includes mitochondrial quality control in the equation, highlighting that efficient

complementation (through fusion) and turnover (through fission) are integral components of the cellular response to changes in nutrient availability (Liesa and Shirihai, 2013).

2. Aims of the work

Mitochondrial dynamics are increasingly emerging as fundamental regulators of cellular and organismal processes. This is also highlighted by the absolute requirement for mitochondrial fusion and fission in a plethora of developmental processes. Indeed, both Mitofusins and Drp1 are essential in early development, and their ablation causes early embryonic lethality (Chen et al., 2003; Wakabayashi et al., 2009). Conditional deletion of both Mitofusins in the heart also causes embryonic lethality due to Notch-mediated inhibition of myocardial differentiation (Kasahara et al., 2013).

The importance of mitochondrial dynamics in brain is evidenced by the primarily neurological phenotypes of diseases of mitochondria-shaping proteins. Indeed, a single case report of a sporadic Drp1 mutation in an infant indicates that loss of Drp1 function in the developing brain leads to severe impairment in brain development (Waterham et al., 2007). Accordingly, loss of function of MFF in humans also causes a severe neurological phenotype (Koch et al., 2016), as does decrease in STAT2, which has been shown to block mitochondrial fission (Shahni et al., 2015). As for mitochondrial fusion, an axonal form of Charcot-Marie-Tooth disease and autosomal dominant optic atrophy result from mutations in MFN2 and OPA1, respectively ((Alexander et al., 2000; Bradbury, 2004); see also 1.1.4.2).

This is reflected in studies on animal models, where embryonic knockout of Mfn1, but not of Mfn2, resulted in early postnatal lethality due to cerebellar defects (Chen 2003). Two separate attempts to ablate Drp1 in the developing brain met with early embryonic lethality, due to severe neurodevelopmental defects (Ishihara et al., 2009; Wakabayashi et al., 2009).

Subsequent attempts to ablate Drp1 in postnatal neurons highlighted its importance in synapse formation and neuronal mitochondrial transport in nigrostriatal dopaminergic neurons (Berthet et al., 2014), in forebrain neurons (Oettinghaus et al., 2016; Shields et al., 2015), and in cerebellar Purkinje cells (Kageyama et al., 2012). Of note, neurodegeneration did not consistently occur in these models, and seems to be a cell-type-specific phenomenon. It has been postulated to be mediated by differential resistance to oxidative

stress, though this was only shown *in vitro* (Kageyama 2009); our own *in vivo* experiments did not show an increase in oxidative stress upon Drp1 ablation (Oettinghaus et al., 2016).

Lately, a relevant role for mitochondrial dynamics has emerged in the hypothalamic circuits that regulate feeding and energy expenditure (Nasrallah and Horvath, 2014). Specifically, Mfn1 and Mfn2 deletion in AgRP-NPY neurons protects mice from diet-induced obesity (Dietrich et al., 2013); conversely, Mfn2 ablation from POMC neurons causes morbid obesity in normal-fed mice (Schneeberger et al., 2013). The former is due to the effect of mitochondrial fusion in regulating cellular ATP levels, while the latter is mainly attributed to Mfn2's role as an ER-mitochondria tether (Gao et al., 2014; Zorzano and Claret, 2015).

Within this framework, and considering that our own Drp1^{flx/flx} CaMK2 α -CreERT2 mice also displayed a prominent and severe metabolic phenotype (Oettinghaus et al., 2016), in this work we sought to further characterize the role of forebrain mitochondrial fission in the systemic regulation of metabolism and energy expenditure.

3. Manuscript

Synaptic dysfunction, memory deficits and hippocampal atrophy due to ablation of mitochondrial fission in adult forebrain neurons

Björn Oettinghaus¹, Jan Michael Schulz², Lisa Michelle Restelli¹, Maria Licci^{1,3}, Claudia Savoia⁴, Alexander Schmidt⁵, Karen Schmitt⁶, Amandine Grimm⁶, Lorenzo Morè⁷, Jürgen Hench¹, Markus Tolnay¹, Anne Eckert⁶, Patrizia D`Adamo⁷, Paul Franken⁸, Naotada Ishihara⁹, Katsuyoshi Mihara^{9,10}, Josef Bischofberger², Luca Scorrano^{4,11*}, and Stephan Frank^{1*}

- ¹) Division of Neuropathology, Institute of Pathology; University Hospital Basel, Basel, 4031, Switzerland
- ²) Division of Neurophysiology, Institute of Physiology, Department of Biomedicine; University of Basel, Basel, 4056, Switzerland
- ³) Department of Neurosurgery; University Hospital Basel, Basel, 4031, Switzerland
- ⁴) Department of Biology, University of Padua, Padua, 35121, Italy
- ⁵) Proteomics Core Facility, Biozentrum, University of Basel, Basel, 4056, Switzerland
- ⁶) Neurobiology Laboratory for Brain and Mental Health, University Psychiatric University Clinics Basel, University of Basel, Basel, 4012, Switzerland
- ⁷) Dulbecco Telethon Institute, San Raffaele Scientific Institute, Milan, 20132, Italy
- ⁸) Faculty of Biology and Medicine, Center for Integrative Genomics, University of Lausanne, Lausanne, 1015, Switzerland
- ⁹) Department of Protein Biochemistry, Institute of Life Science, Kurume University, Kurume, 839-0864, Japan
- ¹⁰) Department of Molecular Biology, Graduate School of Medical Science, Kyushu University, Fukuoka 812-8582, Japan
- ¹¹) Dulbecco-Telethon Institute, Venetian Institute of Molecular Medicine, Padua, 35129, Italy

Running title: Drp1 ablation in adult hippocampal neurons

***Correspondence:** luca.scorrano@unipd.it; stephan.frank@usb.ch

3.1. Summary

Well-balanced mitochondrial fission and fusion processes are essential for nervous system development. Loss of function of the main mitochondrial fission mediator, dynamin-related protein 1 (Drp1), is lethal early during embryonic development or around birth, but the role of mitochondrial fission in adult neurons remains unclear.

Here we show that inducible *Drp1* ablation in neurons of the adult mouse forebrain results in progressive, neuronal subtype-specific alterations of mitochondrial morphology in the hippocampus that are marginally responsive to antioxidant treatment. Furthermore, DRP1 loss affects synaptic transmission and memory function. While these changes culminate in hippocampal atrophy, they are not sufficient to cause neuronal cell death within 10 weeks of genetic *Drp1* ablation.

Collectively, our *in vivo* observations clarify the role of mitochondrial fission in neurons, demonstrating that *Drp1* ablation in adult forebrain neurons compromises critical neuronal functions without causing overt neurodegeneration.

Keywords: autophagy / cell death / dynamin-related protein, Drp1 / mitochondrial dynamics / neurodegeneration

3.2.

3.3. Introduction

In addition to their crucial importance in energy conversion, mitochondria serve many other housekeeping functions, including calcium buffering, amino acid and steroid biosynthesis as well as fatty acids β -oxidation and regulation of cell death. During the past decade, it has become increasingly clear that processes regulating mitochondrial morphology and ultrastructure are influenced by specific cellular requirements upon which mitochondria, in a precisely regulated manner, undergo fusion and division events¹. Maintaining this balance is especially important for highly energy-consuming, polarized cells such as neurons, where single organellar units sprouting from the mitochondrial network are transported along the cytoskeleton into dendrites and spines to meet local energy requirements². In addition, elaborate quality control mechanisms also rely on mitochondrial dynamics: whereas defective organelles are sequestered by fission, enabling their removal from the mitochondrial network^{3,4}, fusion supports qualitative homogeneity of the syncytium through complementation⁵.

Mitochondrial fusion and fission are mediated by large GTPases of the dynamin superfamily⁶. The outer mitochondrial membrane mitofusins 1 (MFN1) and 2 (MFN2) tether mitochondrial membranes by homo- or heterodimer formation⁷, thereby initiating fusion of the organelles, a process that also involves the inner mitochondrial membrane-associated GTPase Optic Atrophy 1 (Opa1)⁸. In addition, MFN2 also mediates contacts between mitochondria and endoplasmic reticulum⁹. The only known mammalian mitochondrial fission protein, Dynamin-Related Protein 1 (Drp1), translocates upon dephosphorylation by calcineurin¹⁰ to fission sites where it binds to mitochondrial fission factor (Mff)¹¹. Drp1 translocation is preceded by ER membranes wrapping around mitochondria to constrict the organelles¹², thereby facilitating the formation of multimeric Drp1 complexes that, upon GTP hydrolysis, further tighten to complete the process of mitochondrial fission¹³.

Genetic evidence in mice and humans indicates that mitochondrial dynamics are crucially important in neurons: in humans, a sporadic dominant negative *DRP1* mutation caused a lethal syndromic defect with abnormal brain development¹⁴; similarly, constitutive *Drp1* knockout in the mouse brain leads to lethal neurodevelopmental defects^{15,16}. While the crucial role of Drp1 during brain development is undisputed, studies on Drp1 function in postmitotic (adult) neurons are scarce; likewise, Drp1 ablation studies in primary cultures have so far failed to yield a conclusive picture. *In vitro*, *Drp1* ablation is reported to lead to a super-elongated neuroprotective^{17–24} or an aggregated mitochondrial phenotype associated with neurodegeneration^{15,16,25–27}. These discrepancies are probably due to different experimental conditions: neuronal health is indeed influenced by the onset and duration of Drp1 inhibition, which varies considerably among the cited reports²⁸, and different types of neuronal cultures studied display different sensitivity to Drp1 inhibition. *In vivo*, Drp1 ablation in Purkinje cells results in oxidative stress and neurodegeneration²⁹ demonstrating that Drp1 is essential for postmitotic neurons' health. In contrast, transient pharmacological Drp1 inhibition is neuroprotective in several mouse ischemia models, indicating that temporarily blocking mitochondrial fission holds therapeutic potential^{30–32}.

To elucidate the consequences of blocked mitochondrial fission in the central nervous system *in vivo*, we bypassed the critical role of Drp1 during brain development by generating *Drp1^{flx/flx}* mice¹⁵ expressing tamoxifen-inducible Cre recombinase under the control of the *CaMKII α* promoter³³. Upon induced *Drp1* deletion in postmitotic adult mouse forebrain neurons, mice develop progressive, neuronal subtype-specific alterations in mitochondrial shape and distribution in the absence of overt neurodegeneration. In addition, respiratory capacity, ATP content, synaptic reserve pool vesicle recruitment as well as spatial working memory are impaired, demonstrating that severely dysregulated mitochondrial dynamics can compromise critical neuronal functions *in vivo* without causing neuronal cell death.

3.4. Results

3.4.1. Inducible *Drp1* ablation in the adult mouse forebrain.

In order to study the effect of mitochondrial fission ablation in adult neurons, we generated a model of inducible *Drp1* ablation in the forebrain by crossing mice with *loxP* sites inserted in the *Drp1* gene (*Drp1^{flx/flx}*)¹⁵ with mice expressing a gene for a tamoxifen-inducible Cre recombinase fusion protein under the control of the *CaMKII α* promoter (Fig. 3.1A)³³, limiting recombination primarily to the forebrain. Eight-week old offspring of these crossings were injected with tamoxifen on five consecutive days (*Drp1* inducibly deleted in the brain, *Drp1^{i Δ b/i Δ b}*), resulting in maximum DRP1 depletion in the hippocampus within 14 days (Fig. 3.1B). Immunohistochemical DRP staining in *Drp1^{i Δ b/i Δ b}* animals 4 weeks post-tamoxifen injection (p.t.i.) confirmed that DRP1 was lacking specifically in hippocampal neurons (Fig. 3.1C) and crosses of *Drp1^{i Δ b/i Δ b}* mice with a reporter strain further confirmed the recombination following tamoxifen injection (Suppl. Fig.1A).

3.4.2. *Drp1* ablation causes progressive changes in mitochondrial morphology.

To characterize the consequences of inducible *Drp1* ablation, we turned to an *in vitro* model of primary cortical neurons isolated from *Drp1^{flx/flx}* mice where we could monitor by confocal microscopy the consequences of Cre recombinase-induced *Drp1* ablation by co-transfecting it with a mitochondria-targeted yellow fluorescent protein (mtYFP). Starting at day 3 following *in vitro* recombination (DIV), mitochondria progressively clustered and aggregated in the soma. Fewer organelles were found within the neurite compartment, where mitochondria also appeared larger in comparison to sham-transfected controls (Fig. 3.2). Comforted by these results, we moved to adult hippocampal neurons *in vivo* to study mitochondrial morphology by immunohistochemistry. At day 10 after *Drp1* ablation, enlarged spherical mitochondria started to aggregate in the perikarya of hippocampal neurons. Whereas 10 days p.t.i. enlarged mitochondria clustered in the perikarya of approx. only 5% of CA1 neurons, in the dentate gyrus (DG) and CA3 hippocampal neurons, mitochondrial morphology changes occurred earlier after *Drp1* ablation. Conversely, 4 weeks p.t.i., neuronal mitochondrial morphology was heavily altered in all three neuronal

subpopulations, mitochondria of CA3 pyramidal neurons appearing considerably less filamentous and more fragmented compared to CA1 and DG neurons (Fig. 3.3). These findings demonstrate that blocking fission alters mitochondrial morphology and distribution in a neuronal subtype-specific manner.

3.4.3. Synaptic transmission is impaired in *Drp1*-deficient CA1 pyramidal neurons.

We next addressed whether the observed mitochondrial morphological defects resulted in any functional consequence by behavioral and electrophysiological tests.

Biocytin filling indicated that dendritic morphology of hippocampal neurons was not altered 4 weeks p.t.i. (Fig. 3.4A). Accordingly, whole-cell patch-clamp recordings revealed that CA1 pyramidal *Drp1*^{iΔb/iΔb} neurons display normal resting membrane potential and action potential (AP) peak amplitudes as well as half-duration (Fig. 3.4B-E). When we explored excitatory synaptic transmission by performing field potential recordings in the hippocampal *Drp1*^{iΔb/iΔb} CA1 region, we observed that stimulation of the Schaffer collaterals evoked field excitatory postsynaptic potentials (fEPSP) with normal paired-pulse facilitation (143%, n=10; t= 100 ms) was similar to that observed in control mice (151%, n=6, p = 0.52), again indicating normal release probability. However, when synaptic transmission was challenged by application of 100 stimuli at either 10 Hz or 100 Hz, frequency-dependent fEPSP facilitation was significantly reduced in *Drp1*^{iΔb/iΔb} brain slices, where synaptic transmission also broke down more rapidly (Fig. 3.5A-C; Suppl. Fig. 3.1D,E). In addition, when subjected to a spontaneous alternation task (a behavioral assay for hippocampus-dependent working memory), short-term working memory was significantly impaired in *Drp1*^{iΔb/iΔb} mice compared to their *Drp1*^{fix/fix} littermates (Fig. 3.5D), not because of impaired visual acuity and olfaction (Suppl. Fig. 3.1F, G). These synaptic transmission deficits are similar to those observed in the neuromuscular junction of *drp1*-mutant *Drosophila*³⁴, which were attributed to a lack of synaptic ATP. We therefore measured oxygen consumption and ATP levels of hippocampal mitochondria, and found oxygen consumption (Fig. 3.5E) as well as ATP content (Fig. 3.5F) to be reduced in *Drp1*-deficient samples. In addition, ultrastructural analysis by transmission electron microscopy (TEM) revealed a significant reduction in presynaptic mitochondria of hippocampal *Drp1*^{iΔb/iΔb} neurons (Fig. 3.5G). The combination of

reduced mitochondrial content in presynaptic terminals and defective ATP production can explain the impaired synaptic function observed in $Drp1^{i\Delta b/i\Delta b}$ mice.

Forebrain-specific neuronal *Drp1* ablation leads to hippocampal atrophy.

Several previous studies indicate that *Drp1* ablation *in vitro* causes a reduction in the number of dendrites, spines, and synapses (reviewed by 28). However, as no substantial changes in dendritic morphology were observed early after *Drp1* ablation (4 weeks p.t.i.; Fig. 3.4A), we performed Golgi silver impregnations on $Drp1^{i\Delta b/i\Delta b}$ brain sections 10 weeks p.t.i.. Sholl analysis revealed that while overall dendritic tree morphometry was unchanged, dendrites were shorter in $Drp1^{i\Delta b/i\Delta b}$ mice (Fig. 3.6A), which was associated with decreased hippocampal volume (Fig. 3.6B). In contrast, cortical or midbrain volumes did not change significantly (Suppl. Fig. 3.1H). To test whether this hippocampal atrophy was associated with loss of spines, we quantified spine numbers on apical dendritic trees of Golgi-impregnated pyramidal CA1 neurons, but did not find any difference (Fig. 3.6C). Likewise, number of synapses, as assessed by co-localization of fluorescent stains for pre- (VGLUT2) and postsynaptic (PSD95) markers in confocal z-stacks, was normal (Fig. 3.6D). Thus, the depletion of mitochondria from presynaptic hippocampal neuron terminals can account for the observed synaptic transmission impairments and the specific deficits in spatial working memory upon *Drp1* ablation. Nevertheless, the maintenance of normal synapse and spine numbers 10 weeks following *Drp1* ablation indicates that mature hippocampal neurons are able to cope with blocked mitochondrial fission with only mild functional alterations.

3.4.4. Adult forebrain neurons do not degenerate within 10 weeks of *Drp1* ablation.

We next verified whether the above-reported changes caused by *Drp1* ablation in the hippocampus led to neurodegeneration. Hippocampal neurons were qualitatively and quantitatively normal in Hematoxylin-Eosin (H&E)-stained hippocampal tissue sections (Fig. 3.7A,B), with no signs of condensed eosinophilic neurons, chromatinolysis, or apoptotic bodies. In addition, *in situ* TUNEL did not detect any evidence of increased cell death in the hippocampus 10 weeks p.t.i. (Fig. 3.7C,D). As neurons are believed to be especially

dependent on ATP produced by oxidative phosphorylation we wondered how they could compensate the reduced ATP production (Fig. 3.5F) to avoid neurodegeneration. Comparative mass spectrometry analyses revealed that levels of glycolysis-related proteins were significantly changed, the rate-limiting enzyme Hexokinase 1 being markedly upregulated (4.37 fold; see Suppl. Table 1). These results indicate that neurons attempt to cope with the metabolic consequences of *Drp1* ablation by upregulating glycolysis.

While *Drp1* ablation in Purkinje cells²⁹ is accompanied by macroautophagy inhibition and reactive oxygen species (ROS) accumulation, extensive TEM analyses did not reveal significant autophagosome accumulation in brain sections from *Drp1*^{iΔb/iΔb} mice; of note, these consisted mostly of double-membrane structures measuring 500 nm (i.e. too small to accommodate mitochondria; Fig S2). Accordingly, comparative mass spectrometry in hippocampal neurons did not reveal significant changes in autophagy-related proteins including p62 and LC3 (Suppl. Table 2). Moreover, levels of ROS (measured by DHR and MitoSox fluorescence on isolated mitochondria), of thiobarbituric acid-reactive substances (TBARS), indicators of lipid peroxidation, as well as of oxidized (vs. total) glutathione were unchanged in mouse brain homogenates 4 weeks p.t.i. (Fig. 3.8A-D). Indeed, our comparative mass spectrometry analyses revealed that 11 out of 48 detected oxidative stress-associated proteins were upregulated in *Drp1*^{iΔb/iΔb} brains 10 weeks p.t.i. (Suppl. Table 3). Ten of these proteins are regulated by the transcription factor nuclear factor erythroid 2 related factor (NRF2), whose inhibitor KEAP1 (Kelch-like ECH-associated protein 1) was significantly downregulated (fold change: 0.38; Q: 0.002; Suppl. Table 3). Among upregulated proteins we identified several glutathione S-transferases, participating in solubilizing peroxidized lipids and xenobiotics, and the multidrug resistance protein 1A, capable of removing toxic components from the cytosol. In contrast, cytosolic and mitochondrial thioredoxins, NRF2 target genes that help reducing oxidized protein, were downregulated. These results indicate that *Drp1* ablation in postmitotic neurons leads to a moderate activation of cellular antioxidant systems, possibly explaining why ROS levels were not increased, but testifying that indeed also in forebrain neurons *Drp1* ablation leads to ROS production. Since in Purkinje cells ROS are involved in the formation of enlarged spherical mitochondrial bodies (mitobulbs)²⁹, we decided to analyze whether treatment of

mice with the mitochondrially targeted antioxidant mitoQ³⁵ for 10 days after the last tamoxifen injection could counteract the mitochondrial morphology phenotype. MitoQ significantly decreased mitobulbs in hippocampal CA1 and granule neurons of the dentate gyrus (Fig. 3.8E). However, in CA3 neurons transformation of mitochondria into mitobulbs is already complete at day 10 after *Drp1* ablation (see Fig. 3.3), and no mitoQ effect was observed, indicating that antioxidant treatment can merely delay the formation of mitobulbs but is not sufficient to suppress it.

In conclusion, unlike Purkinje cells, adult forebrain neurons respond to the increased ROS formation caused by *Drp1* ablation by upregulating the cellular antioxidant defenses that partly neutralize ROS accumulation.

3.5. Discussion

Mitochondrial fragmentation is a hallmark of apoptosis and accordingly of several neurodegenerative disorders. Conversely, the dynamin-related GTPase Drp1 is indispensable for neuronal maturation and brain development^{15,16} and for cerebellar Purkinje cell survival²⁹. Our data conversely demonstrate that adult forebrain and hippocampal neurons display an increased functional reserve that allows them to survive *Drp1* ablation.

In order to bypass the requirement for balanced mitochondrial dynamics during neuronal differentiation and brain development^{15,16}, we devised a model of acute, inducible *Drp1* ablation in adult forebrain including hippocampal neurons. Upon tamoxifen-induced *Drp1* ablation mitochondria appeared enlarged and perinuclearly confined. These neurons were unexpectedly able to cope well with Drp1 ablation: changes in neuronal morphology, oxidative stress and cell death were negligible, whereas the reduction in localized ATP supply to presynaptic terminals impaired synaptic transmission, resulting in early memory defects.

The first visible phenotype of *Drp1*^{iΔb/iΔb} mice, presenting as early as 4 weeks after tamoxifen administration, was a defect in spatial working memory, which could be traced back to the impairment in synaptic transmission upon sustained stimulation.

Accordingly, and in line with the fact that defects in mitochondrial fission impair mitochondrial transport in neurites, presynaptic mitochondria were decreased. A similar electrophysiological phenotype associated with abnormal mitochondrial morphology was observed at neuromuscular junctions of *drp1* mutant flies³⁴. While that phenotype has primarily been attributed to ATP-dependent effects on reserve pool vesicle recycling due to the lack of mitochondria at synaptic boutons and the overall reduction in oxidative phosphorylation, DRP1 may also be directly involved in synaptic vesicle formation, as shown more recently in mouse hippocampal neurons³⁶. Resting electrophysiological properties as well as paired-pulse facilitation, which were all unaffected, argue against a contribution of calcium buffering defects to the overall phenotype (recently reviewed³⁷).

A predictable consequence of inhibiting mitochondrial fission was the change in mitochondrial network morphology, with predominantly enlarged spherical mitochondria that clustered around the nucleus. Of note, while previous reports in Purkinje cells²⁹ attributed these “mitobulbs” to oxidative stress ensuing from defects in autophagy, we did not detect evidence suggesting a significant blockage of the latter *in vivo*, nor the presence of oxidative markers. Therefore, our data indicate that neurons *in vivo* are supported by the brain milieu to keep autophagy at a minimum level, even under stress conditions. This is consistent with reports that autophagy is an extremely rare event in neurons *in vivo*, even after 48 hours of starvation³⁸. Even so, buffering of oxygen radicals by mitoQ administration slowed down the formation of “mitobulbs” in our mice, suggesting that an oxidative stress component is present in *Drp1*-ablated neurons, but efficiently managed by cellular defenses. A possible explanation for this discrepancy is that Purkinje cells represent an exceptionally large and extensively connected neuronal subtype, which might entail very high metabolic activity and associated ROS production (reviewed in³⁹), all of which could contribute to selective vulnerability of this neuronal subtype under certain stress conditions. It is important to note that Purkinje cell death *in vivo* started to occur already at around week 9 after *Drp1* ablation²⁹. On the other hand, in line with the absence of oxidative stress, no neurodegeneration was observed upon 10-week-long *Drp1* ablation in the hippocampus, the time frame when *Drp1*^{iΔb/iΔb} animals had to be sacrificed due to profound systemic-level metabolic changes (manuscript in preparation). Therefore, it cannot be excluded that the

impaired neuronal mitochondrial functions might culminate in hippocampal neuronal death occurring 3 months beyond *Drp1* ablation.

Additionally, it is worth noting that murine Purkinje neuron differentiation continues throughout the first three weeks of life ⁴⁰, the time when the *L7/pcp2* promoter used by Kageyama et al. starts to be active. It may therefore be speculated that *Drp1* ablation in these neurons may still overlap with the final stages of murine cerebellar development and thus also contribute to the observed Purkinje cell degeneration. We can conversely exclude neurodevelopmental defects caused by *Drp1* ablation in our model, as recombination was induced at the age of 8 weeks and dendritic tree morphology as well as synapse and spine numbers were unaffected. Of note, a recent study reporting neurodegeneration upon *Drp1* ablation in postmitotic dopaminergic neurons supports the notion that sensitivity to *Drp1* ablation is neuronal subtype-dependent ⁴¹.

Collectively, our results indicate that adult hippocampal neurons cope with profound impairment of mitochondrial dynamics and function by activating antioxidant and metabolic compensatory mechanisms. Predictably, certain neuronal functions, such as synaptic transmission, can be affected due to depletion of the organelles from presynaptic terminals, culminating in memory deficits. Conversely, these compensatory circuits are sufficient to maintain overall neuronal morphology, synapse and spine numbers and ultimately viability for as long as 3 months following *Drp1* ablation. Our data therefore indicate that forebrain neurons can resist to mitochondrial dysmorphology and dysfunction, a critical feature to protect them and therefore the cognitive functions of higher mammals from mitochondriotoxic stimuli.

3.6. Materials and Methods

3.6.1. Mice

Drp1^{flx/flx} mice¹⁵ were crossed with *CaMKII α CreERT2* (*Cre*⁺) animals, obtained from the European Mouse Mutant Archive (EMMA strain 02125)³³. At 8 weeks of age the resulting *Drp1*^{flx/flx} *Cre*⁺ mice were injected i.p. with 1 mg tamoxifen (Sigma; 10 mg/ml tamoxifen dissolved in a 9:1 ratio of sunflower seed oil to ethanol) twice daily on five consecutive days to induce recombination of the *Drp1* locus. To check for recombination, *Drp1*^{flx/flx} *Cre*⁺ mice were crossed with the RCE:loxP reporter mouse strain (Jackson Laboratories, strain 032037-JAX) harboring the R26R CAG-boosted *Egfp* (RCE) allele with a floxed STOP cassette upstream of the *Egfp* gene.

3.6.2. Histology

Serial coronal cross sections of formalin-fixed, paraffin-embedded (FFPE) mouse brains were prepared and sections representing the coordinates bregma (-1.34 mm) – (-2.46 mm) were selected and stained for COX subunit 1a (Abcam, ab14705). Z-stacks were recorded with an inverted Zeiss Axiovert 200M LSM 510 Meta confocal microscope with a 100x/1.4 Oil DIC objective using Enterprise 405 nm and Argon 488 nm lasers. Z-stacks were projected onto a single plane using ImageJ. Synapse numbers were quantified as described previously⁴². Golgi staining was performed on PBS-perfused, unfixed brains using a commercial kit (FD Neurotechnologies).

Hippocampal volume was calculated from H&E stained 100- μ m-spaced, serial coronal cross sections applying the Cavalieri principle. For cortical and midbrain volume, only sections representing coordinates bregma 1.1 mm – (-1.2 mm) were considered, using corpus callosum as reference. TUNEL staining was performed on frozen, PBS-perfused, fixed brains using a commercial kit (Roche). Confocal images were stitched using a Fiji Plugin⁴³.

3.6.3. Transmission electron microscopy

Semithin sections of osmium-stained hippocampi were prepared in order to identify hippocampal neurons, of which ultrathin sections were prepared. Imaging was done on a

Phillips CM100 transmission electron microscope. Randomly-selected TEM images were used to quantify presynaptic mitochondria of hippocampal synapses.

3.6.4. Electrophysiology

Transverse 350 to 400 μm -thick hippocampal brain slices were cut in a sucrose-based solution. During electrophysiological recordings, slices were continuously superfused with artificial cerebrospinal fluid maintained at 32-33°C. During whole-cell patch-clamp recordings, hippocampal CA1 pyramidal neurons were filled with biocytin for subsequent morphological evaluation. Field excitatory postsynaptic potentials (fEPSP) were recorded with glass pipettes filled with 1 M NaCl placed in the stratum radiatum of the CA1 region. The stimulating electrode was placed \sim 500 μm away to stimulate Schaffer collaterals. Data analysis was performed offline using customized scripts written in python and Stimfit.

3.6.5. Behavioral analyses

Visual performance was tested in the Morris Water tank with a visible platform. Olfaction was checked using the cookie finding test. To score hippocampus-dependent working memory, the spontaneous alternation task was employed in an 8-arm radial maze, based on the spontaneous alternation paradigm⁴⁴.

3.6.6. Western Blot

Proteins of brain lysates were separated on 4-12% BisTris SDS-PAGE gels, blotted onto PVDF membranes using the iBlot Dry Blotting System (Life Technologies), and probed with the indicated primary antibodies and isotype-matched secondary antibodies conjugated to horseradish peroxidase. Signals were detected using ECL (GE Healthcare).

3.6.7. Tissue culture

Cortical neurons from Drp1^{flx/flx} mice were prepared from E16.5 embryos by modifying a previously described method⁴⁵. Prior to plating, cells were electroporated using the Neon Electroporation System (Life Technologies). For complete protocol, please refer to the supplementary information.

3.6.8. Quantitative proteomics

Brain tissue samples were lysed in 2% sodium deoxycholate (DOC), 100 mM ammonium bicarbonate buffer, reduced with 5 mM TCEP and alkylated with 10 mM iodoacetamide. Proteins were then digested by incubation with sequencing-grade modified trypsin (1/50, w/w; Promega, Madison, Wisconsin) overnight at 37°C. The digested samples were subsequently labeled with isobaric tag (TMT 6-plex, Thermo Fisher Scientific) according to the manufacturer's instructions. The TMT labeled samples were re-solubilized to a final concentration of 1 mg/ml and separated on a 12 cm pH 3-10 IPG strip (GE Healthcare) with a 3100 OFFGEL fractionator (Agilent) as previously described⁴⁶.

The setup of the μ RPLC-MS system was as described previously⁴⁷. Chromatographic separation of peptides was carried out using an EASY nano-LC 1000 system (Thermo Fisher Scientific), equipped with a heated RP-HPLC column (75 μ m x 50 cm) packed in-house with 1.9 μ m C18 resin (Reprosil-AQ Pur, Dr. Maisch). Mass spectrometry analysis was performed on a dual pressure LTQ-Elite Orbitrap mass spectrometer equipped with a nanoelectrospray ion source (both Thermo Fisher Scientific).

Using the MASCOT algorithm (Matrix Science, Version 2.4.0), the resulting mgf files were searched against a decoy database containing normal and reverse sequences of the predicted SwissProt entries of *Mus musculus* (www.ebi.ac.uk, release date 16/05/2012) and commonly observed contaminants (in total 33,832 sequences for *Mus musculus*) generated using the SequenceReverser tool from the MaxQuant software (Version 1.0.13.13). Next, database search results were imported to the Scaffold Q+ software (version 4.3.3, Proteome Software Inc., Portland, OR) and the protein false identification rate was set to 1% based on the number of decoy hits.

Protein probabilities were assigned by the Protein Prophet program⁴⁸. Acquired reporter ion intensities in the experiments were employed for automated quantification and statically analyzed using a modified version of our in-house developed SafeQuant R script⁴⁷. In brief, reporter ion intensities were corrected for isotopic impurities according to the manufacturer's instructions. Intensities for each peptide and protein ID were summed, globally normalized across all acquisition runs and employed for ratio calculation and statistical analysis. For complete mass spectrometry materials and methods, please refer to the supplementary information.

3.6.9. Oxygen consumption and ATP levels

Mitochondria were isolated from hippocampus as previously described⁴⁹. Oxygen consumption rate was measured in isolated mitochondria from cortex and hippocampus using a Seahorse Bioscience XF24Analyzer. ATP content from isolated mitochondria was determined by a bioluminescence assay (VialightTM HT; Cambrex Bio Science).

3.7. Acknowledgements

The authors would like to thank M. Rüegg (Biozentrum, University of Basel) for helpful scientific discussions and advice, C. Lautenschlager, M. Bänziger, S. Ipsen (all Institute of Pathology, Basel University) and M. Dürrenberger (Microscopy Center Biozentrum, University of Basel) for their expert help with experimental procedures. MitoQ was kindly provided by M. Murphy (MRC, Cambridge UK), pPGK-Cre was a kind gift from T. Langer (Cologne).

This work was supported by Swiss National Science Foundation grant 31003A_127308, the Novartis Foundation for Medical-Biological Research, the Desirée and Nils Yde Foundation (420-14) and the Nora van Meeuwen-Haefliger Foundation (to S.F.), a grant from the Forschungsfonds of Basel University (to B.O.), and Telethon Italy GGP12162, GPP10005, AIRC Italy, ERC ERMITO, FP7 CIG CristOpa, MIUR FIRB Automed (to L.S.).

3.7.1. Authors' Contributions

B.O., J.M.S., L.M.R., M.L., C.S., K.S., A.G., and L.M. performed experiments. J.B., A.S., J.H., A.E., P. D`A., P.F., and M.T. analyzed and interpreted experimental data. N.I. and K.M. provided reagents. L.S. and S.F. conceived the project, coordinated and supervised research. B.O., L.M.R., L.S. and S.F. wrote the manuscript.

3.8. References

1. Nunnari J, Suomalainen A. Mitochondria: In Sickness and in Health. *Cell* 2012; **148**: 1145–1159.
2. Sheng Z-H. Mitochondrial trafficking and anchoring in neurons: New insight and implications. *J Cell Biol* 2014; **204**: 1087–1098.
3. McLelland G-L, Soubannier V, Chen CX, McBride HM, Fon EA. Parkin and PINK1 function in a vesicular trafficking pathway regulating mitochondrial quality control. *EMBO J* 2014; **33**: 282–295.
4. Twig G, Elorza A, Molina AJ, Mohamed H, Wikstrom JD, Walzer G *et al*. Fission and selective fusion govern mitochondrial segregation and elimination by autophagy. *Embo J* 2008; **27**: 433–46.
5. Chen H, Chomyn A, Chan DC. Disruption of Fusion Results in Mitochondrial Heterogeneity and Dysfunction. *J Biol Chem* 2005; **280**: 26185–26192.
6. Blik AM van der, Shen Q, Kawajiri S. Mechanisms of Mitochondrial Fission and Fusion. *Cold Spring Harb Perspect Biol* 2013; **5**: a011072.

7. Koshiba T, Detmer SA, Kaiser JT, Chen H, McCaffery JM, Chan DC. Structural Basis of Mitochondrial Tethering by Mitofusin Complexes. *Science* 2004; **305**: 858–862.
8. Cipolat S, de Brito OM, Dal Zilio B, Scorrano L. OPA1 requires mitofusin 1 to promote mitochondrial fusion. *Proc Natl Acad Sci U S A* 2004; **101**: 15927–15932.
9. De Brito OM, Scorrano L. Mitofusin 2 tethers endoplasmic reticulum to mitochondria. *Nature* 2008; **456**: 605–610.
10. Cereghetti GM, Stangherlin A, Martins de Brito O, Chang CR, Blackstone C, Bernardi P *et al.* Dephosphorylation by calcineurin regulates translocation of Drp1 to mitochondria. *Proc Natl Acad Sci U S A* 2008; **105**: 15803–8.
11. Otera H, Wang C, Cleland MM, Setoguchi K, Yokota S, Youle RJ *et al.* Mff is an essential factor for mitochondrial recruitment of Drp1 during mitochondrial fission in mammalian cells. *J Cell Biol* 2010; **191**: 1141–58.
12. Friedman JR, Lackner LL, West M, DiBenedetto JR, Nunnari J, Voeltz GK. ER tubules mark sites of mitochondrial division. *Science* 2011; **334**: 358–62.
13. Bui HT, Shaw JM. Dynamin Assembly Strategies and Adaptor Proteins in Mitochondrial Fission. *Curr Biol* 2013; **23**: R891–R899.
14. Waterham HR, Koster J, van Roermund CW, Mooyer PA, Wanders RJ, Leonard JV. A lethal defect of mitochondrial and peroxisomal fission. *N Engl J Med* 2007; **356**: 1736–41.
15. Ishihara N, Nomura M, Jofuku A, Kato H, Suzuki SO, Masuda K *et al.* Mitochondrial fission factor Drp1 is essential for embryonic development and synapse formation in mice. *Nat Cell Biol* 2009; **11**: 958–66.

16. Wakabayashi J, Zhang Z, Wakabayashi N, Tamura Y, Fukaya M, Kensler TW *et al.* The dynamin-related GTPase Drp1 is required for embryonic and brain development in mice. *J Cell Biol* 2009; **186**: 805–16.
17. Barsoum MJ, Yuan H, Gerencser AA, Liot G, Kushnareva Y, Graber S *et al.* Nitric oxide-induced mitochondrial fission is regulated by dynamin-related GTPases in neurons. *Embo J* 2006; **25**: 3900–11.
18. Cheung EC, McBride HM, Slack RS. Mitochondrial dynamics in the regulation of neuronal cell death. *Apoptosis* 2007; **12**: 979–92.
19. Costa V, Giacomello M, Hudec R, Lopreiato R, Ermak G, Lim D *et al.* Mitochondrial fission and cristae disruption increase the response of cell models of Huntington's disease to apoptotic stimuli. *EMBO Mol Med* 2010; **2**: 490–503.
20. Dagda RK, Merrill RA, Cribbs JT, Chen Y, Hell JW, Usachev YM *et al.* The spinocerebellar ataxia 12 gene product and protein phosphatase 2A regulatory subunit Bbeta2 antagonizes neuronal survival by promoting mitochondrial fission. *J Biol Chem* 2008; **283**: 36241–8.
21. Meuer K, Suppanz IE, Lingor P, Planchamp V, Goricke B, Fichtner L *et al.* Cyclin-dependent kinase 5 is an upstream regulator of mitochondrial fission during neuronal apoptosis. *Cell Death Differ* 2007; **14**: 651–61.
22. Tian C, Murrin LC, Zheng JC. Mitochondrial fragmentation is involved in methamphetamine-induced cell death in rat hippocampal neural progenitor cells. *PLoS ONE* 2009; **4**: e5546.
23. Young KW, Pinon LG, Bampton ET, Nicotera P. Different pathways lead to mitochondrial fragmentation during apoptotic and excitotoxic cell death in primary neurons. *J Biochem Mol Toxicol* 2010; **24**: 335–41.

24. Yuan H, Gerencser AA, Liot G, Lipton SA, Ellisman M, Perkins GA *et al.* Mitochondrial fission is an upstream and required event for bax foci formation in response to nitric oxide in cortical neurons. *Cell Death Differ* 2007; **14**: 462–71.
25. Lee YJ, Jeong SY, Karbowski M, Smith CL, Youle RJ. Roles of the mammalian mitochondrial fission and fusion mediators Fis1, Drp1, and Opa1 in apoptosis. *Mol Biol Cell* 2004; **15**: 5001–11.
26. Uo T, Dworzak J, Kinoshita C, Inman DM, Kinoshita Y, Horner PJ *et al.* Drp1 levels constitutively regulate mitochondrial dynamics and cell survival in cortical neurons. *Exp Neurol* 2009; **218**: 274–85.
27. Wang X, Su B, Lee HG, Li X, Perry G, Smith MA *et al.* Impaired balance of mitochondrial fission and fusion in Alzheimer's disease. *J Neurosci* 2009; **29**: 9090–103.
28. Oettinghaus B, Licci M, Scorrano L, Frank S. Less than perfect divorces: dysregulated mitochondrial fission and neurodegeneration. *Acta Neuropathol* 2012; **123**: 189–203.
29. Kageyama Y, Zhang Z, Roda R, Fukaya M, Wakabayashi J, Wakabayashi N *et al.* Mitochondrial division ensures the survival of postmitotic neurons by suppressing oxidative damage. *J Cell Biol* 2012; **197**: 535–551.
30. Grohm J, Kim S-W, Mamrak U, Tobaben S, Cassidy-Stone A, Nunnari J *et al.* Inhibition of Drp1 provides neuroprotection in vitro and in vivo. *Cell Death Differ* 2012; **19**: 1446–1458.
31. Park SW, Kim KY, Lindsey JD, Dai Y, Heo H, Nguyen DH *et al.* A selective inhibitor of drp1, mdivi-1, increases retinal ganglion cell survival in acute ischemic mouse retina. *Invest Ophthalmol Vis Sci* 2011; **52**: 2837–43.

32. Zhang N, Wang S, Li Y, Che L, Zhao Q. A selective inhibitor of Drp1, mdivi-1, acts against cerebral ischemia/reperfusion injury via an anti-apoptotic pathway in rats. *Neurosci Lett* 2013; **535**: 104–109.
33. Erdmann G, Schutz G, Berger S. Inducible gene inactivation in neurons of the adult mouse forebrain. *BMC Neurosci* 2007; **8**: 63.
34. Verstreken P, Ly CV, Venken KJ, Koh TW, Zhou Y, Bellen HJ. Synaptic mitochondria are critical for mobilization of reserve pool vesicles at *Drosophila* neuromuscular junctions. *Neuron* 2005; **47**: 365–78.
35. Kelso GF, Porteous CM, Coulter CV, Hughes G, Porteous WK, Ledgerwood EC *et al.* Selective Targeting of a Redox-active Ubiquinone to Mitochondria within Cells Antioxidant and antiapoptotic properties. *J Biol Chem* 2001; **276**: 4588–4596.
36. Li H, Alavian KN, Lazrove E, Mehta N, Jones A, Zhang P *et al.* A Bcl-xL–Drp1 complex regulates synaptic vesicle membrane dynamics during endocytosis. *Nat Cell Biol* 2013; **15**: 773–785.
37. Williams GSB, Boyman L, Chikando AC, Khairallah RJ, Lederer WJ. Mitochondrial calcium uptake. *Proc Natl Acad Sci U S A* 2013; **110**: 10479–10486.
38. Mizushima N, Yamamoto A, Matsui M, Yoshimori T, Ohsumi Y. In Vivo Analysis of Autophagy in Response to Nutrient Starvation Using Transgenic Mice Expressing a Fluorescent Autophagosome Marker. *Mol Biol Cell* 2004; **15**: 1101–1111.
39. Kern JK, Jones AM. Evidence of Toxicity, Oxidative Stress, and Neuronal Insult in Autism. *J Toxicol Environ Health Part B* 2006; **9**: 485–499.

40. Sudarov A, Joyner AL. Cerebellum morphogenesis: the foliation pattern is orchestrated by multi-cellular anchoring centers. *Neural Develop* 2007; **2**: 26.
41. Berthet A, Margolis EB, Zhang J, Hsieh I, Zhang, J, Hnasko T *et al.* Loss of Mitochondrial Fission Depletes Axonal Mitochondria in Midbrain Dopamine Neurons. *J Neurosci* 2014.
42. Ippolito DM, Eroglu C. Quantifying Synapses: an Immunocytochemistry-based Assay to Quantify Synapse Number. *J Vis Exp* 2010. doi:10.3791/2270.
43. Preibisch S, Saalfeld S, Tomancak P. Globally optimal stitching of tiled 3D microscopic image acquisitions. *Bioinformatics* 2009; **25**: 1463–1465.
44. Ragozzino ME, Unick KE, Gold PE. Hippocampal acetylcholine release during memory testing in rats: augmentation by glucose. *Proc Natl Acad Sci U S A* 1996; **93**: 4693–4698.
45. Abramov AY, Scorziello A, Duchen MR. Three Distinct Mechanisms Generate Oxygen Free Radicals in Neurons and Contribute to Cell Death during Anoxia and Reoxygenation. *J Neurosci* 2007; **27**: 1129–1138.
46. Beck M, Schmidt A, Malmstroem J, Claassen M, Ori A, Szymborska A *et al.* The quantitative proteome of a human cell line. *Mol Syst Biol* 2011; **7**: 549.
47. Glatter T, Ludwig C, Ahrné E, Aebersold R, Heck AJR, Schmidt A. Large-Scale Quantitative Assessment of Different In-Solution Protein Digestion Protocols Reveals Superior Cleavage Efficiency of Tandem Lys-C/Trypsin Proteolysis over Trypsin Digestion. *J Proteome Res* 2012; **11**: 5145–5156.
48. Nesvizhskii AI, Keller A, Kolker E, Aebersold R. A statistical model for identifying proteins by tandem mass spectrometry. *Anal Chem* 2003; **75**: 4646–4658.

49. Rhein V, Song X, Wiesner A, Ittner LM, Baysang G, Meier F *et al.* Amyloid- β and tau synergistically impair the oxidative phosphorylation system in triple transgenic Alzheimer's disease mice. *Proc Natl Acad Sci* 2009; **106**: 20057–20062.

3.9. Figure legends

Fig. 3.1 Drp1 ablation in postmitotic forebrain neurons.

(A) $Drp1^{flx/flx}$ and $Drp1^{flx/flx} CaMKII\alpha CreERT2^{-/+}$ mice were crossed, resulting in a Mendelian distribution of alleles. At 8 weeks of age animals were injected with tamoxifen for 5 consecutive days to induce recombination of the floxed *Drp1* locus.

(B) Mice of the indicated genotype were sacrificed at indicated time points after tamoxifen injection. Hippocampal lysates were separated by SDS-PAGE and immunoblotted using indicated antibodies.

(C) Immunohistochemical staining (NovaRED, counterstain Hematoxyllin) for Drp1 was performed on hippocampal CA1 FFPE tissue sections of $Drp1^{i\Delta b/i\Delta b}$ mice 4 weeks p.t.i.. Arrows indicate unstained hippocampal dendrites. Scale bar 5 μ m.

Fig. 3.2 Mitochondrial morphology in primary neuronal cultures after Drp1 ablation.

(A) Primary cortical neurons isolated from $Drp1^{flx/flx}$ E17 embryos were co-electroporated with mYFP- and Cre-expression constructs prior to seeding. Images were taken at the indicated time points of differentiation.

Fig. 3.3 Mitochondrial morphology in the hippocampus after Drp1 ablation.

Mice of the indicated genotype were killed at indicated times after tamoxifen injection. Coronal sections of FFPE brains of $Drp1^{i\Delta b/i\Delta b}$ and control mice were immunostained for cytochrome c oxidase subunit 1. Images show CA1 and CA3 pyramidal neurons and dentate gyrus. (DG) granule cells. Scale bar 10 μ m.

Fig. 3.4 Electrophysiological properties are not affected in Drp1-ablated neurons.

- (A)** Acute hippocampal slices of Drp1^{iΔb/iΔb} 4 weeks p.t.i. and control animals were prepared. CA1 pyramidal neurons were patch-clamped and infused with biocytin, which was revealed by immunofluorescence. Scale bar 40 μm. Note the regular dendritic morphology.
- (B-D)** One-second-long current steps of increasing amplitude were injected to induce action potentials in Drp1^{iΔb/iΔb} 4 weeks p.t.i. and control CA1 pyramidal neurons; maximal amplitude and half width were plotted. Data represent average ±SEM of at least 7 neurons.
- (E)** Resting membrane potential of Drp1^{iΔb/iΔb} 4 weeks p.t.i. and control CA1 pyramidal neurons. Data represent average ±SEM of at least 7 neurons.

Fig. 3.5 Impaired synaptic transmission in Drp1-ablated neurons.

- (A)** Representative field excitatory postsynaptic potentials (fEPSP) before and after 10s of 10Hz stimulation. fEPSPs were recorded in the CA1 stratum radiatum in Drp1^{iΔb/iΔb} and control hippocampal slice cultures upon Schaffer collateral stimulation.
- (B)** Mean slope of fEPSPs during the time course of a 10s 10Hz stimulation was plotted. Data represent average ±SEM of at least 6 neurons.
- (C)** Maximal mean fEPSP slope after 10s 10Hz stimulation. Data represent average ±SEM of at least 6 neurons.
- (D)** Drp1^{iΔb/iΔb} 4 weeks p.t.i. and control animals were placed in an 8-arm radial maze which they were left to systematically explore. Correct alternation of arm visits was scored. Data represent average ±SEM of at least 6 animals.
- (E)** Oxygen consumption rate of isolated hippocampal mitochondria of Drp1^{iΔb/iΔb} and control mice was measured with a Seahorse Bioscience XF24 Analyzer. Substances were injected at the indicated time points. Data represent average ±SEM of at least 4 animals whose hippocampi were pooled; measurements performed with at least 6 replicates.
- (F)** ATP content of isolated hippocampal mitochondria of Drp1^{iΔb/iΔb} and control mice as measured with a bioluminescence assay. Data represent average ±SEM of at least 4 animals whose hippocampi were pooled; measurements were performed with at least 8 replicates.
- (G)** Synapses in TEM images of Drp1^{iΔb/iΔb} 4 weeks p.t.i. and control hippocampi were screened for presynaptic mitochondria. Data represent average ±SEM of at least 4 animals of which at least 100 synapses each were screened. TEM image shows a representative

synaptic structure with a presynaptic mitochondrion (M), presynaptic vesicles (V) and a postsynaptic dense area (PSD). Scale bar 150 nm. Asterisks denote p-values of an unpaired, two-tailed Student's t-test: *:p<0.05

Fig. 3.6 Long-term Drp1 ablation causes hippocampal atrophy.

(A) Representative camera lucida drawings and Sholl analysis of Golgi-stained Drp1^{iΔb/iΔb} 10 weeks p.t.i. and control CA1 pyramidal neurons. Each data point represents number of intersections of the dendritic tree with concentric perisomatic rings of increasing diameter (exemplified by dashed circles). Data represent average ±SEM of at least 100 neurons.

(B) Hippocampal volume was recorded on H&E-stained, serial coronal cross sections of Drp1^{iΔb/iΔb} animals 8-weeks p.t.i. applying the Cavalieri principle. For cortical and midbrain volumes, only sections representing the coordinates bregma 1.1 mm – (-1.2 mm) were considered. Data represent average ±SEM of at least 5 animals.

(C) Number of spines visualized by Golgi staining per μm dendrite length (apical dendritic tree of CA1 pyramidal neurons). Data represent average ±SEM of at least 3 animals of which 1000 spines were counted.

(D) Coronal cross sections of Drp1^{iΔb/iΔb} 10 weeks p.t.i. and control brains co-stained with presynaptic VGLUT2 (green) and postsynaptic marker PSD95 (red). A 150μm x 150μm x 5μm confocal image stack in the CA1 stratum radiatum was recorded and the number of overlapping puncta was determined. Data represent average ±SEM of at least 5 animals of which 4 stacks each were recorded. Scale bar 5 μm. Asterisks denote p-values of an unpaired, two-tailed Student's t-test: *:p<0.05

Fig. 3.7 Drp1 ablation does not lead to hippocampal neurodegeneration.

(A) H&E-staining of coronal cross sections of FFPE ^{Δb/iΔb} 10 weeks p.t.i. and control brains showing the hippocampus and a magnification of the CA1 region. Scale bars 1 mm (left) and 50 μm (right).

(B) Neuronal nuclei in the CA1 region were quantified manually. Data represent average ±SEM of at least 5 animals of which at least 200 nuclei each were counted.

(C) *In situ* TUNEL of coronal cross sections of frozen Drp1^{iΔb/iΔb} 10 weeks p.t.i. and control brains showing hippocampus. Positive control was preincubated with DNase I; negative control incubated without terminal deoxynucleotidyl transferase. Scale bar 1 mm.

(D) Neuronal nuclei in the CA1 region were quantified over a 250 μm length. Data represent average ±SEM of at least 5 animals.

Fig. 3.8 The antioxidant mitoQ ameliorates mitochondrial morphology in Drp1-deficient CA1 and DG hippocampal neurons.

(A+B) Oxidative stress levels represented by DHR and MitoSox fluorescence in cortical and hippocampal tissue homogenates of Drp1^{iΔb/iΔb} 4 weeks p.t.i. and control mice. Data represent average ±SEM of at least 4 animals (tissue pooled) and measurements were performed with a minimum of 4 replicates.

(C) TBARS levels, reflecting lipid peroxidation, in Drp1^{iΔb/iΔb} 4 weeks p.t.i. and control cortical and hippocampal lysates measured by colorimetric assay. Data represent average ±SEM of at least 6 animals.

(D) Ratio of oxidized to total glutathione in hippocampal lysates of Drp1^{iΔb/iΔb} 4 weeks p.t.i. and control mice measured by colorimetric assay. Data represent average ±SEM of at least 6 animals.

(E) Drp1^{iΔb/iΔb} animals treated or not with daily mitoQ injections of 20 mg/kg i.p. were sacrificed 10 days p.t.i. and coronal cross sections of FFPE brains immunostained for cytochrome c oxidase subunit 1. Mitobulbs of randomly selected areas within the indicated hippocampal subregions were quantified. Scale bar 10 μm. Data represent average ±SEM of at least 4 animals. Asterisks denote p-values of an unpaired, two-tailed Student's t-test. *: p<0.05

Supplementary Fig.1

(A-C) CamK2 CreERT2 mice were crossed with a GFP reporter strain. Following tamoxifen injections at 8 weeks of age, coronal cross sections of FFPE brains were immunostained for

GFP (red) and incubated with DAPI (blue). Magnification of the hippocampal CA1(A); CA3(B) and DG (C) region. Scale bar 50 μ m.

(D) Field excitatory postsynaptic potentials (fEPSPs) were recorded in the CA1 stratum radiatum in 4-week-Drp1-ablated and control hippocampal slice cultures after Schaffer collateral stimulation. Mean slope of fEPSPs during the time course of a 100Hz stimulation. Data represent average \pm SEM of at least 6 neurons.

(E) Maximal mean fEPSP slope after 100 Hz stimulation. Data represent average \pm SEM of at least 6 neurons.

(F) Visual performance of 4-week-Drp1-ablated and control mice was tested in the Morris Walter tank with a visible platform. Data represent average \pm SEM of at least 6 animals.

(G) Olfaction of 4-week-Drp1-ablated and control mice was tested using the cookie finding test. The time required to find a cookie hidden inside the mouse`s cage was measured. Data represent average \pm SEM of at least 6 animals.

(H) Cortical and midbrain volumes were recorded on H&E-stained, serial coronal cross sections of 8-week-Drp1-ablated animals applying the Cavalieri principle. Only sections representing the coordinates bregma 1.1 mm – (-1.2 mm) were considered. Data represent average \pm SEM of at least 5 animals.

Supplementary Fig.2

(A) Intraneuronal autophagosome-like structures in TEM images of hippocampal neurons of *Drp1*^{iΔb/iΔb} mice at 4 weeks p.t.i. were quantified. Data represent average ±SEM of at least 4 animals of which at least 100 neurons each were screened. Representative examples are shown. Scale bar 500 nm

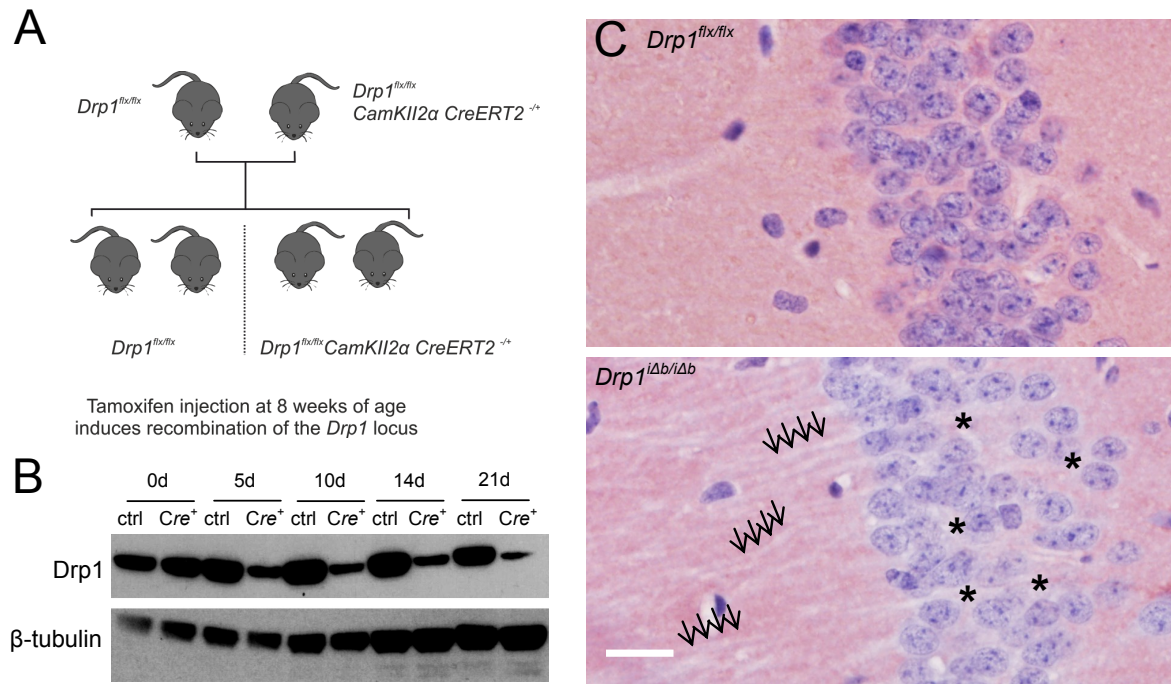


Figure 1, Oettinghaus et al.
Revised ms CDD-14-1068R

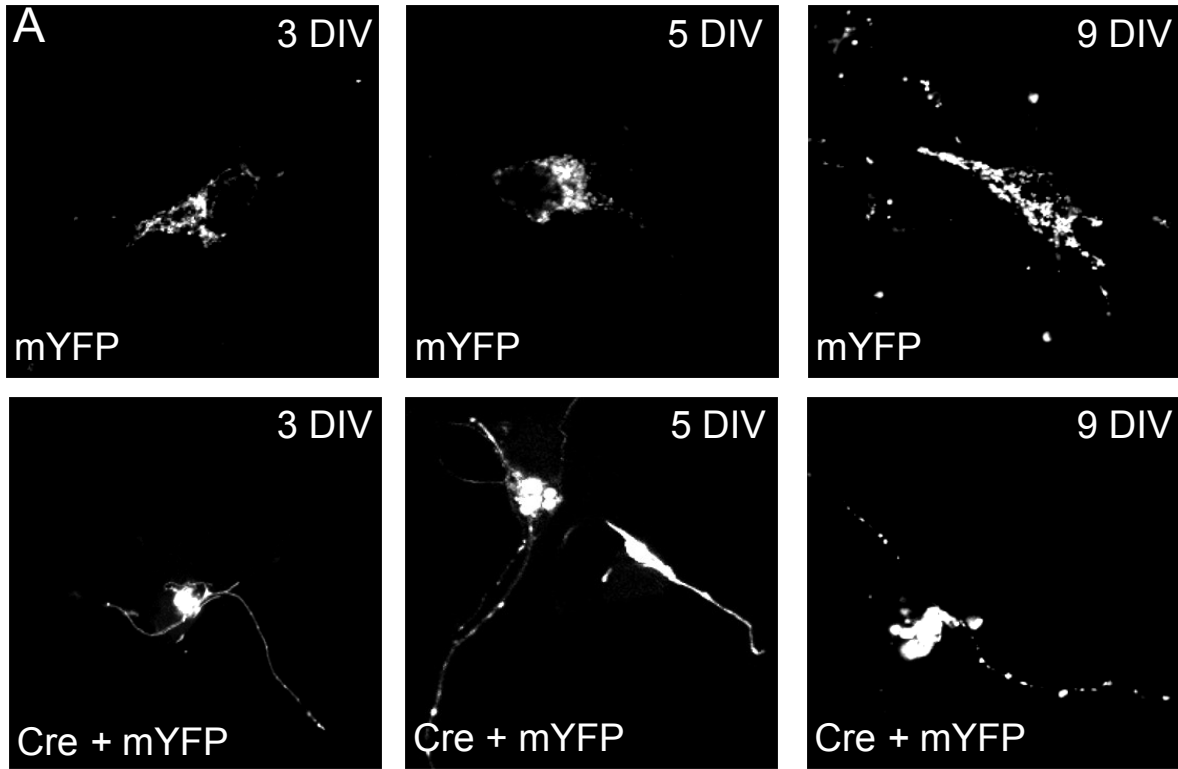


Figure 2, Oettinghaus et al.
Revised ms CDD-14-1068R

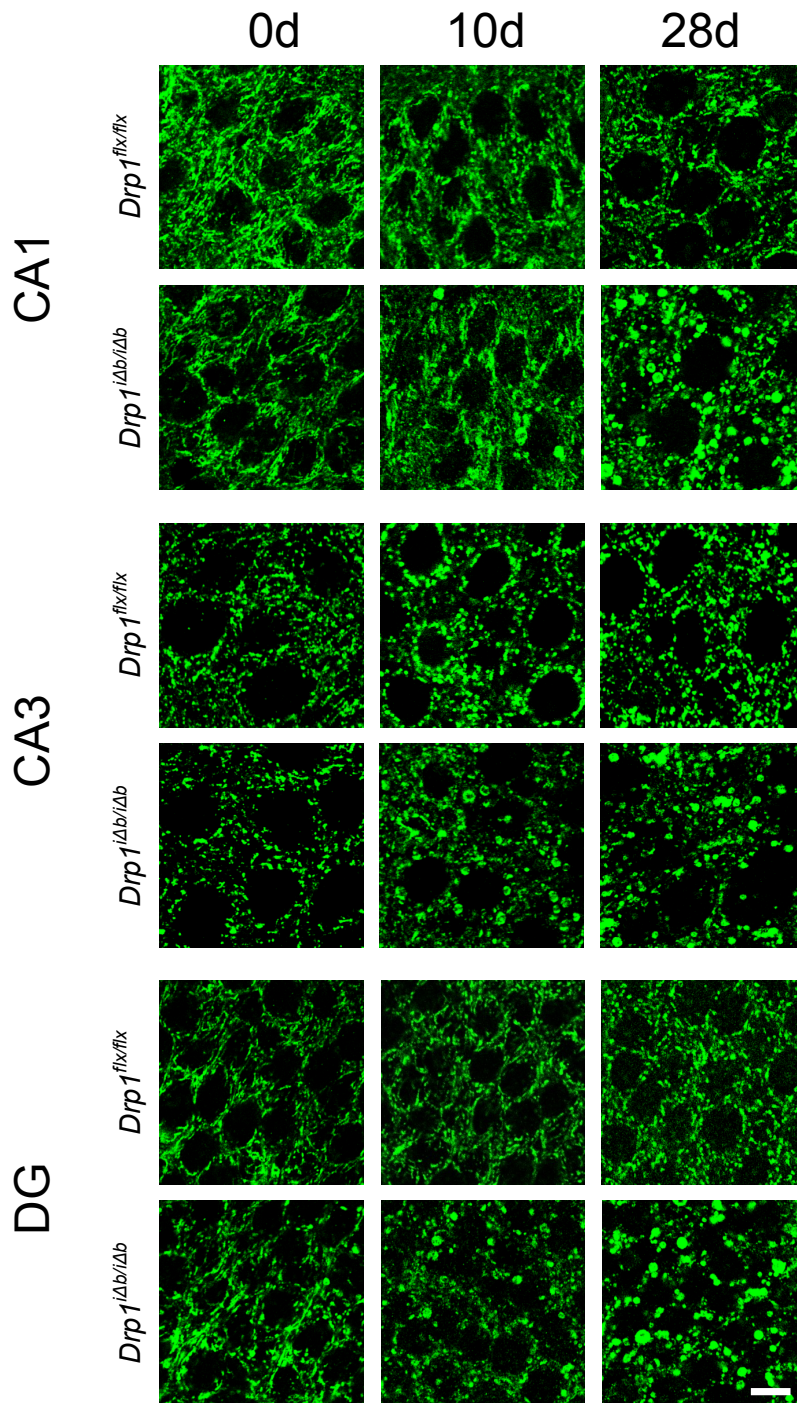


Figure 3, Oettinghaus et al.
Revised ms CDD-14-1068R

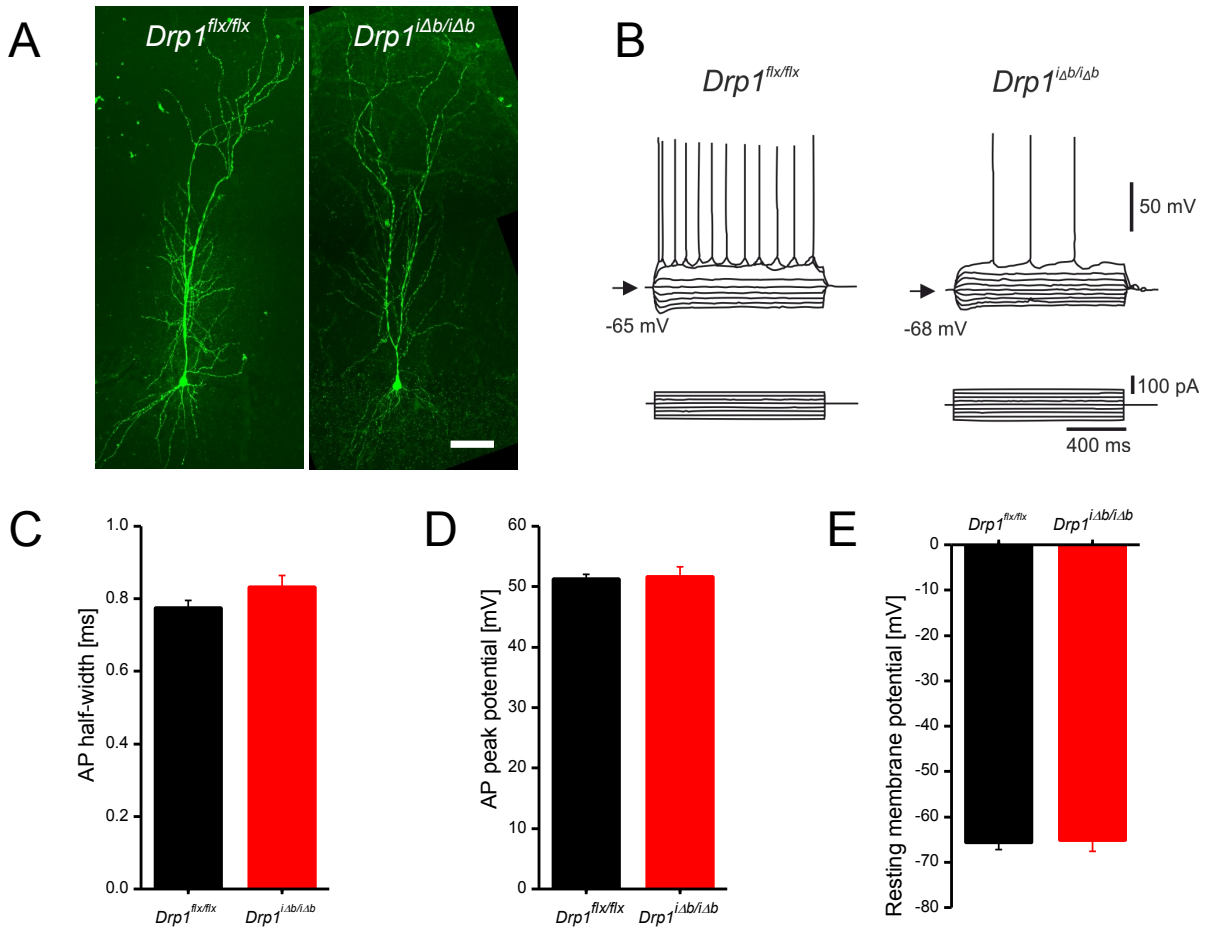


Figure 4, Oettinghaus et al.
Revised ms CDD-14-1068R

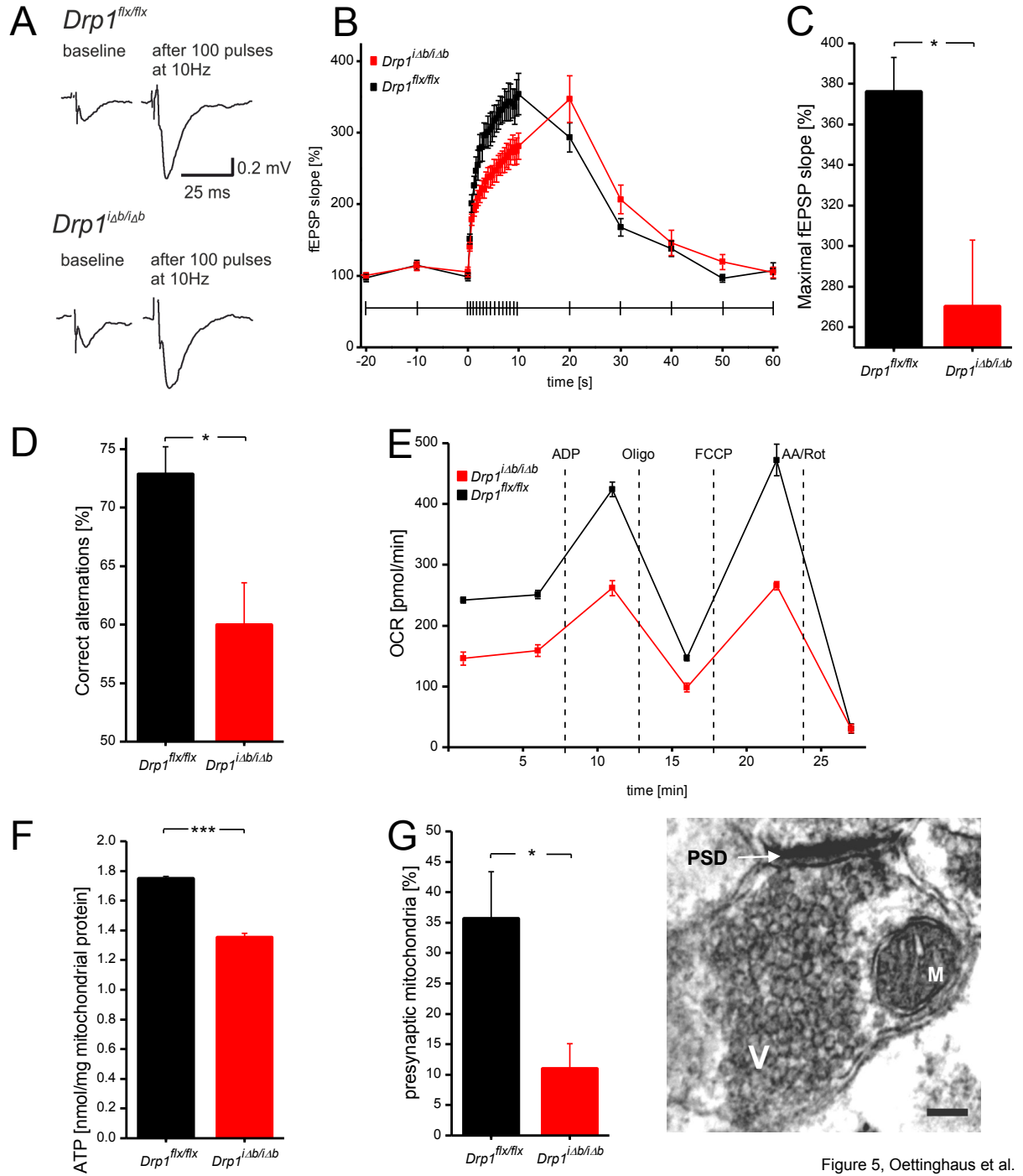


Figure 5, Oettinghaus et al.
 Revised ms CDD-14-1068R

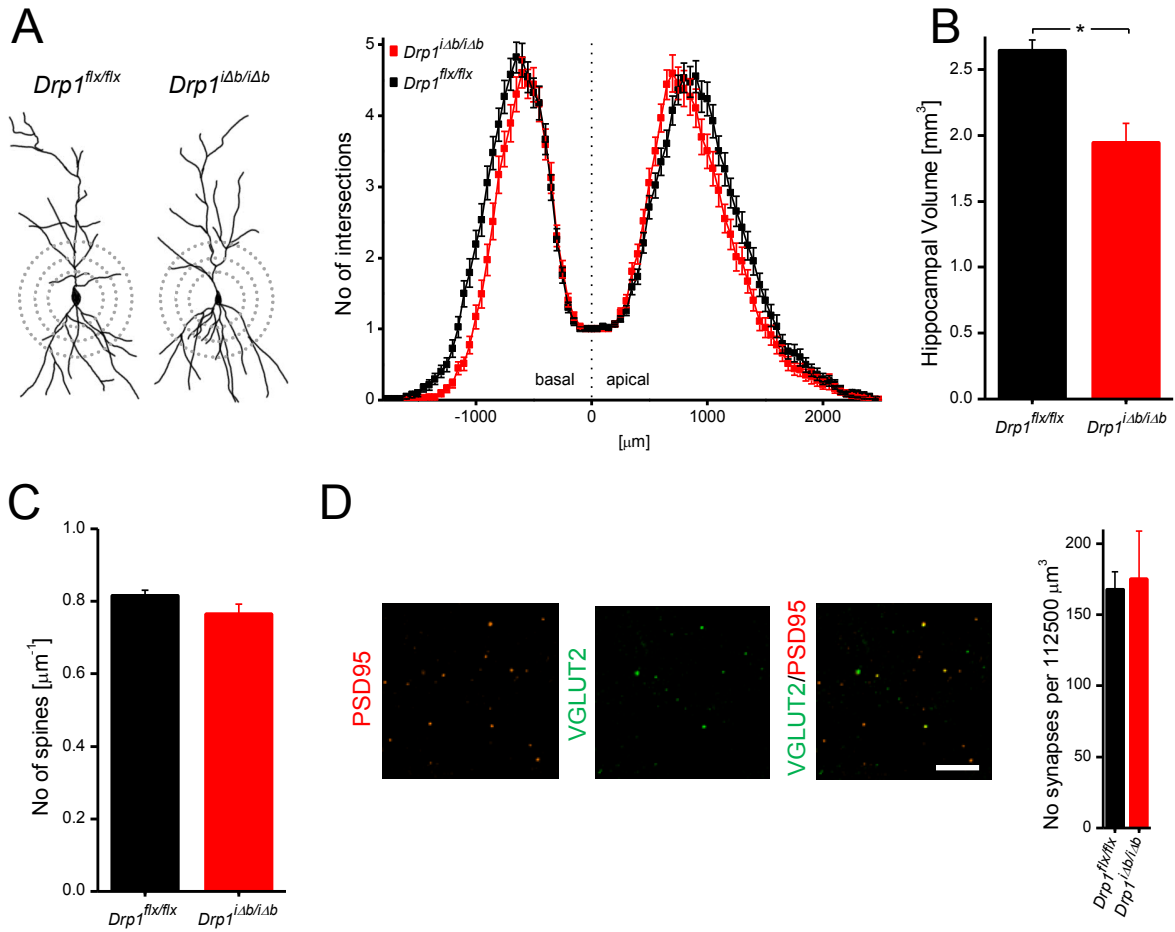


Figure 6, Oettinghaus et al.
Revised ms CDD-14-1068R

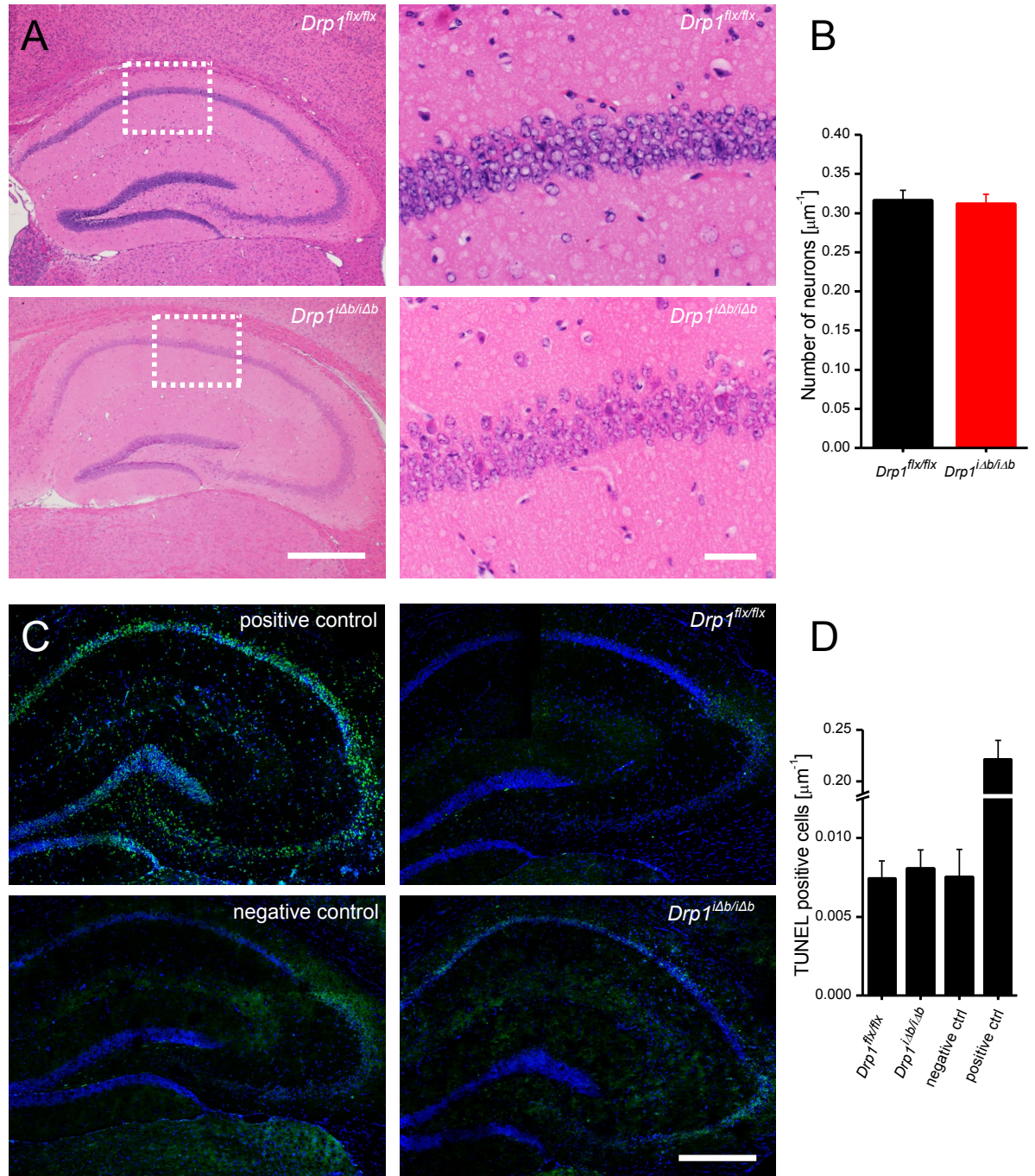


Figure 7. Oettinghaus et al.
Revised ms CDD-14-1068R

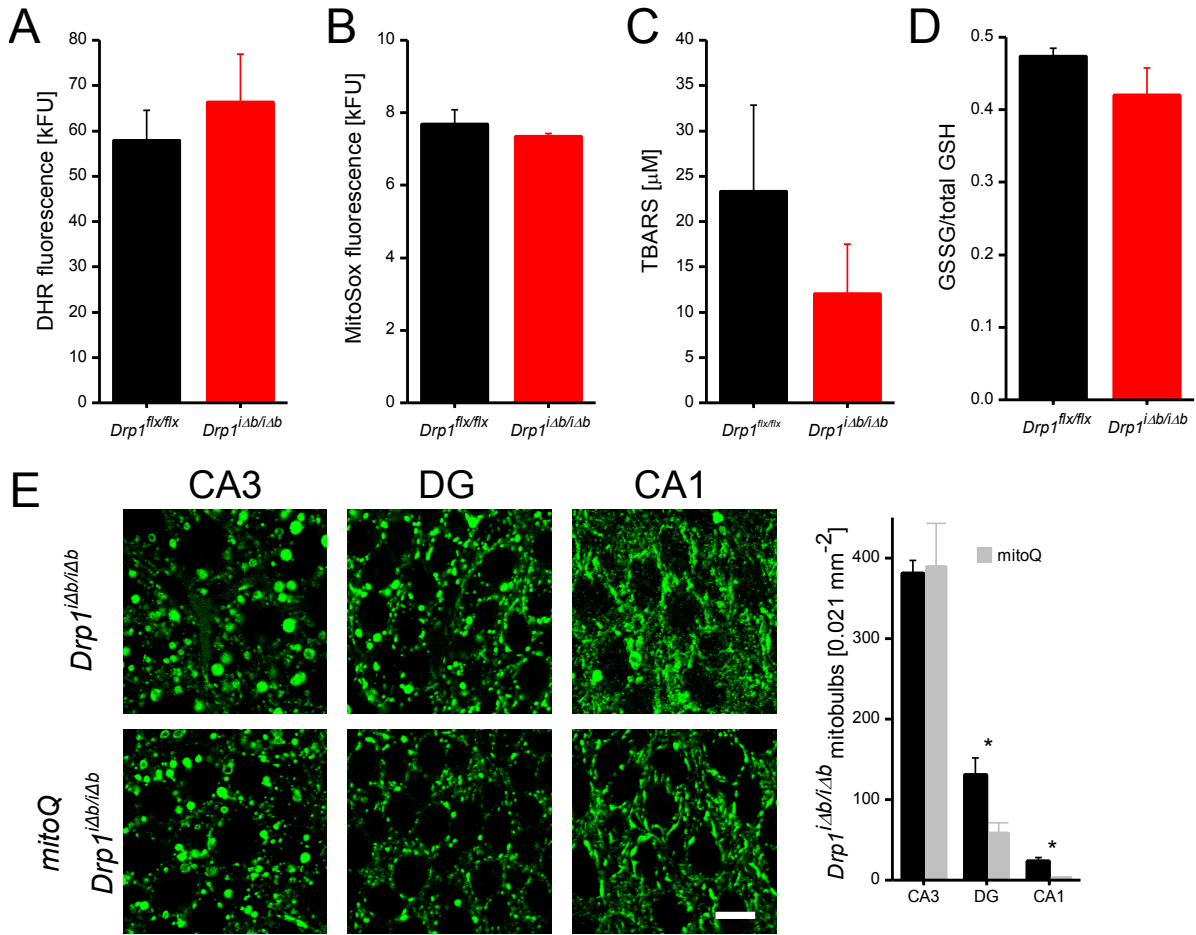
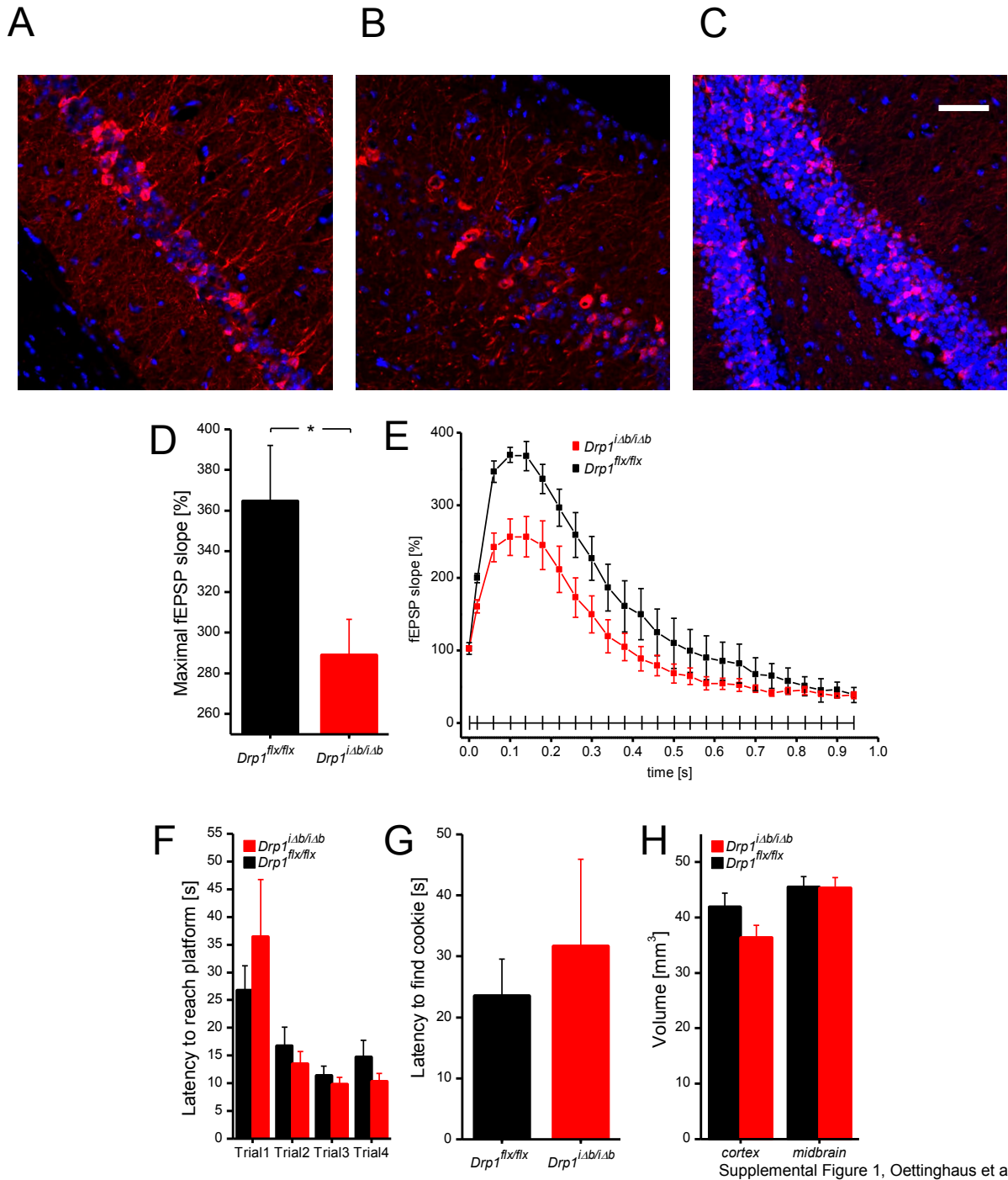
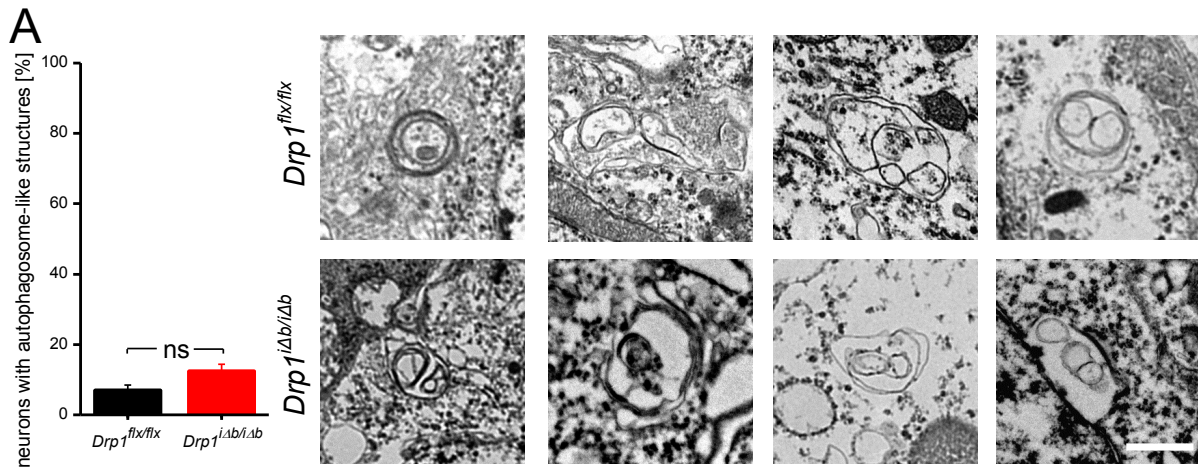


Figure 8, Oettinghaus et al.
Revised ms CDD-14-1068R



Supplemental Figure 1, Oettinghaus et al.
Revised ms CDD-14-1068R



Supplemental Figure 2, Oettinghaus et al.
 Revised ms CDD-14-1068R

Table S1 Levels of glycolytic proteins

Protein	Gene	FC	Q-Value
Fructose-bisphosphate aldolase A	Aldoa	0.55	0.0084 *
Brain protein 44 (mitochondrial pyruvate carrier)	Brp44	0.71	0.0344 *
Phosphoglycerate mutase 1	Pgam1	0.80	0.0468 *
L-lactate dehydrogenase A chain	Ldha	0.81	0.1861
Triosephosphate isomerase	Tpi1 PE	0.82	0.1000
6-phosphofructokinase, liver type	Pfkl	0.85	0.2662
Phosphoglycerate kinase 1	Pgk1	0.85	0.3055
6-phosphofructokinase type C	Pfkp	0.89	0.2499
Glucose-6-phosphate isomerase	Gpi	0.89	0.2568
Alpha-enolase	Eno1	0.91	0.2470
Glyceraldehyde-3-phosphate dehydrogenase	Gapdh	0.99	0.8268
Pyruvate kinase isozymes M1/M2	Pkm2	1.00	0.7776
L-lactate dehydrogenase B chain	Ldhb	1.04	0.7919
Solute carrier family 2, facilitated glucose transporter member 3	Slc2a3	1.08	0.2199
Enolase-phosphatase E1	Enoph1	1.10	0.4551
6-phosphofructokinase, muscle type	Pfkm	1.10	0.6907
Bisphosphoglycerate mutase	Bpgm	1.12	0.9618
Gamma-enolase	Eno2	1.17	0.3132
Phosphoglycerate mutase 2	Pgam2	1.21	0.5752
Glucose transporter 1 (GLUT1)	Slc2a1	1.37	0.0439 *
Hexokinase-1	Hk1	4.37	0.0016 *

Fold change (FC) value describes *Drp1^{flx/flx} Cre⁺* vs *Drp1^{flx/flx}* protein levels in mixed cortical /hippocampal homogenates analyzed by quantitative mass spectrometry. Q<0.05:*

Table S2 Levels of autophagy related proteins in Drp1 ablated brain homogenates

Protein	Gene	FC	Q-Value
Cysteine protease ATG4C	Atg4c	0.60	0.0966
Ragulator complex protein LAMTOR3	Lamtor3	0.83	0.5414
Rapamycin-insensitive companion of mTOR	Rictor	0.86	0.0617
Autophagy-related protein 9A	Atg9a	0.87	0.1119
Hamartin	Tsc1	0.93	0.8762
Autophagy-related protein 2 homolog A	Atg2a	0.94	0.2891
Tuberin	Tsc2	0.97	0.8646
Autophagy-related protein	Atg13	1.03	0.5822
Sequestosome / p62	Sqstm1	1.04	0.8268
Cysteine protease ATG4B	Atg4b	1.07	0.4169
Serine/threonine-protein kinase mTOR	Mtor	1.08	0.3113
Ubiquitin-like modifier-activating enzyme ATG7	Atg7	1.09	0.3400
Autophagy-related protein 2 homolog B	Atg2b	1.09	0.4264
Microtubule-associated proteins 1A/1B light chain 3A	Map1lc3a	1.09	0.1735
GTP-binding protein Rheb	Rheb	1.11	0.5684
Microtubule-associated proteins 1A/1B light chain 3B	Map1lc3b	1.12	0.2273
Regulatory-associated protein of mTOR	Rptor	1.13	0.3207
Ubiquitin-like-conjugating enzyme ATG3	Atg3	1.16	0.0729
Beclin-1	Becn1	1.17	0.0741
Ubiquitin-like protein ATG12	Atg12	1.20	0.1165
Autophagy-related protein 16-1	Atg16l1	1.23	0.0892
Autophagy protein 5	Atg5	1.33	0.0117 *

Fold change (FC) value describes $Drp1^{flx/flx} Cre^+$ vs $Drp1^{flx/flx}$ protein levels in mixed cortical /hippocampal homogenates analyzed by quantitative mass spectrometry. Q<0.05:*

Table S3 Levels of oxidative stress related proteins in Drp1 ablated brain homogenates

Protein	Gene	FC	Q-Value
Kelch-like ECH-associated protein 1	Keap1	0.38	0.0023 ***
Thioredoxin, mitochondrial	Txn2	0.67	0.0134 *
Thioredoxin-dependent peroxide reductase, mitochondrial	Prdx3	0.77	0.0297 *
Thioredoxin	Txn	0.77	0.0286 *
Thioredoxin reductase 2, mitochondrial	Txnrd2	0.77	0.0964
Multidrug resistance-associated protein 1	Abcc1	0.80	0.5612
Microsomal glutathione S-transferase 3	Mgst3	0.80	0.6265
6-phosphogluconate dehydrogenase, decarboxylating	Pgd	0.84	0.0531
Sulfiredoxin-1	Srxn1	0.85	0.1128
Phospholipid hydroperoxide glutathione peroxidase, mitochondrial	Gpx4	0.85	0.1769
Flavin reductase (NADPH)	Blvrb	0.86	0.3307
Superoxide dismutase [Mn], mitochondrial	Sod2	0.94	0.5272
Glutathione S-transferase A2	Gsta2	0.94	0.2818
UTP--glucose-1-phosphate uridylyltransferase	Ugp2	0.98	0.9543
Thioredoxin reductase 1, cytoplasmic	Txnrd1	0.99	0.9485
Thioredoxin reductase 1, cytoplasmic	Txnrd1	0.99	0.9485
Peroxiredoxin-2	Prdx2	0.99	0.5531
Heme oxygenase 2	Hmox2	1.01	0.7210
Sequestosome-1	Sqstm1	1.04	0.8268
Glutathione S-transferase A4	Gsta4	1.04	0.4437
4-trimethylaminobutyraldehyde dehydrogenase	Aldh9a1	1.07	0.3152
Peroxiredoxin-1	Prdx1	1.10	0.5576
Glutathione synthetase	Gss	1.11	0.1446
Glutamate--cysteine ligase regulatory subunit	Gclm	1.12	0.1312
Glutathione peroxidase 1	Gpx1	1.12	0.6620
Retinal dehydrogenase 1	Aldh1a1	1.12	0.2235
Glutathione reductase, mitochondrial	Gsr	1.13	0.5022
Transketolase	Tkt	1.14	0.1258
Glutathione S-transferase P 1	Gstp1	1.14	0.2150
NAD(P)H dehydrogenase [quinone] 1	Nqo1	1.15	0.1912
Pirin	Pir	1.16	0.3966
Superoxide dismutase [Cu-Zn]	Sod1	1.18	0.1725
Glucose-6-phosphate 1-dehydrogenase X	G6pdx	1.21	0.0806
Glutathione S-transferase kappa 1	Gstk1	1.26	0.0532
Fatty aldehyde dehydrogenase	Aldh3a2	1.27	0.0375 *
Catalase	Cat	1.29	0.0514
Glutathione S-transferase Mu 2	Gstm2	1.31	0.1557
Glutamate--cysteine ligase catalytic subunit	Gclc	1.32	0.0200 *
Glutathione S-transferase Mu 5	Gstm5	1.36	0.0139 *
Glutathione S-transferase theta-1	Gstt1	1.38	0.0724
Multidrug resistance protein 1A	Abcb1a	1.39	0.0216 *
Epoxide hydrolase 1	Ephx1	1.39	0.0081 **
Glutathione S-transferase Mu 7	Gstm7	1.40	0.0324 *
Beta-glucuronidase	Gusb	1.42	0.0552 *
Peroxiredoxin-4	Prdx4	1.44	0.0132 *
Ferritin heavy chain	Fth1	1.48	0.0409 *

Glutathione S-transferase omega-1	Gsto1	1.51	0.0067 **
Glutathione S-transferase Mu 1	Gstm1	2.00	0.0120 *

Fold change (FC) value describes $Drp1^{flx/flx} Cre^+$ vs $Drp1^{flx/flx}$ protein levels in mixed cortical /hippocampal homogenates analyzed by quantitative mass spectrometry. Bold print indicates target genes of Nrf2. Note that the Nrf2 inhibitor Keap1 is down regulated. Q<0.05:*; Q<0.01:**; Q<0.005:***

4. Experimental procedures

For mouse lines, Western blot analysis, electron microscopy, immunohistochemistry and proteomics please refer to the Materials and Methods paragraph in the Manuscript section (3.5).

4.1. Mouse lines

$Drp1^{flx/flx}$ $CaMK2\alpha::CreERT2$ have been described in Oettinghaus et al., 2016. $Fgf21^{flx/flx}$ mice were purchased from Jackson Labs (strain number 022361) and bred to $Drp1^{flx/flx}$ $CaMK2\alpha::CreERT2$ for at least two generations before experiments.

4.2. Mitochondrial membrane potential measurement

Mitochondria were isolated from freshly harvested hippocampus of $Drp1^{flx/flx}$ Cre^+ and control mice 4 weeks PTI, with the protocol described in Oettinghaus et al., 2016 (Manuscript section). Isolated mitochondria were loaded with TMRM and R123 fluorescent dyes for mitochondrial membrane potential according to manufacturers' instructions, then imaged on a VictorX5 multi-label plate reader (PerkinElmer).

4.3. Oxygraph measurements

Mitochondria were isolated from freshly-harvested hippocampi with a magnetic beads isolation kit (Miltenyi Biotec), according to manufacturer's instructions. 100 μ g of isolated mitochondria (as measured by total mitochondrial protein) were used.

The activity of the individual mitochondrial complexes was analyzed using an Oxygraph-2k high-resolution respirometer (Oroboros Instruments), as described in (Haegler et al., 2015).

Briefly, complexes I and III were analyzed using:

- L-glutamate/malate (10 and 5 mM, respectively) as substrates
- ADP (2 mM)
- Oligomycin (1 μ M) to inhibit complex V
- FCCP (carbonyl cyanide *p*-(trifluoromethoxyl)-phenyl-hydrazone, 10 μ M) to stimulate maximal electron transport chain activity
- Rotenone (0.5 μ M) as inhibitor of complex I
- Duroquinol (500 μ M) to reduce complex III

Complexes II and IV were analyzed using:

- Succinate (10 mM) as substrate in the presence of rotenone (0.5 μ M) to block complex I
- ADP (2 mM)
- Oligomycin (1 μ M) to inhibit complex V
- FCCP (carbonyl cyanide *p*-(trifluoromethoxyl)-phenyl-hydrazone, 10 μ M) to stimulate maximal electron transport chain activity
- Complex III inhibitor antimycin A (2.5 μ M)
- N,N,N',N'-tetramethyl-*p*-phenylenediamine (TMPD)/ascorbate (0.5 mM and 2 mM, respectively) to investigate complex IV activity
-

4.4. ER morphology evaluation

Morphological analysis of ER and mitochondria was performed using Fiji. Minimal mitochondrial radial diameter was calculated using a rotating calipers algorithm; roundness of the ER was calculated using the standard Fiji shape descriptors.

4.5. Metabolic Measurements

CLAMS (Columbus Instruments) were used to measure metabolic parameters; Drp1^{flx/flx} Cre⁺ and control mice were monitored for 72 h following a 48-h acclimation period.

An EcoMRI-100 qNMR (EchoMRI Medical Systems) was used to monitor body composition (i.e. lean versus fat mass) in mice.

For the glucose/pyruvate tolerance test, mice 9 weeks PTI were starved overnight and injected i.p. with 2g/kg glucose. Blood glucose was monitored from the tail vein using Accu Check Aviva test strips (Roche). For the insulin tolerance test, mice 9 weeks PTI were injected i.p. with 7.5 U/kg insulin (Actrapid Human Insulin A10AB01 100U/ml) and tail vein blood glucose concentration was monitored.

4.6. Western blot

Western blot was performed as indicated in Oettinghaus et al., 2016 (Manuscript section). Antibodies used were Drp1 (BD Biosciences, 611112), ATF4 (Santa Cruz, sc-200), Bip (BD Biosciences, 610978), eIF2 α total (Cell Signaling, 5324), eIF2 α P51 (Cell Signaling 3398), Akt1 (Cell Signaling, 9272), Akt1-P S473 (Cell Signaling, 4060), actin (Thermo Scientific; MA1-91399), Ucp1 (Abcam, ab10983), Hsp60 (ADI-SPA-807-E, Enzo).

Secondary antibodies were anti mouse-HRP (GE Healthcare; NA931) and anti rabbit (GE Healthcare; NA934); signal was detected with Amersham ECL Prime Western Blotting Detection Reagent (GE Healthcare; RPN2232) in conjunction with Amersham Hyperfilm (GE Healthcare; 28-9068-44) or the C300 chemiluminescence imager (Azure).

4.7. ELISA

ELISA were performed on either serum or plasma samples, according to manufacturer's instructions. For metabolic hormones, blood was collected in the morning between 9-10 AM by tail vein or heart puncture.

The following assays were used: serum Corticosterone: (Arbor Assays; K014-H1), T4 (Callbiotech; t4044T-100), Leptin (BioVendor, RD291001200R), active Ghrelin (Millipore, EZRGRA-90K), Fgf21 (BioVendor; RD291108200R), CRH (MBS727471, mybiosource), ACTH (M046006, MD Biosciences), Insulin (90080, Crystal Chem), L-amino acids (MAK002-1KT, Sigma).

4.8. Quantitative real-time PCR

Organs were collected from PBS-perfused mice and RNA was isolated using Qiagen kits (RNeasy Lipid Tissue Kit for adipose tissue; 74804, RNeasy Fibrous Tissue kit for muscle; 74704; RNeasy kit for other organs 74104). Reverse-Transcription was performed using the High-Capacity cDNA Reverse Transcription Kit (Invitrogen; 4368814). Quantitative real-time PCR was performed using TaqMan assays (Life Technologies) on a 7900HT Real-Time PCR System (Applied Biosystems). The following Taqman assays were used: Fgf21 (Mm00840165_g1), 18S (Mm03928990_g1), CHOP (Mm01135937_g1), PPAR α (m00440939_m1), PPAR δ (Mm00803184_m1), PGC-1 α (Mm01208835_m1), PGC-1 β (Mm00504720_m1), ATF4 (Mm00515325_g1), Akt1 (Mm01331626_m1), PI3K (Mm00803160_m1), Yme1l1 (Mm00496843_m1), Clpp (Mm00489940_m1), Hsp10 (Mm00434083_m1). Cross-threshold (Ct) values were normalized to 18S Ct values.

4.9. Pharmacological treatments

When indicated, mice were fed 0.4%-TUDCA-supplemented chow starting after the last tamoxifen injection for the entire time of the experiment.

GSK2606414 was dissolved in vehicle (0.5% hydroxypropylmethyl cellulose + 0.1% Tween-80 in water at pH 4.0) and was administered by oral gavage, twice a day for 5 consecutive days, at a concentration of 50 mg/kg; control mice received only vehicle with the same treatment schedule (Moreno et al., 2013).

4.10. BAT sympathectomy

Adult mice (>20g body weight) were weighed preoperatively and anesthetized with ketamine and xylazine (ketamine, 138mg/kg; xylazine, 6,9mg/kg). Sufficient narcosis was verified by testing missing pain reflexes. The completely anesthetized mouse was shaved in the dorsal neck on an area of approx. 1 cm² and the area disinfected.

The skin of the disinfected neck area was incised in anterior-to-posterior direction on a length of 1 – 1.5 cm, and rinsed with sterile saline. The brown adipose tissue (BAT) is located right beneath a layer of white adipose tissue (WAT). In order to be able to sever all 5 BAT-innervating nerves, the WAT layer was slightly lifted with a forceps, until the 5-tiered nerve bundle was exposed, of which all 5 branches were cut, taking care to avoid Sulzer's vein.

After denervation, the tissues were repositioned; the cutis was then stitched with U-sutures. The operated mouse was placed on a warm pad to avoid postoperative body temperature drop. Postoperatively, mice received a subcutaneous injection of 0.5 ml Ringer solution to compensate for intraoperative fluid losses, as well as preventive analgesia (0.05 mg/kg body weight buprenorphine).

For the half sympathectomy, only the nerve bundle innervating the right BAT was cut. For sham-operated mice, the entire procedure was reproduced up to the exposure of the nerve bundle, after which tissues were repositioned and the mouse sutured.

To verify the success of the surgery, half-sympathectomized mice were kept at 4°C for 48 hours to stimulate Ucp1 expression, then immediately sacrificed.

5. Results

5.1. Drp1 ablation in adult mouse forebrain impairs mitochondrial structure and respiratory activity

In our inducible mouse model, tamoxifen injection (1 mg, two times a day, for 5 consecutive days) at 8 weeks after birth causes the ablation of the *Drp1* gene only in neurons of the forebrain (*Drp1^{flx/flx} CaMKII α ::CreERT2*; hereafter, *Drp1^{flx/flx} Cre⁺*) (Figure 5.1 A). In line with *Drp1*'s role as a fission mediator, its ablation led to a marked enlargement of hippocampal mitochondria, which appeared rounded and clustered around neuronal nuclei already 4 weeks post tamoxifen injection (PTI; Figure 5.1 B). This was also confirmed by ultrastructural analyses, which showed that mitochondria of *Drp1*-ablated neurons were larger, rounded and mostly devoid of cristae (Figure 5.1 C-E). The disorganized internal structure notwithstanding, mitochondrial membrane potential, as measured by two separate fluorescent probes, TMRM and R123 (Tetramethylrhodamine methylester and Rhodamine 123), was preserved in mitochondria from hippocampus 4 weeks PTI (Figure 5.1 F).

In line with the disorganized state of the cristae, the activity of the respiratory complexes was also compromised; specifically, the activity of complex II was decreased already in the early stages of the phenotype (4 weeks PTI; Figure 5.1 G-H), while all complexes – I through IV – showed some degree of impairment at the end stages of the phenotype (10 weeks PTI; Figure 5.1 I-J).

5.2. Drp1-ablated mice develop a catabolic phenotype

Shortly after developing mild memory defects as early as 4 weeks PTI (see manuscript section, 3.3.3; (Oettinghaus et al., 2016)), *Drp1*-ablated mice experienced a progressive drop in body weight (Figure 5.2 B) and died between 9 and 12 weeks PTI (Figure 5.2 A). This was accompanied by a significant drop in body temperature in the days preceding death (Figure

5.2 C), and by a decrease, already 4 weeks PTI, of cold tolerance, as indicated by the inability to maintain a physiological body temperature after 4 hours at 4°C (Figure 5.2 D).

Further analyses performed in CLAMS metabolic cages showed that $Drp1^{flx/flx} Cre^+$ mice have a lower respiratory exchange ratio (RER; Figure 5.2 E), which is the ratio of the volume of CO_2 produced to the volume of O_2 consumed. Complete oxidation of glucose would yield 6 CO_2 molecules for 6 O_2 molecules consumed; thus, the RER of an organism consuming only glucose would be 1. Conversely, full oxidation of fatty acid chains requires more oxygen molecules than it releases CO_2 , and therefore β -oxidation lowers the RER. In this case, the lowering of the RER in $Drp1^{flx/flx} Cre^+$ mice indicates that they have an increased preference for lipid β -oxidation as fuel source. Accordingly, total body fat mass, assessed by EchoMRI, was decreased in $Drp1^{flx/flx} Cre^+$ mice (Figure 5.2 F). The loss of stored lipids could also be appreciated on the histological level, where white adipose tissue (WAT) presented with depleted fat vacuoles, and brown adipose tissue (BAT) ranged from smaller vacuoles to completely devoid of lipid droplets in $Drp1^{flx/flx} Cre^+$ mice (Figure 5.2 G-H). Finally, we detected increased BAT activity, reflected by a trend of increased *Ucp1* expression 10 weeks PTI (Figure 5.2 I-J).

5.3. Metabolic pathways that regulate fuel choice in $Drp1^{flx/flx} Cre^+$ mice

In order to elucidate whether the partial switch in fuel utilization was due to a compromised ability to metabolize glucose, we performed a glucose tolerance test, injecting 2g/kg glucose and measuring its clearance from the circulation at 8 weeks PTI. While absolute glucose levels were decreased in $Drp1^{flx/flx} Cre^+$ mice, both before and throughout the challenge, the rate and kinetics of glucose clearance were comparable (Figure 5.3 A). Likewise, an insulin tolerance test did not highlight any differences in insulin sensitivity (0.75 U/kg; Figure 5.3 B). Finally, a pyruvate tolerance test (2g/kg challenge) revealed a non-significant trend of increase in hepatic gluconeogenesis (Figure 5.3 C). These data, together with the observation that steady-state insulin levels were comparable between $Drp1^{flx/flx}$ and $Drp1^{flx/flx} Cre^+$ mice (Figure 5.3 D) rule out a prominent role for glucose dysmetabolism as a cause for the fuel switch.

We then focused on the regulation of feeding, hypothesizing that diminished nutrient intake could alter fuel choice. However, we found food consumption to actually increase in $Drp1^{flx/flx} Cre^+$ mice at 7 weeks PTI; only at the pre-terminal stages of the phenotype did $Drp1^{flx/flx} Cre^+$ mice decrease their food intake (Figure 5.3 E). Accordingly, at 10 weeks PTI, satiety hormone leptin was within normal ranges, while active ghrelin, which signals hunger, showed a non-significant trend of increase in $Drp1^{flx/flx} Cre^+$ mice (Figure 5.3 F-G).

Finally, we focused our attention on hormone systems that regulate metabolism and energy expenditure. Thyroid hormone T4 was decreased in $Drp1^{flx/flx} Cre^+$ mice, but only at 10 weeks PTI, which makes it unlikely that a thyroid deficiency underlies the early alterations in energy metabolism that we report (Figure 5.3 H). However, corticosterone, the main circulating glucocorticoid in rodents, was consistently and significantly increased in $Drp1^{flx/flx} Cre^+$ mice from 6 weeks PTI (Figure 5.3 I); possibly due to negative feedback, corticosterone-inducing hormones ACTH and CRH were not significantly increased in $Drp1^{flx/flx} Cre^+$ mice at 10 weeks PTI (Figure 5.3 J-K).

5.4. Drp1-ablated brain regions secrete metabolic cytokine Fgf21 in an eIF2 α -ATF4-mediated fashion

A plausible link between increased corticosterone and mitochondrial defects is Fgf21, a circulating cytokine that is canonically produced by the liver and WAT in response to starvation ((Fisher and Maratos-Flier, 2015); see intro paragraph 1.2.1.4). Of note, recent work has shown that disrupting mitochondrial function in muscle can lead to ectopic Fgf21 secretion (Suomalainen et al., 2011; Tynysmaa et al., 2010); furthermore, Fgf21 exerts some of its functions by acting on the CNS to induce CRH synthesis and corticosterone production, in addition to the activation of the sympathetic branch of the autonomic nervous system (Bookout et al., 2013; Owen et al., 2014).

Indeed, ELISA showed a very modest, but significant increase in circulating Fgf21 in $Drp1^{flx/flx} Cre^+$ mice (Figure 5.4 A). Though no expression of Fgf21 has ever been reported in the brain (Suomalainen et al., 2011), we tested by qRT-PCR whether the mitochondrial defect induced by Drp1 ablation could be the driver for Fgf21 production in $Drp1^{flx/flx} Cre^+$ mice. Indeed, we found that the hippocampus and cortex of $Drp1^{flx/flx} Cre^+$ mice express Fgf21 mRNA from the

early stages of the phenotype; conversely, no change in Fgf21 expression was detected in its canonical source organs (muscle, liver and WAT), nor in the cerebellum, where the CaMKII α promoter is not active (Figure 5.4 B).

Having ascertained the source of the circulating Fgf21, we set out to identify the mechanism mediating its transcription; among the transcription factors known to control Fgf21 expression, only ATF4 was upregulated in Drp1-ablated brains (Figure 5.4 C). Western Blot analyses further confirmed that AKT1, one of the candidate activators of Fgf21 synthesis, was not phosphorylated (Figure 5.4 D-E).

ATF4 is a transcription factor and a crucial node in the integrated stress response, which responds to different forms of stress via a decrease in global translation and the activation of specific transcriptional programs aimed at damage control (Donnelly 2013). Eukaryotic translation initiation factor 2 α (eIF2 α) phosphorylation is the checkpoint upstream of ATF4 that regulates its expression: phosphorylated eIF2 α hampers binding of the ribosome to the translation initiation complex, inhibiting translation of most mRNAs; however, ATF4 and other stress response mRNAs possess upstream open reading frames (uORFs) that allow them to be preferentially translated only when eIF2 α is phosphorylated.

Through Western Blot analysis, we confirmed both the ATF4 increase and the phosphorylation of eIF2 α in the hippocampi of Drp1^{fix/fix} Cre⁺ mice (Figure 5.4 F-H); the same pattern was observed for the cortex (data not shown). Furthermore, canonical ATF4 target gene *CHOP* underwent an upregulation similar to that of Fgf21 in the hippocampus and cortex of Drp1^{fix/fix} Cre⁺ mice (Figure 5.4 I).

Four different eIF2 α kinases are known, reflecting different stress conditions that trigger the ISR. PERK responds to ER stress, in the form of misfolded proteins. General Control Nonderepressible 2 (GCN2) is a sensor for amino acid deficiency, and it is activated by uncharged tRNAs. PKR is activated by double-stranded RNAs, and it signals viral infections; of note, it has also been reported to transduce the mitochondrial unfolded protein response (Rath et al., 2012). Finally, HRI becomes activated in the absence of heme (Donnelly et al., 2013).

All four kinases phosphorylate eIF2 α on the same residue, Ser51, and antibodies that detect the activation of the upstream kinases did not prove to be sensitive enough to be used on brain tissue, even after phospho-protein enrichment (data not shown); therefore, the detection of the arm(s) of the ISR that are responsible for eIF2 α phosphorylation must be achieved through the identification of the upstream stress that triggers the cascade.

5.5. Drp1 ablation in neurons causes ER stress

Given the close physical and functional connection that mitochondria share with the ER, we first focused on this organelle. Evaluation of EM images from hippocampus 4 weeks PTI revealed that the rough ER (rER) in Drp1^{flx/flx} Cre⁺ brains is round and swollen, much unlike the flat rER cisternae in their Drp1^{flx/flx} counterparts (Figure 5.5 A-B).

In addition, ER stress marker Bip/GRP78 was upregulated in Drp1^{flx/flx} Cre⁺ mice as early as 4 weeks PTI, and remained increased in the later stages of the phenotype (Figure 5.5 C-D). Taken together, these data indicate that throughout the phenotype a response against ER stress is active in Drp1^{flx/flx} Cre⁺ brains.

5.6. Pharmacological inhibition of ER stress does not prevent Fgf21 expression

In order to verify the contribution of ER stress to the cascade that results in Fgf21 expression, we treated the mice with orally-bioavailable chemical chaperone tauroursodeoxycholic acid (TUDCA, 0.4%-supplemented chow, from tamoxifen injection throughout the phenotype; (Lo et al., 2013)). However, while TUDCA treatment did lower Bip and P-eIF2 α levels in both genotypes, confirming its brain localization and activity, eIF2 α phosphorylation remained higher in TUDCA-treated Drp1^{flx/flx} Cre⁺ mice compared to Drp1^{flx/flx} (Figure 5.6 A-C). Furthermore, weight monitoring showed no improvement of TUDCA-treated Drp1^{flx/flx} Cre⁺ mice (Figure 5.6 D). Accordingly, Fgf21 mRNA expression remained elevated in TUDCA-treated brains, as did that of ATF4 target gene *CHOP*, though to a lesser extent than Fgf21 (Figure 5.6 E-F).

Given that TUDCA is a chemical with a broad spectrum of activity, and that it can also have antioxidant effects, we chose to repeat the rescue experiment with a targeted PERK inhibitor, GSK2606414 (hereafter, GSK), which has been reported to decrease ER stress in a mouse model of prion disease (Moreno et al., 2013). In addition, as sustained systemic inhibition of the ER stress response can have repercussions on normal physiology, we treated mice 7 weeks PTI for 5 consecutive days (50 mg/kg, every 12 hours). Nevertheless, weight monitoring again showed a strong negative effect of GSK treatment on mouse viability, with a 10% loss over less than a week (Figure 5.6 G). Indeed, while GSK treatment did slightly decrease eIF2 α phosphorylation and ATF4 (Figure 5.6 H-K), it failed to prevent the increase in Fgf21 and CHOP mRNA (Figure 5.6 L-M), indicating that the ISR pathway is still active in Drp1^{flx/flx} Cre⁺ brains in the presence of PERK inhibitor GSK.

Overall, while ER stress certainly is present in Drp1^{flx/flx} Cre⁺ brains, its inhibition alone is not sufficient to prevent Fgf21 expression and phenotype onset, suggesting that one or more of the other ISR branches may be contributing to the cellular response to Drp1 ablation.

5.7. Lack of mtUPR activation and evidence for amino acid deprivation and iron handling alterations in Drp1^{flx/flx} Cre⁺ mice

Considering the effect of Drp1 ablation on mitochondrial energy production (Figure 5.1 F-H) and internal structure (Figure 5.1 C-E), it is conceivable that mitochondrial translation would be impaired, resulting in the accumulation of unfolded proteins and activation of the mtUPR. mtUPR is a recently-discovered, mitochondria-specific response to proteotoxic stress, the relevance of which has so far only been demonstrated *in vitro* in mammals; of note, the central regulator of mammalian mtUPR is transcription factor CHOP ((Mottis et al., 2014); see 1.1.3.2). However, this was not the case: at 10 weeks PTI, protein levels of Hsp60 and mRNA levels of Hsp10, ClpP and Yme1l were unchanged between Drp1^{flx/flx} and Drp1^{flx/flx} Cre⁺ brains (Figure 5.7 A-C).

ID	Protein	Gene	FC	Q-Value
Q64433	10 kDa heat shock protein, mitochondrial (Hsp10)	Hspe1	0.98	0.6229
P63038	60 kDa heat shock protein, mitochondrial (Hsp60)	Hspd1	0.85	0.0185 *
Q9JHS4	ATP-dependent Clp protease ATP-binding subunit clpX-like, mitochondrial (ClpP)	Clpx	0.85	0.0422 *
Q99M87	DnaJ homolog subfamily A member 3, mitochondrial	Dnaja3	0.91	0.2022

Table 5.1 mtUPR-related genes from proteomics, 10 weeks PTI. Asterisks denote q values as follows. *: $p < 0.05$; **: $p < 0.01$; ***: $p < 0.001$.

In order to gain a better insight in the cellular processes taking place in $Drp1^{flx/flx} Cre^+$ brains, we performed total proteomics analysis on pooled hippocampi and cortices from mice 10 weeks PTI. Analysis of mtUPR-associated proteins confirmed that no mtUPR is in place in $Drp1^{flx/flx} Cre^+$ mice 10 weeks PTI, with two out of four genes being even significantly decreased (Table 5.1).

We then evaluated the role of amino acid deprivation in ISR activation; mitochondria are an important biosynthetic hub for de novo amino acid production, which may be affected by $Drp1$ ablation and the ensuing energy defects. Additionally, though neurons preferentially oxidize glucose to produce ATP, they may turn to alternative fuel sources when under energetic stress. Total amino acid content revealed that while the hippocampus showed a moderate decrease in amino acids, they were significantly increased in the cortex of $Drp1^{flx/flx} Cre^+$ mice (Figure 5.7 D).

In addition, among the significantly different hits in our proteomics analysis, we identified aminoacyl-tRNA synthetases as enriched, with a remarkable distribution: 80% of cytosolic aminoacyl-tRNA synthetases were significantly upregulated in $Drp1^{flx/flx} Cre^+$ brains, while their mitochondrial counterparts were mostly downregulated (Figure 5.7 E). While this is not conclusive evidence that amino acid deprivation is occurring in $Drp1^{flx/flx} Cre^+$ brains, it does suggest that alterations in amino acid metabolism occur upon $Drp1$ ablation.

Finally, we considered heme metabolism, as a large fraction of the biosynthetic pathway that produces heme resides within mitochondria, and it exploits the mitochondrial

membrane potential to carry iron atoms across the IMM. Indeed, coproporphyrinogen-III oxidase and ferrochelatase, two mitochondria-localized components of the heme biosynthetic pathway, were downregulated, as was frataxin (Table 5.2).

ID	Protein	Gene	FC	Q-Value
P10518	Delta-aminolevulinic acid dehydratase	Alad	1.00	0.5238
P22315	Ferrochelatase, mitochondrial	Fech	0.78	0.0071 **
O35943	Frataxin, mitochondrial	Fxn	0.85	0.0125 *
P36552	Oxygen-dependent coproporphyrinogen-III oxidase, mitochondrial	Cpox	0.77	0.0148 *
P22907	Porphobilinogen deaminase	Hmbs	1.06	0.1691
P51175	Protoporphyrinogen oxidase	Ppox	0.91	0.1215
Q8CAK1	Putative transferase CAF17 homolog, mitochondrial	lba57	0.90	0.0887
Q9CQN6	Transmembrane protein 14C	Tmem14c	1.05	0.4674
P70697	Uroporphyrinogen decarboxylase	Urod	0.85	0.1122
P51163	Uroporphyrinogen-III synthase	Uros	0.85	0.1815

Table 5.2 Heme-related genes from proteomics, 10 weeks PTI. Asterisks denote q values as follows. *: p<0.05; **: p<0.01; ***: p<0.001.

Of note, iron storage protein ferritin H was significantly upregulated in $Drp1^{flx/flx} Cre^+$ brains (Table 5.3).

ID	Protein	Gene	FC	Q-Value
P09528	Ferritin heavy chain	Fth1	1.27	0.0409 *
P29391	Ferritin light chain 1	Ftl1	1.04	0.2494
O35943	Frataxin, mitochondrial	Fxn	0.85	0.0125 *

Table 5.3 Iron storage-related genes from proteomics, 10 weeks PTI. Asterisks denote q values as follows. *: p<0.05; **: p<0.01; ***: p<0.001.

Therefore, we conclude that a combination of impaired amino acid and iron metabolism, in addition to ER stress, may contribute to the activation of the integrated stress response in $Drp1^{flx/flx} Cre^+$ mice.

5.8. Genetic rescue

Given the complexity of the catabolic phenotype caused by Drp1 ablation in the brain, we sought to verify whether Fgf21 was indeed the only mediator of the spectrum of metabolic alterations we observed. To this end, we crossed Drp1^{flx/flx} Cre⁺ mice to Fgf21^{flx/flx} mice, generating triple transgenic mice where recombination of both Fgf21 and Drp1 was driven by tamoxifen-inducible Cre, expressed under the control of the CaMKII α promoter (Drp1^{flx/flx}, Fgf21^{flx/flx}, CaMKII α ::CreERT2, hereafter Drp1^{flx/flx} Fgf21^{flx/flx} Cre⁺). As for double transgenics, Drp1^{flx/flx} Fgf21^{flx/flx} Cre⁺ mice were injected with tamoxifen 8 weeks after birth, and their progress monitored.

Survival analysis revealed no significant change in viability between double and triple transgenics (Figure 5.8 A). On the other hand, body weight was moderately improved in Drp1^{flx/flx} Fgf21^{flx/flx} Cre⁺ mice compared to Drp1^{flx/flx} Cre⁺ mice (Figure 5.8 B).

qRT-PCR analysis in brain showed a significant decrease of Fgf21 in the hippocampi of Drp1^{flx/flx} Fgf21^{flx/flx} Cre⁺ mice; there was, however, some residual expression, which may still be able to drive the phenotype (Figure 5.8 C). Of note, CHOP expression was not affected by the deletion of Fgf21 in the triple transgenics (Figure 5.8 D).

5.9. Figures

Figure 5.1 Mitochondrial morphology and function in Drp1-ablated neurons

(A) Tamoxifen-induced Drp1 ablation. Lysates of hippocampus and cortex from Drp1^{flx/flx} and Drp1^{flx/flx} Cre⁺ mice were separated by SDS-PAGE and immunoblotted with the indicated antibodies.

(B) Mitochondrial morphology after Drp1 ablation. Representative images of CA1 pyramidal neurons from of Drp1^{flx/flx} and Drp1^{flx/flx} Cre⁺ mice 4 weeks PTI immunostained for cytochrome c oxidase subunit 1 (green) and with DAPI (blue). Scale bar: 10 μ m.

(C) Mitochondrial ultrastructure after Drp1 ablation. Representative TEM images of mitochondria of hippocampal neurons of Drp1^{flx/flx} and Drp1^{flx/flx} Cre⁺ mice 4 weeks PTI. “N” indicates the nucleus and “M” indicates mitochondria. Scale bar: 1 μ m.

(D) Smallest radial diameter. Mitochondria from TEM images of Drp1^{flx/flx} and Drp1^{flx/flx} Cre⁺ mice 4 weeks PTI were measured. Data represent average \pm SEM of at least 4 animals of which at least 100 mitochondria were measured.

(E) Mitochondria with abnormal cristae. TEM images from Drp1^{flx/flx} and Drp1^{flx/flx} Cre⁺ mice 4 weeks PTI were evaluated for abnormal mitochondria. Data represent average \pm SEM of at least 4 animals of which at least 100 mitochondria were scored.

(F) Mitochondrial membrane potential. Fluorescence intensity of mitochondrial membrane potential probes TMRM and R123, in mitochondria isolated from hippocampus from Drp1^{flx/flx} and Drp1^{flx/flx} Cre⁺ mice 4 weeks PTI. Please note the double Y axis; kFU: thousands of fluorescence units. Data represent average \pm SEM of 4 animals.

(G-J) Respiratory complexes activity. Isolated mitochondria from Drp1^{flx/flx} and Drp1^{flx/flx} Cre⁺ mice 4 and 10 weeks PTI were assayed for oxygen consumption upon sequential addition of the indicated substrates. Mal/Glut – Malate and Glutamate; Oligo – Oligomycin; Rot – Rotenone; Duro – Duroquinone; Succ/Rot – Succinate and Rotenone; AntiA – Antimycin A; Asc – Ascorbate. For concentrations, please refer to the Experimental Procedures section.

Asterisks denote p values of an unpaired, two-tailed Student’s t test; in case of multiple comparisons, one-way ANOVA followed by Dunnett’s or Sidak’s post hoc method was applied. *: p<0.05; **: p<0.01; ***: p<0.001.

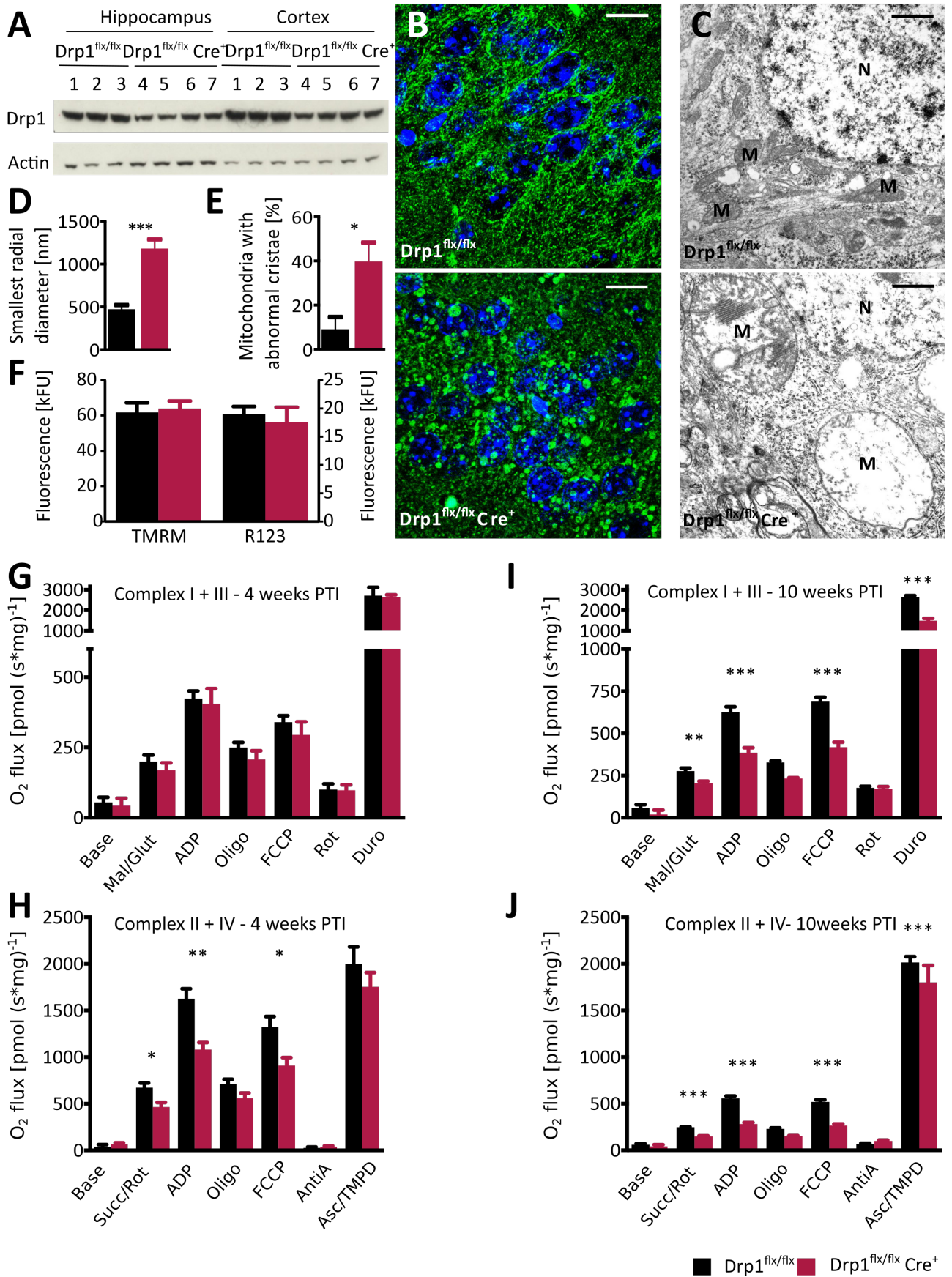


Figure 5.1

Figure 5.2 Macroscopic metabolic alterations in $Drp1^{flx/flx} Cre^+$ mice

(A) Mouse viability after Drp1 ablation. Kaplan-Meier plot of $Drp1^{flx/flx}$ and $Drp1^{flx/flx} Cre^+$ mice. At least 15 mice per group were monitored.

(B) Body weight monitoring after Drp1 ablation. Sex-sorted body weight of $Drp1^{flx/flx}$ and $Drp1^{flx/flx} Cre^+$ mice at the indicated time points. Data represent average \pm SEM of at least 6 animals.

(C) Body temperature monitoring after Drp1 ablation. Body temperature of $Drp1^{flx/flx} Cre^+$ mice plotted as a function of time before death. Data represent average \pm SEM of at least 8 animals.

(D) Cold resistance test. Body temperature of $Drp1^{flx/flx}$ and $Drp1^{flx/flx} Cre^+$ mice before and after 4 hours at 4°C. Data represent average \pm SEM of at least 6 animals.

(E) Respiratory exchange ratio. $Drp1^{flx/flx}$ and $Drp1^{flx/flx} Cre^+$ mice were tested for metabolic parameters in CLAMS cages 4 weeks PTI. Data represent average \pm SEM of at least 8 animals.

(F) Body fat percentage. $Drp1^{flx/flx}$ and $Drp1^{flx/flx} Cre^+$ mice 4 weeks PTI were tested for lean and fat mass in an EchoMRI. Data represent average \pm SEM of at least 8 animals.

(G-H) Histology of WAT (G) and BAT (H). H&E staining of FFPE white and brown adipose tissue sections of $Drp1^{flx/flx}$ and $Drp1^{flx/flx} Cre^+$ mice was performed 10 weeks PTI. White adipose tissue was classified by cell size and brown adipose tissue by vacuole size in a blinded fashion. Chi-square test for trend analysis was performed. WAT, $p = 0.0075$; BAT, $p = 0.0249$.

(I) BAT activation. Lysates of BAT from $Drp1^{flx/flx}$ and $Drp1^{flx/flx} Cre^+$ mice 10 weeks PTI were separated by SDS-PAGE and immunoblotted with the indicated antibodies.

(J) UCP1 quantification. Relative intensity of UCP1 and actin bands were measured. Data represent average \pm SEM of at least 5 animals.

Asterisks denote p values of an unpaired, two-tailed Student's t test; in case of multiple comparisons, one-way ANOVA followed by Dunnett's or Sidak's post hoc method was applied. *: $p < 0.05$; **: $p < 0.01$; ***: $p < 0.001$.

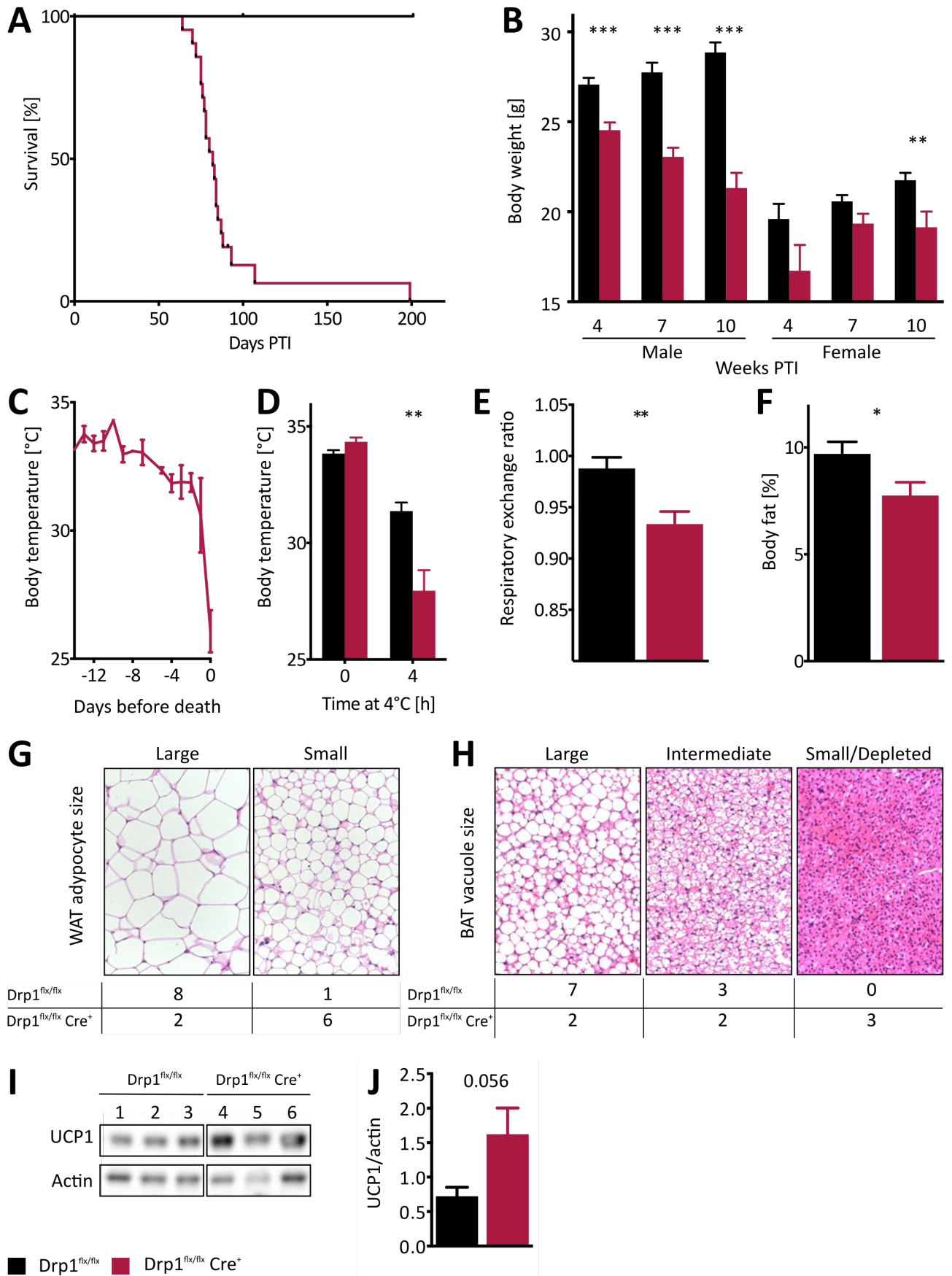


Figure 5.2

Figure 5.3 Clinical chemistry and hormones in $Drp1^{flx/flx} Cre^+$ mice

(A) Glucose tolerance test. $Drp1^{flx/flx}$ and $Drp1^{flx/flx} Cre^+$ mice 10 weeks PTI were starved overnight and injected with 2 g/kg glucose, and their glucose levels were measured in tail vein blood at the indicated time points. Data represent average \pm SEM of at least 7 animals.

(B) Insulin tolerance test. $Drp1^{flx/flx}$ and $Drp1^{flx/flx} Cre^+$ mice 10 weeks PTI were starved overnight and injected with 7.5 U/kg glucose, and their glucose levels were measured in tail vein blood at the indicated time points. Data represent average \pm SEM of at least 5 animals.

(C) Pyruvate tolerance test. $Drp1^{flx/flx}$ and $Drp1^{flx/flx} Cre^+$ mice 9 weeks PTI were starved overnight and injected with 2 g/kg pyruvate, and their glucose levels were measured in tail vein blood at the indicated time points. Data represent average \pm SEM of at least 5 animals.

(D) Plasma insulin. ELISA measurement of plasma insulin levels in $Drp1^{flx/flx}$ and $Drp1^{flx/flx} Cre^+$ mice 10 weeks PTI. Positive control represents $Drp1^{flx/flx}$ mice starved overnight. Data represent average \pm SEM of at least 7 animals.

(E) Food intake monitoring. $Drp1^{flx/flx}$ and $Drp1^{flx/flx} Cre^+$ mice were housed in single cages and their food intake monitored at the indicated time point. Food consumption was normalized to body weight. Data represent average \pm SEM of at least 4 animals.

(F-G) Plasma leptin (F) and ghrelin (G). ELISA measurement of plasma leptin and ghrelin levels in $Drp1^{flx/flx}$ and $Drp1^{flx/flx} Cre^+$ mice 10 weeks PTI. Data represent average \pm SEM of at least 4 animals.

(H-I) Serum T4 (H) and corticosterone (I). ELISA measurement of serum T4 and corticosterone levels in $Drp1^{flx/flx}$ and $Drp1^{flx/flx} Cre^+$ mice at the indicated time points. Data represent average \pm SEM of at least 4 animals.

(J-K) Plasma CRH (J) and ACTH (K). ELISA measurement of plasma CRH and ACTH levels in $Drp1^{flx/flx}$ and $Drp1^{flx/flx} Cre^+$ mice 10 weeks PTI. Data represent average \pm SEM of at least 4 animals.

Asterisks denote p values of an unpaired, two-tailed Student's t test; in case of multiple comparisons, one-way ANOVA followed by Dunnett's or Sidak's post hoc method was applied. *: $p < 0.05$; **: $p < 0.01$; ***: $p < 0.001$.

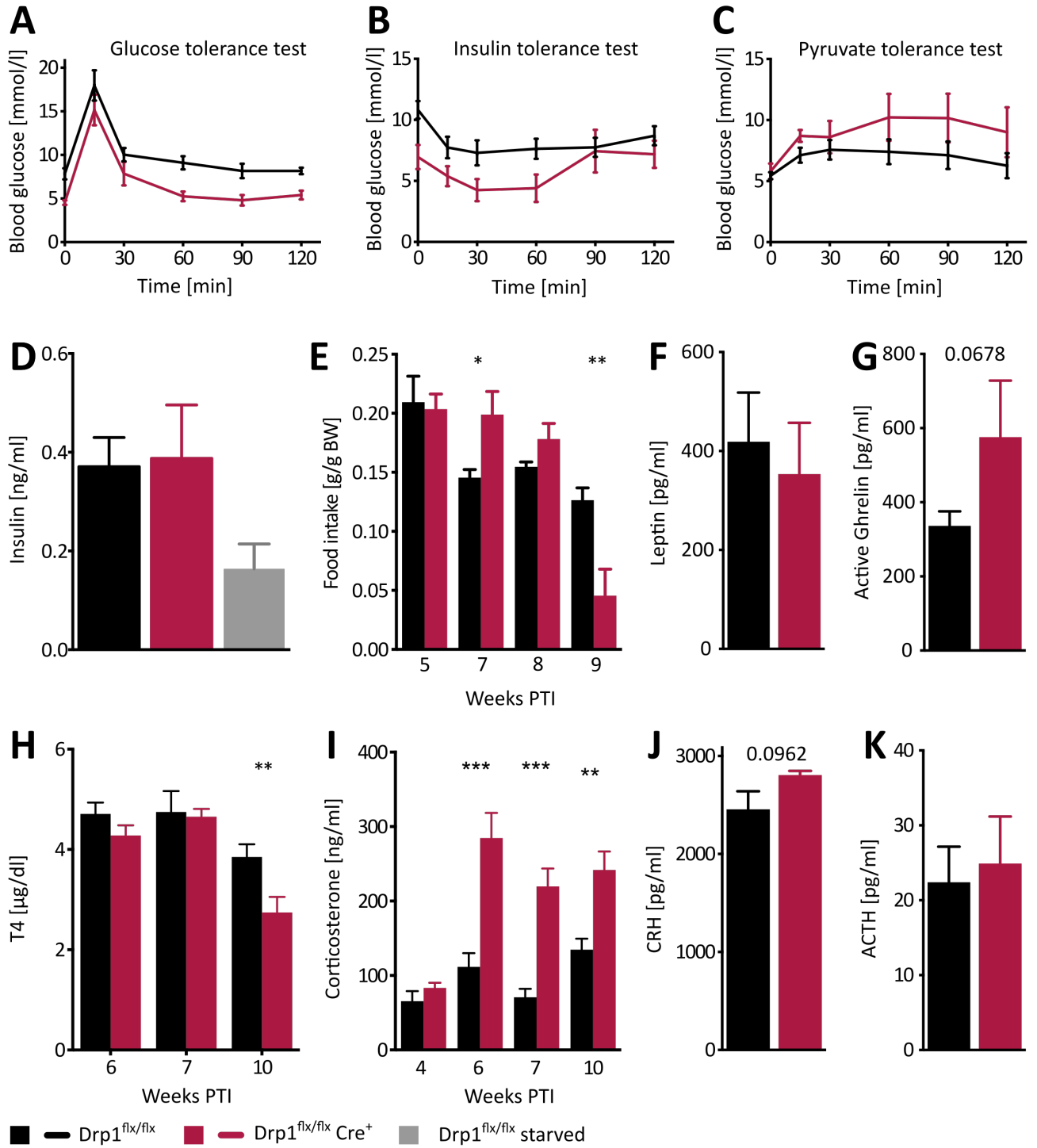


Figure 5.3

Figure 5.4 Production of Fgf21 in Drp1^{flx/flx} Cre⁺ mice

(A) Plasma Fgf21. ELISA measurement of plasma Fgf21 levels in Drp1^{flx/flx} and Drp1^{flx/flx} Cre⁺ mice at the indicated time points. Data represent average \pm SEM of at least 3 animals.

(B) Fgf21 expression in different organs. qRT-PCR analysis was performed on the indicated organs and brain areas to assay for Fgf21 expression at the indicated time points. Fgf21 ct values were normalized against 18S rRNA ct values. Data represent average \pm SEM of at least 4 animals.

(C) Transcription factor expression in the hippocampus. qRT-PCR analysis was performed on hippocampi from Drp1^{flx/flx} and Drp1^{flx/flx} Cre⁺ mice 10 weeks PTI to assay for transcription factor expression. mRNA ct values were normalized against 18S rRNA ct values. Data represent average \pm SEM of at least 4 animals.

(D) AKT activation. Lysates of hippocampus from Drp1^{flx/flx} and Drp1^{flx/flx} Cre⁺ mice 10 weeks PTI were separated by SDS-PAGE and immunoblotted with the indicated antibodies.

(E) Phospho-AKT quantification. Relative intensity of AKT P473 and total AKT bands were measured. Data represent average \pm SEM of at least 4 animals.

(F) Integrated stress response activation. Lysates of hippocampus from Drp1^{flx/flx} and Drp1^{flx/flx} Cre⁺ mice 4 and 10 weeks PTI were separated by SDS-PAGE and immunoblotted with the indicated antibodies.

(G-H) Phospho-eIF2 α (G) and ATF4 (H) quantification. Relative intensity of P-eIF2 α and total eIF2 α bands and of ATF4 and actin bands, respectively, were measured. Data represent average \pm SEM of at least 4 animals.

(I) CHOP expression in brain. qRT-PCR analysis was performed on the indicated brain areas to assay for CHOP expression at the indicated time points. Fgf21 ct values were normalized against 18S rRNA ct values. Data represent average \pm SEM of at least 4 animals.

Asterisks denote p values of an unpaired, two-tailed Student's t test; in case of multiple comparisons, one-way ANOVA followed by Dunnett's or Sidak's post hoc method was applied. *: p<0.05; **: p<0.01; ***: p<0.001.

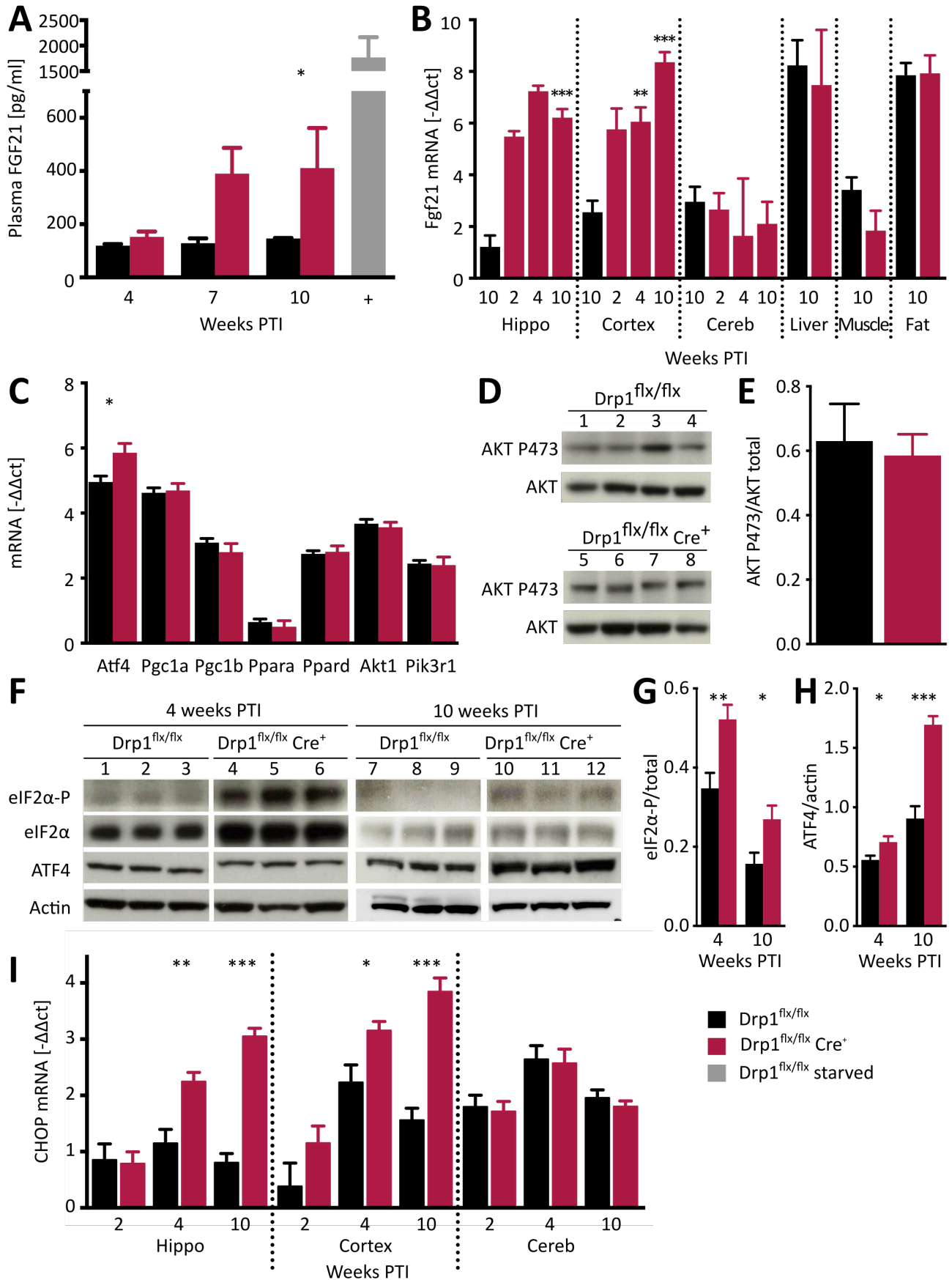


Figure 5.4

Figure 5.5 ER stress in Drp1^{flx/flx} Cre⁺ mice

(A) ER ultrastructure after Drp1 ablation. Representative TEM images of ER of hippocampal neurons of Drp1^{flx/flx} and Drp1^{flx/flx} Cre⁺ mice 4 weeks PTI. “N” indicates the nucleus and “M” indicates mitochondria. Arrows indicate ER. Scale bar: 1 μ m.

(B) ER circularity. Evaluation of the circularity of ER structures in hippocampi of Drp1^{flx/flx} and Drp1^{flx/flx} Cre⁺ mice based on the formula $(4\pi * \text{Area})/\text{Perimeter}^2$. Data represent average \pm SEM of at least 4 animals of which rER structures of at least 50 neurons were measured.

(C) ER stress activation. Lysates of hippocampus from Drp1^{flx/flx} and Drp1^{flx/flx} Cre⁺ mice 10 weeks PTI were separated by SDS-PAGE and immunoblotted with the indicated antibodies.

(D) Bip quantification. Relative intensity of Bip and actin bands were measured. Data represent average \pm SEM of at least 4 animals.

Asterisks denote p values of an unpaired, two-tailed Student’s t test; in case of multiple comparisons, one-way ANOVA followed by Dunnett’s or Sidak’s post hoc method was applied. *: p<0.05; **: p<0.01; ***: p<0.001.

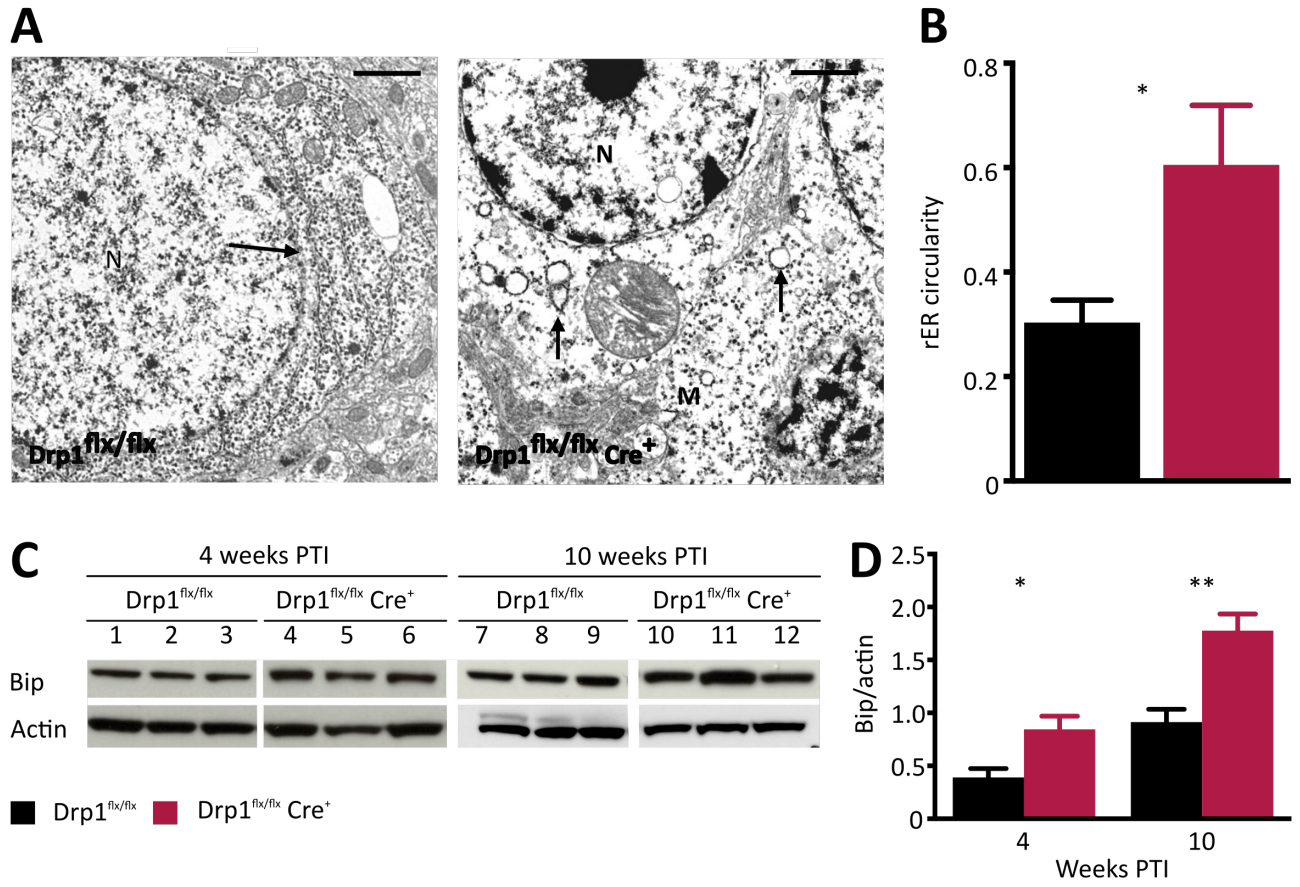


Figure 5.5

Figure 5.6 Pharmacological ER stress rescue

(A) ER stress response activation after TUDCA treatment. Lysates of hippocampus from $Drp1^{flx/flx}$ and $Drp1^{flx/flx} Cre^+$ mice 10 weeks PTI with or without TUDCA treatment were separated by SDS-PAGE and immunoblotted with the indicated antibodies.

(B) Bip quantification. Relative intensity of Bip and actin bands were measured. Data represent average \pm SEM of at least 4 animals.

(C) Weight monitoring during TUDCA treatment. Percent change of body weight is plotted as a function of time for $Drp1^{flx/flx}$ and $Drp1^{flx/flx} Cre^+$ mice with or without TUDCA treatment. Data represent average \pm SEM of at least 5 animals.

(D) Phospho-eIF2 α quantification. Relative intensity of P-eIF2 α and total eIF2 α bands were measured. Data represent average \pm SEM of at least 4 animals.

(E) Fgf21 expression after TUDCA treatment. qRT-PCR analysis was performed on hippocampus from $Drp1^{flx/flx}$ and $Drp1^{flx/flx} Cre^+$ mice with or without TUDCA treatment to assay for Fgf21 expression 10 weeks PTI. Fgf21 ct values were normalized against 18S rRNA ct values. Data represent average \pm SEM of at least 4 animals.

(F) CHOP expression after TUDCA treatment. qRT-PCR analysis was performed on hippocampus from $Drp1^{flx/flx}$ and $Drp1^{flx/flx} Cre^+$ mice with or without TUDCA treatment to assay for CHOP expression 10 weeks PTI. CHOP ct values were normalized against 18S rRNA ct values. Data represent average \pm SEM of at least 4 animals.

(G) Weight monitoring during GSK treatment. Percent change of body weight after 5-days GSK treatment in $Drp1^{flx/flx}$ and $Drp1^{flx/flx} Cre^+$ mice. Data represent average \pm SEM of at least 5 animals.

(H) ER stress response activation after GSK treatment. Lysates of hippocampus from $Drp1^{flx/flx} Cre^+$ mice 7 weeks PTI with or without GSK treatment were separated by SDS-PAGE and immunoblotted with the indicated antibodies.

(I-K) Bip (I), P-eIF2 α (J) and ATF4 (K) quantification. Relative intensity of Bip, ATF4 and actin bands, and of P-eIF2 α and total eIF2 α , respectively, were measured. Data represent average \pm SEM of at least 4 animals.

(L) Fgf21 expression after GSK treatment. qRT-PCR analysis was performed on hippocampus from $Drp1^{flx/flx}$ and $Drp1^{flx/flx} Cre^+$ mice with or without GSK treatment to assay for Fgf21 expression. Fgf21 ct values were normalized against 18S rRNA ct values. Data represent average \pm SEM of at least 4 animals.

(M) CHOP expression after GSK treatment. qRT-PCR analysis was performed on hippocampus from $Drp1^{flx/flx}$ and $Drp1^{flx/flx} Cre^+$ mice with or without GSK treatment to assay for CHOP expression. CHOP ct values were normalized against 18S rRNA ct values. Data represent average \pm SEM of at least 4 animals.

Asterisks denote p values of an unpaired, two-tailed Student's t test; in case of multiple comparisons, one-way ANOVA followed by Dunnett's or Sidak's post hoc method was applied. *: $p < 0.05$; **: $p < 0.01$; ***: $p < 0.001$.

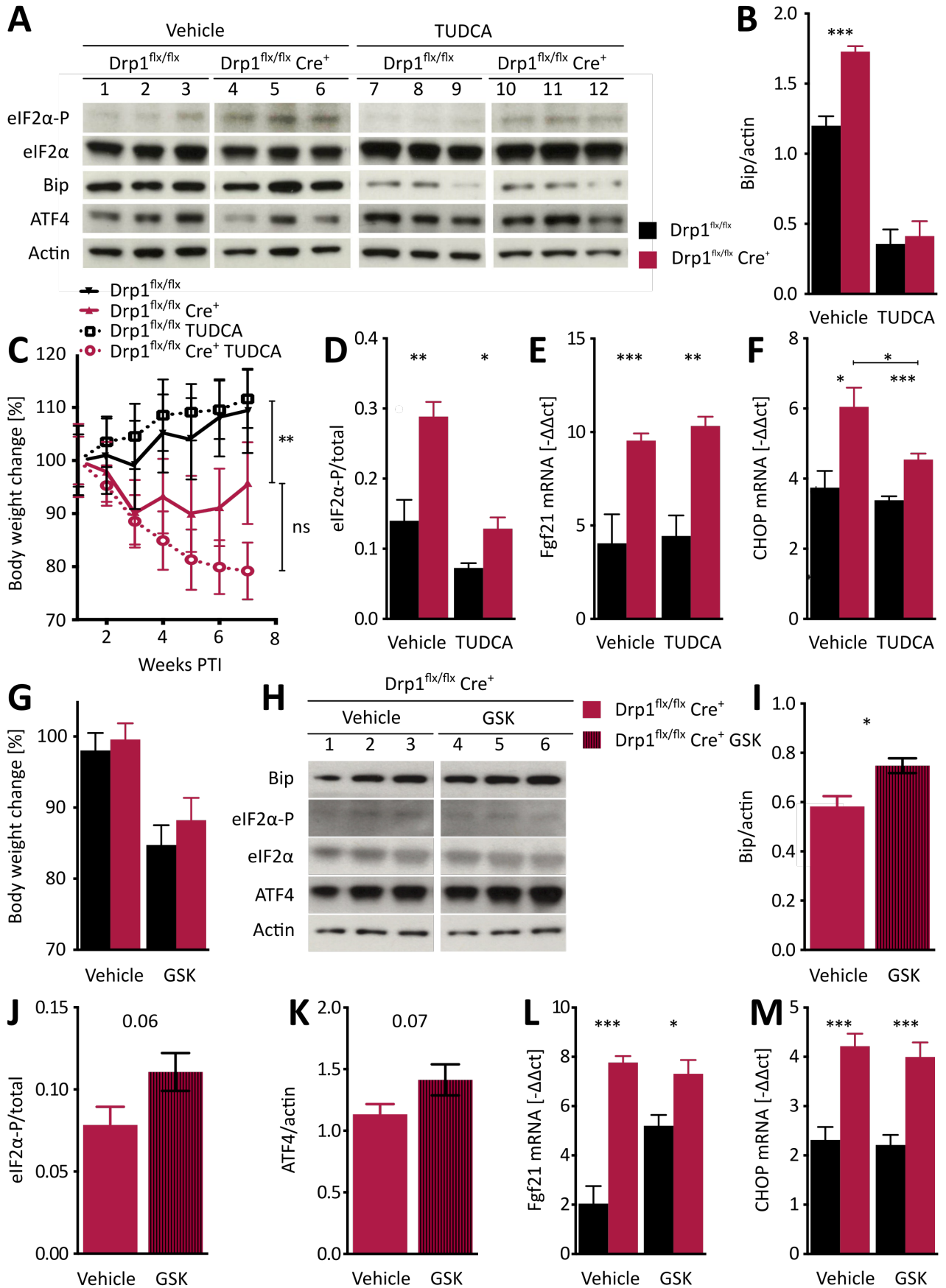


Figure 5.6

Figure 5.7 Integrated stress response in Drp1^{flx/flx} Cre⁺ mice

(A) mtUPR activation. Lysates of hippocampus from Drp1^{flx/flx} and Drp1^{flx/flx} Cre⁺ mice 10 weeks PTI were separated by SDS-PAGE and immunoblotted with the indicated antibodies.

(B) Hsp60 quantification. Relative intensity of Hsp60 and actin bands were measured. Data represent average \pm SEM of at least 4 animals.

(C) mtUPR proteases expression in the hippocampus. qRT-PCR analysis was performed on hippocampi from Drp1^{flx/flx} and Drp1^{flx/flx} Cre⁺ mice 10 weeks PTI to assay for the expression of mtUPR proteases. mRNA ct values were normalized against 18S rRNA ct values. Data represent average \pm SEM of at least 4 animals.

(D) Free amino acids. Free L-amino acids in lysates from the indicated brain areas from Drp1^{flx/flx} and Drp1^{flx/flx} Cre⁺ mice 10 weeks PTI. Data represent average \pm SEM of at least 5 animals.

(E) Aminoacyl tRNA synthetases. Fold change (Drp1^{flx/flx} Cre⁺ / Drp1^{flx/flx}) values from cytosolic and mitochondrial aminoacyl tRNA synthetases are plotted as a function of their q-value in the proteomics screen.

Asterisks denote p values of an unpaired, two-tailed Student's t test; in case of multiple comparisons, one-way ANOVA followed by Dunnett's or Sidak's post hoc method was applied. *: p<0.05; **: p<0.01; ***: p<0.001.

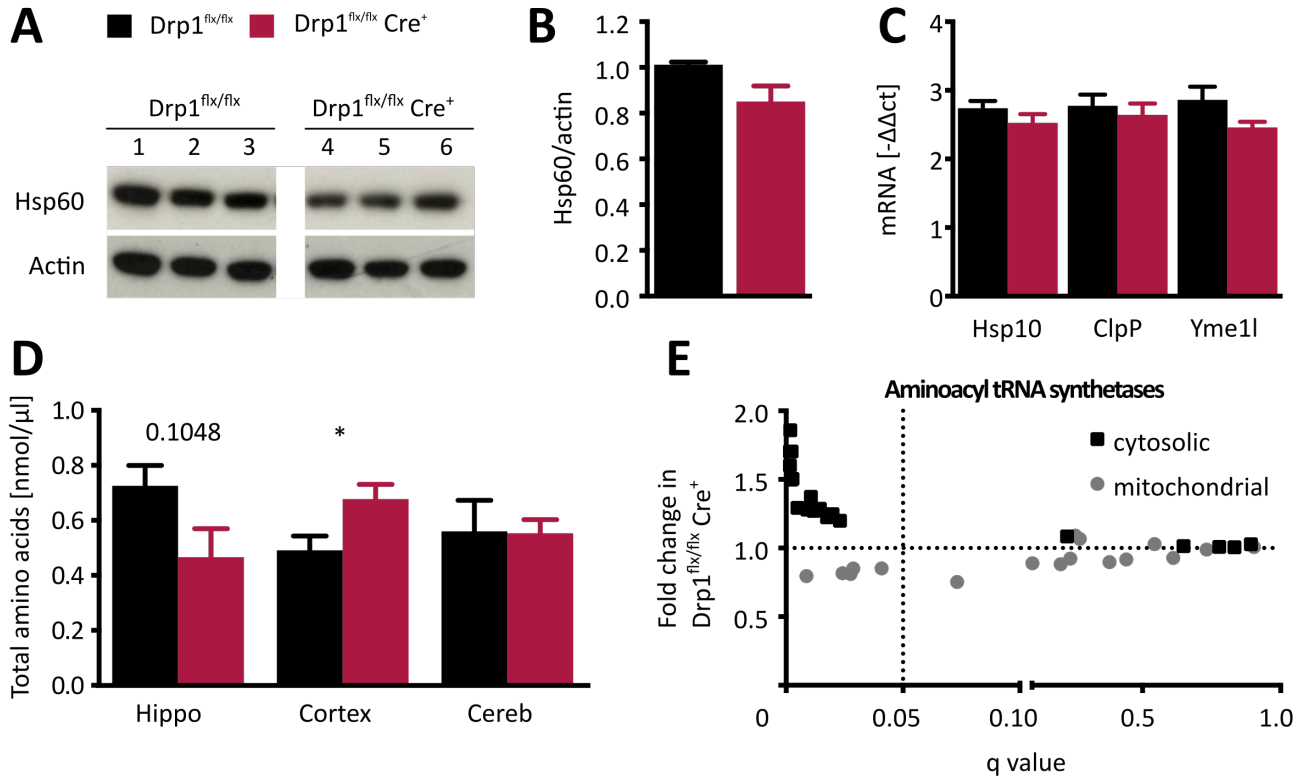


Figure 5.7

Figure 5.8 Genetic rescue

(A) Mouse viability after Drp1 and Fgf21 ablation. Kaplan-Meier plot of Drp1^{flx/flx} Fgf21^{flx/flx} and Drp1^{flx/flx} Fgf21^{flx/flx} Cre⁺ mice. At least 10 mice per group were monitored.

(B) Body weight monitoring after Drp1 and Fgf21 ablation. Body weight of Drp1^{flx/flx} Fgf21^{flx/flx} and Drp1^{flx/flx} Fgf21^{flx/flx} Cre⁺ mice are plotted as a function of time after tamoxifen injection. Data represent average \pm SEM of at least 6 animals.

(C) Fgf21 expression after GSK treatment. qRT-PCR analysis was performed on hippocampus from Drp1^{flx/flx} Fgf21^{flx/flx} and Drp1^{flx/flx} Fgf21^{flx/flx} Cre⁺ mice with or without GSK treatment to assay for Fgf21 expression. Fgf21 ct values were normalized against 18S rRNA ct values. Data represent average \pm SEM of at least 4 animals.

(D) CHOP expression after GSK treatment. qRT-PCR analysis was performed on hippocampus from Drp1^{flx/flx} Fgf21^{flx/flx} and Drp1^{flx/flx} Fgf21^{flx/flx} Cre⁺ mice with or without GSK treatment to assay for CHOP expression. CHOP ct values were normalized against 18S rRNA ct values. Data represent average \pm SEM of at least 4 animals.

Asterisks denote p values of an unpaired, two-tailed Student's t test; in case of multiple comparisons, one-way ANOVA followed by Dunnett's or Sidak's post hoc method was applied. *: p<0.05; **: p<0.01; ***: p<0.001.

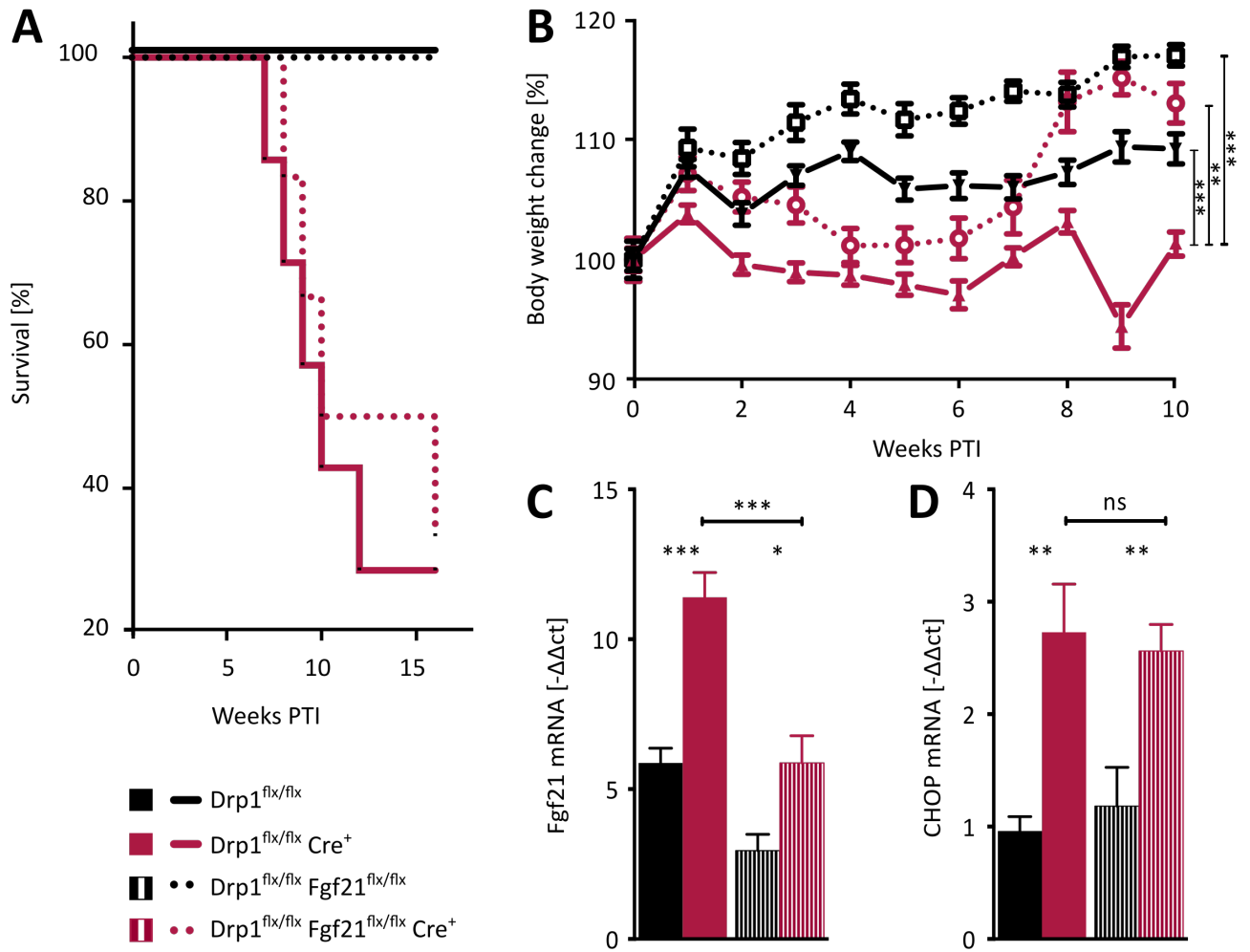


Figure 5.8

6. Discussion

This work stems from our group's published observation that conditional Drp1 ablation in adult neurons leads to defects in neuronal function and long-term potentiation establishment, culminating in behavioral alterations (Oettinghaus et al., 2016). We then set out to complete the characterization of the neuronal phenotype of Drp1 ablation, and examined the systemic consequences of the disruption of mitochondrial fission in adult neurons. Remarkably, we found that Drp1 deletion triggers the activation of a likely multi-branched response that culminates in ectopic Fgf21 expression in the brain. Paracrine action of Fgf21 on its hypothalamic receptor then initiates an uncoordinated catabolic switch in the systemic metabolism of the animals, which results in lethality (Figure 6.1).

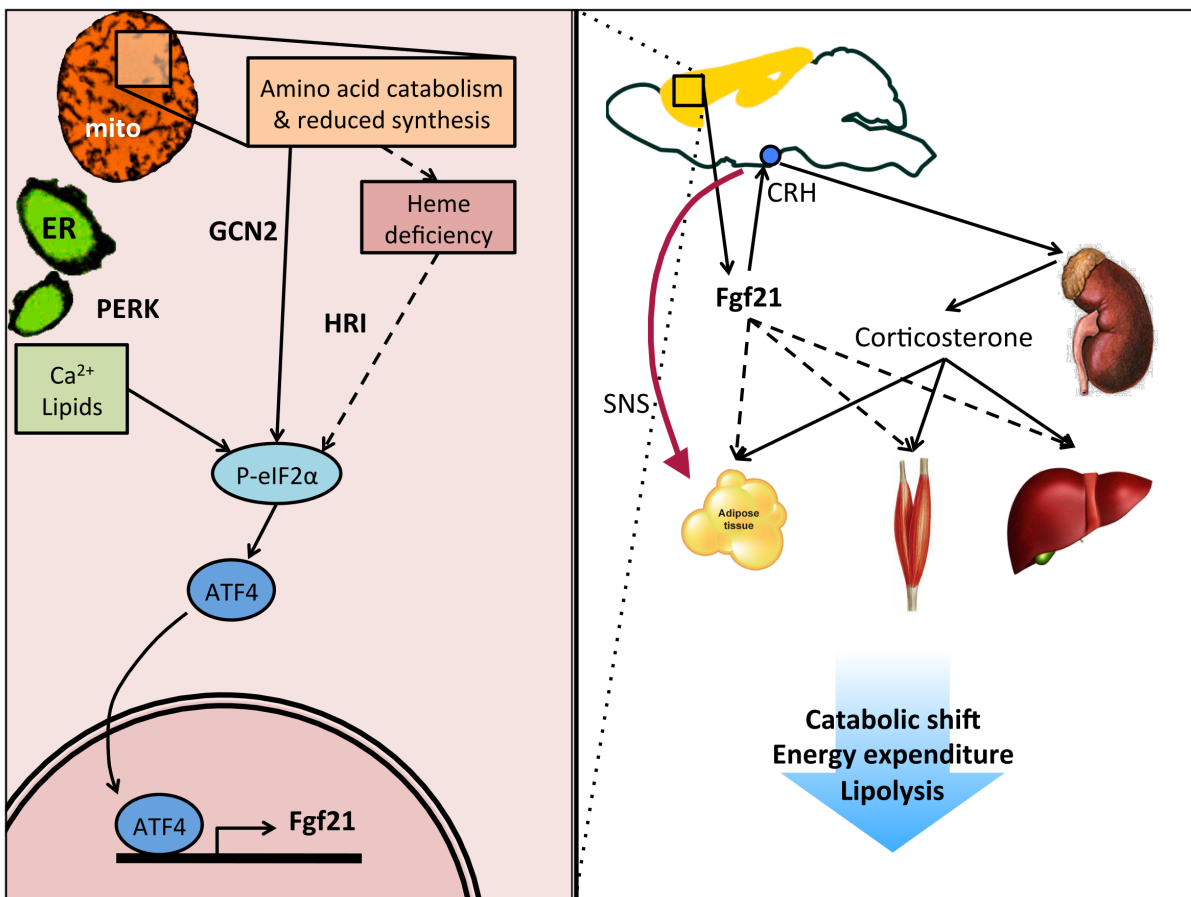


Figure 6.1 Graphical abstract. Left, Drp1 ablation in neurons activates a combination of ISR branches, resulting in Fgf21 transcription by Atf4. Right, Fgf21 exerts a paracrine action on its hypothalamic receptors, stimulating corticosterone production and sympathetic nervous system activation. The combination of these stimuli shifts systemic metabolism towards energy expenditure, resulting in lethality. SNS: Sympathetic Nervous System.

6.1. Drp1 deletion in forebrain neurons activates the integrated stress response

In accordance with our published findings (Oettinghaus et al., 2016), mitochondria in the hippocampi of Drp1-ablated mice are spherical and grossly enlarged. This is paralleled by disruption of the cristae structure, which likely affects respiratory complex assembly (Figure 5.1).

It is interesting to note that despite massive structural defects, Drp1-deficient mitochondria are still able to maintain their membrane potential (Figure 5.1 F). One possible explanation is based on the observation that, according to our proteomics screen, Drp1^{flx/flx} Cre⁺ brains strongly upregulate mitochondrial uncoupler Ucp5 (fold change 1.55, q value 0.021). Little is known about this brain-specific uncoupling protein: recent work has shown that it is upregulated upon oxidative insults in dopaminergic neurons (Ho et al., 2005), and, counterintuitively, its increase protects MPTP-treated neurons from mitochondrial membrane potential loss (Kwok et al., 2010). Whether Ucp5 can regulate mitochondrial membrane potential by modulating the proton leak, or whether other mechanisms are in place to explain its activity, is not yet clear (Cardoso et al., 2014). On the other hand, it is also possible that the mitochondrial purification protocol used for membrane potential measurement, which is based on sequential centrifugation steps, is biased towards smaller, healthier mitochondria, and therefore excludes the extreme cases that are represented in the EM images (Figure 5.1 C).

Nevertheless, the decreased activity of all respiratory complexes at 10 weeks PTI is a strong hint that in the later stages of the phenotype mitochondrial membrane potential is likely impaired, though we lack an accurate measurement at this time point.

Within this framework, it is surprising that no signs of mtUPR activation were detectable at 10 weeks PTI; nevertheless, as the mtUPR is a first-line, rectifying response to misfolded proteins, it is possible that analysis of earlier time points (2-4 weeks PTI) would yield a different pattern of upregulation of stress markers.

Predictably, biosynthetic activities that reside within mitochondria show some degree of impairment in Drp1-ablated neurons. Proteins that are responsible for iron utilization in

heme biosynthesis – e.g. ferrochelatase, which catalyzes the final step of heme assembly (Richardson et al., 2010), and frataxin, which has been proposed as a metabolic switch between Fe-S cluster and heme biosynthetic pathways (Becker et al., 2002; Richardson et al., 2010) – are downregulated; conversely, iron storage protein ferritin is upregulated in the cytosol (Table 5.2 and 5.3).

In light of the fact that mitochondrial iron import is mediated by specialized channel mitoferrin in a manner that is membrane-potential-dependent (Lill et al., 2006; Shaw et al., 2006; Zhang et al., 2005), a possible scenario is that iron would accumulate in the cytosol because it is unable to cross the IMM; conversely, within mitochondria, iron-related biosynthetic processes would be halted. Of note, lack of heme and Fe-S prosthetic groups would negatively affect a plethora of respiratory complex subunits, in which these cofactors are fundamental for electron transfer. Indeed, proteomics results show a drastic downregulation of both β subunits of hemoglobin (0.22 and 0.28 fold, q value 0.026), which may further corroborate the heme deficiency hypothesis.

Amino acid metabolism is also likely to be affected by Drp1 ablation: on one hand, energy defects would impair de novo synthesis; on the other hand, amino acids may be needed as alternative fuel sources – within the neurons themselves or in the surrounding glia. Indeed, while signs of global defects in amino acid metabolism throughout the brain are present, it is interesting to note that the cortex is able to maintain an elevated amino acid pool, while the hippocampus is depleted (Figure 5.7 D); of note, amino acid levels of Drp1^{flx/flx} cortex and hippocampus are also different. Remarkably, one specific area of the cortex, the anterior piriform cortex, is the only known sensor for amino acid limitation in the brain, and it acts in a GCN2-dependent manner to regulate feeding behavior and increase de novo biosynthesis (Hao et al., 2005). This phenomenon raises the interesting possibility that, throughout the brain, different responses are enacted upon Drp1 ablation. Indeed, this aligns with existing studies that report different degrees of sensitivity to Drp1 deletion in different neuronal subpopulations (Berthet et al., 2014; Kageyama et al., 2012; Oettinghaus et al., 2016; Shields et al., 2015).

Further insight into the biosynthetic state of Drp1-ablated brains would come from a shotgun metabolomics approach (currently ongoing), eventually complemented by carbon tracing, which would allow for the identification of metabolites and synthesis intermediates, and define a clearer picture of active metabolic networks (see for instance (Nilsson et al., 2014)).

In addition to the disruption of their resident activities, Drp1-ablated mitochondria also affect neighboring organelles, foremost among them the ER. In fact, it is likely that the marked enlargement of Drp1-deficient mitochondria prevents, or at least diminishes, its physical association to the MAMs within the ER. This could result in functional uncoupling, e.g. loss of coordinated calcium handling or of lipid transport. The electrophysiological work-up (Figure 3.4 C-D) argues against a significant alteration of calcium regulation. On the other hand, defects in lipid metabolism would explain the circular ER morphology we observed 4 weeks PTI (Figure 5.1 C). Compellingly, two proteins of the prohibitin family that were significantly upregulated in our proteomics screen, Erlin-1 and Erlin-2 (1.6 and 2.2 fold respectively, q values 0.047 and 0.007), are highly enriched in ER-resident lipid rafts and at MAMs (Browman et al., 2006). Furthermore, there are reports of direct PERK activation by ER membrane lipid saturation, irrespective of protein synthesis status (Volmer et al., 2013). This is of special interest in our model, where we were unable to verify the activation of the IRE1 and the ATF6 branch of ER stress (data not shown).

Compounded with previous reports of mitochondrial dynamics being tightly linked to ER stress, these data confirm that, like Mfn2 (Debattisti 2014, Diaz 2015, Schneeberger 2013, Munoz 2013, Ngoh 2012), also Drp1 deficiency results in ER stress. However, aside from few reports indicating a possible alternative localization and membrane tubulation activity of Drp1 to the ER (Pitts et al., 1999; Yoon et al., 1998), there is little mechanistic evidence of how Drp1 deficiency would mediate ER stress. Analysis of mitochondrial and ER lipid content, in combination with published FRET sensors that evaluate ER-mitochondria apposition (Csordás et al., 2010), would certainly be of interest in this regard.

In spite of evidence supporting the activation of different branches of the integrated stress response, the specific detection of the eIF2 α -phosphorylating kinase in our model was not

technically feasible. This is due in part to the inabundance of these proteins and the asynchronous nature of their activation, and in part to the poor performance of existing antisera (Prof. David Ron, Cambridge, UK, personal communication). Nevertheless, although we lack a full understanding of the combination of signals that trigger eIF2 α phosphorylation, our data do show that the integrated stress response is activated in Drp1^{flx/flx} Cre⁺ brains, already in the early stages of the phenotype. Of note, it could be argued that the observed upregulation of cytosolic aminoacyl tRNA synthetases is a consequence, rather than a cause, of ISR activation, as these genes are transcriptional targets of ATF4 (Han et al., 2013). Nevertheless, the consensus in the field is that ATF4 does not always transcribe the full range of its target genes, but rather functions in a combinatorial manner with other transcription factors, which determine the scope and the nature of the response (Kilberg et al., 2009).

One single attempt at a pharmacological rescue with recently published small-molecule inhibitor of P-eIF2 α ISRIB (Sidrauski et al., 2013) failed to decrease ATF4 in Drp1^{flx/flx} Cre⁺ brains (data not shown); thus, a better dose titration needs to be performed to ensure sufficient bioavailability in the brain during a long-term treatment.

ATF4 is a transcription factor that binds to conserved CCAAT-enhancer binding protein-activating transcription factor response elements (CARE) to mediate expression of target genes. It does not, however, act independently, but it is always found in combination with other transcription factors (e.g. members of the C/EBP family, ATF3); thus, the general consensus is that the combination of binding sites and of the respective transcription factors will determine whether a gene is expressed in response to certain ATF4-inducing stresses (Kilberg et al., 2009). In our mouse model, Chromatin ImmunoPrecipitation (ChIP) would be instrumental not only in confirming ATF4 presence on the Fgf21 promoter, but also to identify other co-regulated genes that could constitute a specific signature of mitochondrial dysfunction due to fission deletion.

Overall, though the data show a marked and early-onset ER stress response in Drp1^{flx/flx} Cre⁺ brains, the failure of two separate rescue approaches to significantly reduce the ISR response raises the possibility that more than one branch, or alternatively different

combinations of branches in different brain regions, are responsible for the activation of the integrated stress response via eIF2 α phosphorylation.

6.2. Ectopic Fgf21 expression in Drp1^{flx/flx} Cre⁺ brains causes a systemic catabolic phenotype

One remarkable finding of this work is that Drp1 ablation causes the forebrain to produce metabolic cytokine Fibroblast Growth Factor 21 (Fgf21). Of note, there is one report of glial cells expressing Fgf21 when in culture, and also of steady-state protein expression of Fgf21 in untreated rodent brain (Mäkelä et al., 2014); we were, however, unable to reproduce this finding in the brains of untreated mice (data not shown). Even so, the general consensus is that the brain does not canonically express relevant levels of Fgf21 (Fisher and Maratos-Flier, 2015; Suomalainen et al., 2011). This raises a number of interesting possibilities, both for the understanding of Fgf21 physiology and for the potential diagnostic applications of such a finding.

While the spectrum of systemic actions of Fgf21 is still being dissected (Fisher and Maratos-Flier, 2015), a prominent role for the CNS in the coordination of Fgf21 action is emerging. Indeed, hypothalamic coreceptor KLB is indispensable for Fgf21 action, and intracerebroventricular (icv) injection of Fgf21 is sufficient to induce all associated metabolic alterations (Bookout et al., 2013; Owen et al., 2014). In contrast, in our model, localized Fgf21 production in the brain does not recapitulate all the canonical features of increased Fgf21 signaling: specifically, while corticosterone production and lipolysis do occur, there is no comparable change in glucose clearance or in insulin sensitivity (Figure 5.3 A-C), nor in ketone bodies generation (data not shown).

The apparent disagreement with the icv injection experiments can be explained by the fact that, in our model, Fgf21 production is very localized, and its presence in the general circulation, though statistically significant, is likely negligible, since it is one order of magnitude lower than the canonical starvation-induced Fgf21 increase (Figure 5.4 A). On the other hand, icv-injected Fgf21 would still be able to access the general circulation, as it

crosses the blood-brain barrier, and the administered dose was several orders of magnitude greater than our detected circulating Fgf21 (in the range of μ grams/day; (Douris et al., 2015; Owen et al., 2014)).

Of note, published work, as well as our own experiments (data not shown), indicate that the CamK2 α promoter that drives Cre expression in our model is active also in the suprachiasmatic and paraventricular nuclei of the hypothalamus (Bookout et al., 2013; Owen et al., 2014). This would imply that autocrine signaling, in addition to paracrine action of hippocampus- and cortex-produced Fgf21, is in place.

Ours is the first report of Fgf21 expression having deleterious effects in mice, aside from the observation that Fgf21 administration can lead to bone loss (Kolumam et al., 2015; Wu et al., 2013a). The general agreement in the field is actually that Fgf21 administration improves a number of metabolic parameters (Degirolamo et al., 2016; Kharitononkov and DiMarchi, 2015); constitutive overexpression of Fgf21 is even associated to a lean phenotype and increased longevity (Zhang et al., 2012). In light of our results, we postulate that the concerted action of the central and peripheral Fgf21 target organs is critical for the metabolism-enhancing effects of Fgf21. We believe that, in our model, exclusively activating the CNS-controlled component of Fgf21 signaling results in excessive catabolism and lethality. Further analysis of organ-specific signaling pathways would be required to demonstrate that Fgf21-dependent cascades are active in the CNS but not in the periphery. However, to conclusively demonstrate the separation of central and peripheral Fgf21 signaling, organ-specific KLB knockout mice would be required.

Two aspects of Fgf21 physiology that do become activated in our model system are corticosterone production and sympathetic nervous system activation, both through CRH induction in the paraventricular nucleus (Owen et al., 2014). The former results in sustained high levels of circulating corticosterone, while the latter conveys the lipolysis signal from the CNS to the BAT. Though we could not detect a statistically significant increase in circulating CRH in our mice (Figure 5.3 J), possibly due to negative feedback by corticosterone, we did

see a trend of increase; these results could be corroborated by qRT-PCR analysis on hypothalamus from $Drp1^{flx/flx} Cre^+$ mice.

It is unclear how a state of continuously high corticosterone does not result in a Cushing-like phenotype in our mice, considering that, normally, pharmacological Cushing induction is already visible over a 3-week pharmacological treatment (Cassano et al., 2012). As no Cushing-like symptoms were observed in the Fgf21-overexpressing mice either (Zhang et al., 2012), one could speculate that Fgf21 is able to compensate the effects of corticosterone; of course one alternative interpretation in the constitutive overexpressing mouse is that Fgf21 expression from birth triggers an adaptation to glucocorticoids (this aspect was not examined in the original paper).

Nevertheless, the mixed results from the genetic rescue (Figure 5.8), conditionally ablating Fgf21 in the same cells where Drp1 was ablated, suggest an additional layer of complexity in the phenotype. Indeed, tamoxifen-injected $Drp1^{flx/flx} Fgf21^{flx/flx} Cre^+$ mice have decreased, but not completely abolished, Fgf21 expression (Figure 5.8 C), which makes it difficult to conclusively prove a causal role for Fgf21 in mediating the phenotype. As it is, we cannot mechanistically dissect whether the improved weight profile but unchanged lethality in triple transgenic mice is due to residual Fgf21 activity or to the fact that other processes, and not Fgf21 alone, are causally involved in the phenotype.

There are two possible explanations for the incomplete deletion of Fgf21 in $Drp1^{flx/flx} Fgf21^{flx/flx} Cre^+$ mice:

- (I) That Cre activation by tamoxifen was not sufficient to recombine the Fgf21 locus in all cells in which Drp1 recombination occurred. The confirmation of this hypothesis would be rather laborious, as one could not accurately distinguish between the un-recombined neuronal Fgf21 locus and the surrounding un-recombined glia. A longer tamoxifen treatment might be effective to allow for full recombination in this case.
- (II) That the source of Fgf21 is not only neurons, where the Cre is expressed, but also the surrounding glia, sensing energetic distress in neurons. Intriguingly, the one

report indicating Fgf21 expression in the brain then claims that glial cells *in vitro* produce Fgf21. In situ hybridization setup is currently ongoing to verify whether Fgf21 mRNA can be detected as colocalizing with astrocytic, neuronal, microglial or oligodendroglial markers. One alternative, complementary approach would be to perform single-cell RNA-sequencing on a cell suspension from Drp1^{flx/flx} Cre⁺ brains (and eventually on triple transgenics; see for instance (Darmanis et al., 2015; Johnson et al., 2015)); in addition to revealing the source of Fgf21, this experiment would also yield further insight into which cellular responses are activated in which cell type. Such a mechanistic dissection of neuron-glia crosstalk would undoubtedly shed some light on the largely controversial topic of intercellular metabolism within the CNS (Magistretti and Allaman, 2015).

There is, naturally, the additional possibility that Fgf21 deletion is not sufficient to rescue the phenotype of Drp1^{flx/flx} Cre⁺ mice because it is not the main mediator of the systemic metabolic shift. While the evidence of corticosterone production and BAT lipolysis is compelling, discrete aspects of the phenotype could have other explanations.

For instance, other proteins and polypeptides have been associated to BAT activation and systemic metabolic effects, foremost among them irisin (Boström et al., 2012) and mitochondria-derived peptide MOTS-C (Lee et al., 2015). While they did not appear to be present in our proteomics panel, further confirmation of their absence in Drp1^{flx/flx} Cre⁺ brains would strengthen the case for Fgf21, as would a full Fgf21 ablation in all cells.

It could be argued that sympathetic nervous system-induced lipolysis and corticosterone could recapitulate most of the observed phenotype. An accurate approach to dissect the relative contribution of each process to the phenotype would be to target them individually. First, sympathetic nervous system activity can be systemically attenuated with β -blockers, which have a well-known pharmacology and are compatible with a long-term treatment. It is important to note that broad-range β -blockers would have to be employed, in order to target canonical β 1 and β 2 adrenoreceptors in addition to β 3, which is expressed in BAT (Kajimura and Saito, 2014).

Second, corticosterone synthesis can be blocked by ketoconazole or other inhibitors of steroidogenesis, which are currently used as a treatment for Cushing's syndrome (Daniel and Newell-Price, 2015).

Third, the sympathetic connection between the brain and BAT, mediating lipolysis, can be surgically ablated (sympathectomy). This approach is currently ongoing, with the technique established (Figure 6.2 A-B) and the first mouse cohort operated and under monitoring (Figure 6.2 C). For the other two approaches, animal permission is pending.

While the ongoing experiments will confirm the relative contribution of secondary factors to the overall phenotype, our data convincingly pinpoint *Fgf21* as a marker for mitochondrial dynamics dysfunction in the brain. An interesting follow-up project would be the systematic investigation of *Fgf21* expression in diseases of primary mitochondrial morphology dysfunction (See chapter 1.1.4.2), as well as in conditions in which mitochondrial dynamics are affected as a downstream effect of an unrelated pathogenic mutation (Chapter 1.1.4.1); for instance, a tauopathy mouse model overexpressing the pathological P301L-mutated Tau protein has been reported to show increased ISR activation (Radford et al., 2015).

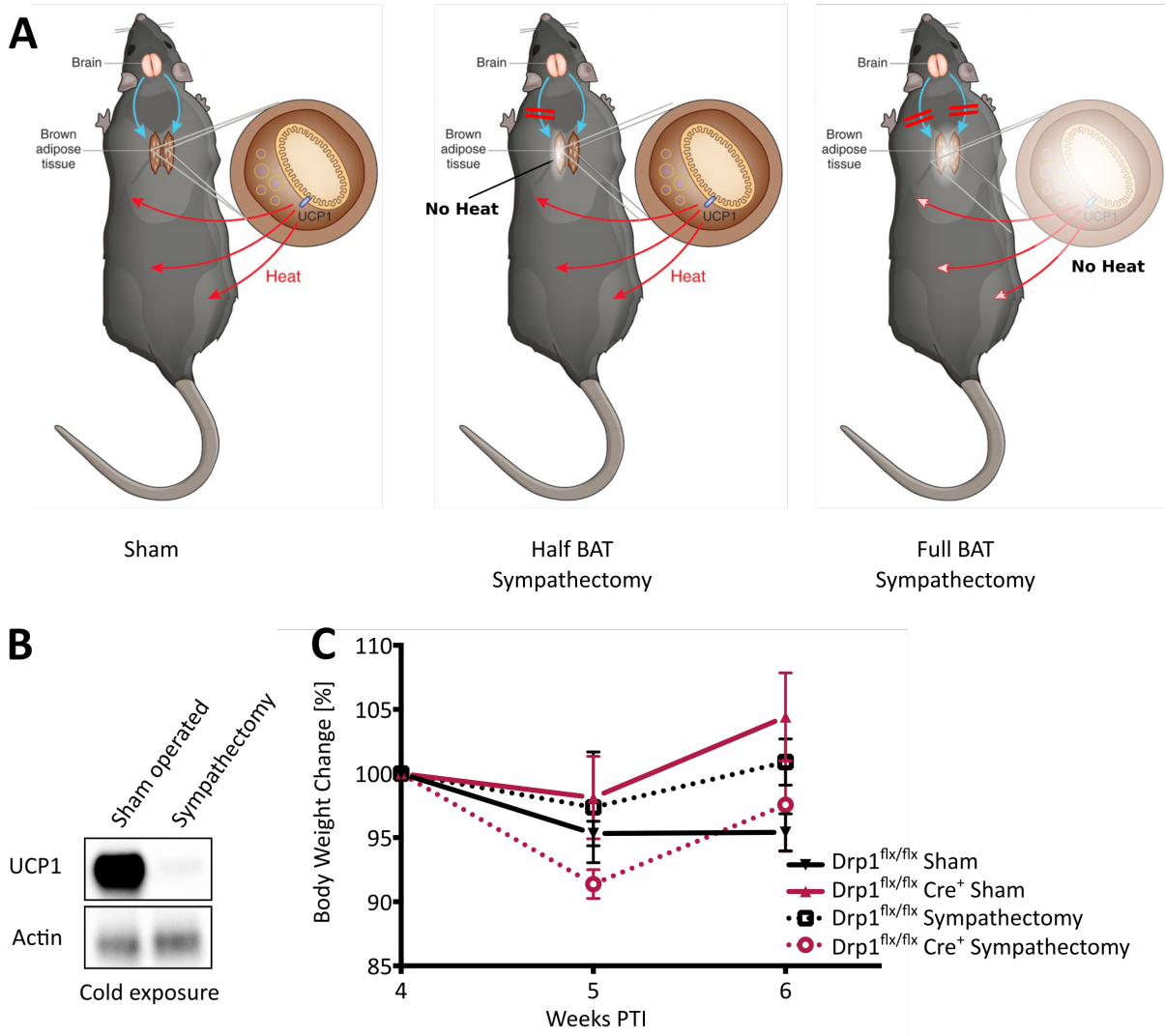


Figure 6.2 Sympathectomy model. (A) Surgery rationale. In untreated mice, there are two nerve bundles connecting the brain to the BAT; a half sympathectomy allows one to verify the extent of denervation; a full sympathectomy completely ablates BAT sympathetic innervation and the ensuing UCP1-mediated thermogenesis. (B) UCP1 protein levels after half sympathectomy. The two samples are derived from the same mouse, which has undergone a half sympathectomy and then has been placed at 4°C for 48 hours to induce thermogenesis. (C) Full sympathectomy monitoring. A cohort of mice was fully denervated (or sham operated), and monitoring is still ongoing. % body weight is plotted as a function of time.

6.3. Conclusion and perspectives

Our data show that irreversible Drp1 ablation, even when confined to adult neurons, gives rise to a stress response that culminates in the death of the animal. This piece of information complements a body of work indicating Drp1 blockage as an effective way of delaying or preventing apoptosis in case of acute stress in the CNS (Estaquier and Arnoult, 2007; Frank et al., 2001; Lee et al., 2004; Li et al., 2015; Liu et al., 2015a; Xie et al., 2013), and it poses the caveat that such blockage needs to be reversible and short-term. Previous work had primarily exploited pharmacological Drp1 inhibitor mdivi-1 (Cassidy-Stone et al., 2008); whereas the results of these studies were encouraging, mdivi-1 suffers from a number of off-target effects which effectively preclude its use as a therapeutic agent *in vivo*. In fact, mdivi-1 inhibits mitochondrial respiration even in the absence of Drp1, and it affects cell membrane potential and ion currents (Qian et al., 2014; So et al., 2012). As such, while still a valuable research tool, mdivi-1 will need to be vastly improved before it can be considered as a therapeutic strategy (Qian et al., 2013).

One promising alternative to pharmacological Drp1 inhibition is a newly-discovered Drp1 peptide inhibitor, P110, which interferes with Drp1 binding to its receptor Fis1, and has been shown to prevent mitochondrial fission in a cell model of PD (Qi et al., 2013); further research will need to confirm whether lack of activity of P110 on Mff-driven mitochondrial fission, which is the most prevalent, will affect its potential uses.

Another potential target that has recently emerged as a regulator of mitochondrial fission is its upstream phosphatase, calcineurin; indeed, systemic and skeletal muscle-specific deletion of calcineurin results in a hyperelongated mitochondrial phenotype (Pfluger et al., 2015). This raises the possibility that one could act on Drp1 by inhibiting its activator calcineurin, rather than on Drp1 itself.

Of special relevance to this work is the observation that calcineurin ablation leads to resistance to diet-induced obesity and ensuing comorbidities (Pfluger et al., 2015).

Remarkably, though the authors state that neuron-derived orphan receptor 1 (*NOR-1*) elevation is responsible for the systemic metabolic effects of calcineurin deletion, without any mechanistic confirmation, *Fgf21* mRNA is also upregulated in their microarray analysis.

An interesting issue that emerges from our work is that *Fgf21*, which has so far been touted as a universally positive metabolism-enhancing agent, can actually be lethal when its bioavailability is altered. This hypothesis, if corroborated by further experiments, will undoubtedly need to inform therapy design, given that *Fgf21*-mimicking compounds are being explored as pharmacological treatments for type-2 diabetes and obesity, with promising results (Fisher and Maratos-Flier, 2015; Gaich et al., 2013).

In conclusion, our work highlights a novel link between mitochondrial fission and *Fgf21*, and opens up new avenues of research into the influence of neuronal mitochondrial morphology in the central regulation of systemic metabolism.

7. References

- Ackema, K.B., Hench, J., Böckler, S., Wang, S.C., Sauder, U., Mergentaler, H., Westermann, B., Bard, F., Frank, S., and Spang, A. (2014). The small GTPase Arf1 modulates mitochondrial morphology and function. *EMBO J.* *33*, 2659–2675.
- Alexander, C., Votruba, M., Pesch, U.E., Thiselton, D.L., Mayer, S., Moore, A., Rodriguez, M., Kellner, U., Leo-Kottler, B., Auburger, G., et al. (2000). OPA1, encoding a dynamin-related GTPase, is mutated in autosomal dominant optic atrophy linked to chromosome 3q28. *Nat Genet* *26*, 211–215.
- Anand, B.K., and Brobeck, J.R. (1951). Hypothalamic control of food intake in rats and cats. *Yale J. Biol. Med.* *24*, 123–140.
- Anand, R., Wai, T., Baker, M.J., Kladt, N., Schauss, A.C., Rugarli, E., and Langer, T. (2014). The i-AAA protease YME1L and OMA1 cleave OPA1 to balance mitochondrial fusion and fission. *J. Cell Biol.* *204*, 919–929.
- Anikster, Y., Kleta, R., Shaag, A., Gahl, W.A., and Elpeleg, O. (2001). Type III 3-methylglutaconic aciduria (optic atrophy plus syndrome, or Costeff optic atrophy syndrome): identification of the OPA3 gene and its founder mutation in Iraqi Jews. *Am. J. Hum. Genet.* *69*, 1218–1224.
- Antignani, A., and Youle, R.J. (2006). How do Bax and Bak lead to permeabilization of the outer mitochondrial membrane? *Curr. Opin. Cell Biol.* *18*, 685–689.
- Aponte, Y., Atasoy, D., and Sternson, S.M. (2011). AGRP neurons are sufficient to orchestrate feeding behavior rapidly and without training. *Nat. Neurosci.* *14*, 351–355.
- Arasaki, K., Shimizu, H., Mogari, H., Nishida, N., Hirota, N., Furuno, A., Kudo, Y., Baba, M., Baba, N., Cheng, J., et al. (2015). A role for the ancient SNARE syntaxin 17 in regulating mitochondrial division. *Dev. Cell* *32*, 304–317.
- Area-Gomez, E., de Groof, A., Boldogh, I., Bird, T., Gibson, G., Koehler, C., Yu, W., Duff, K., Yaffe, M., Pon, L., et al. (2009). Presenilins are enriched in endoplasmic reticulum membranes associated with mitochondria. *Am. J. Pathol.* *175*, 1810–1816.
- Babbar, M., and Sheikh, M.S. (2013). Metabolic Stress and Disorders Related to Alterations in Mitochondrial Fission or Fusion. *Mol. Cell. Pharmacol.* *5*, 109–133.
- Badman, M.K., Pissios, P., Kennedy, A.R., Koukos, G., Flier, J.S., and Maratos-Flier, E. (2007). Hepatic fibroblast growth factor 21 is regulated by PPARalpha and is a key mediator of hepatic lipid metabolism in ketotic states. *Cell Metab.* *5*, 426–437.
- Barneo-Muñoz, M., Juárez, P., Civera-Tregón, A., Yndriago, L., Pla-Martin, D., Zenker, J., Cuevas-Martín, C., Estela, A., Sánchez-Aragó, M., Forteza-Vila, J., et al. (2015). Lack of GDAP1 induces neuronal calcium and mitochondrial defects in a knockout mouse model of charcot-marie-tooth neuropathy. *PLoS Genet.* *11*, e1005115.
- Barsoum, M.J., Yuan, H., Gerencser, A.A., Liot, G., Kushnareva, Y., Gräber, S., Kovacs, I., Lee, W.D., Waggoner, J., Cui, J., et al. (2006). Nitric oxide-induced mitochondrial fission is regulated by dynamin-related GTPases in neurons. *EMBO J.* *25*, 3900–3911.
- Baughman, J., Perocchi, F., Girgis, H., Plovanich, M., Belcher-Timme, C., Sancak, Y., Bao, X., Strittmatter, L., Goldberger, O., Bogorad, R., et al. (2011). Integrative genomics identifies MCU as an essential component of the mitochondrial calcium uniporter. *Nature* *476*, 341–345.
- Becker, E.M., Greer, J.M., Ponka, P., and Richardson, D.R. (2002). Erythroid differentiation and protoporphyrin IX down-regulate frataxin expression in Friend cells: characterization of frataxin expression compared to molecules involved in iron metabolism and hemoglobinization. *Blood* *99*, 3813–3822.
- Berthet, A., Margolis, E.B., Zhang, J., Hsieh, I., Zhang, J., Hnasko, T.S., Ahmad, J., Edwards, R.H., Sesaki, H., Huang, E.J., et al. (2014). Loss of Mitochondrial Fission Depletes Axonal Mitochondria in Midbrain Dopamine Neurons. *J. Neurosci.* *34*, 14304–14317.

- Betley, J.N., Cao, Z.F.H., Ritola, K.D., and Sternson, S.M. (2013). Parallel, redundant circuit organization for homeostatic control of feeding behavior. *Cell* *155*, 1337–1350.
- Bookout, A.L., de Groot, M.H., Owen, B.M., Lee, S., Gautron, L., Lawrence, H.L., Ding, X., Elmquist, J.K., Takahashi, J.S., Mangelsdorf, D.J., et al. (2013). FGF21 regulates metabolism and circadian behavior by acting on the nervous system. *Nat Med* *19*, 1147–1152.
- Boron, W.F., and Boulpaep, E.L. (2009). *Medical physiology : a cellular and molecular approach* (Philadelphia, PA: Saunders/Elsevier).
- Bossy, B., Petrilli, A., Klinglmayr, E., Chen, J., Lütz-Meindl, U., Knott, A.B., Masliah, E., Schwarzenbacher, R., and Bossy-Wetzel, E. (2010). S-Nitrosylation of DRP1 does not affect enzymatic activity and is not specific to Alzheimer's disease. *J. Alzheimers Dis. JAD* *20 Suppl 2*, S513–S526.
- Boström, P., Wu, J., Jedrychowski, M.P., Korde, A., Ye, L., Lo, J.C., Rasbach, K.A., Boström, E.A., Choi, J.H., Long, J.Z., et al. (2012). A PGC1- α -dependent myokine that drives brown-fat-like development of white fat and thermogenesis. *Nature* *481*, 463–468.
- Bouchard, C., and Tremblay, A. (1990). Genetic effects in human energy expenditure components. *Int. J. Obes. 14 Suppl 1*, 49–55; discussion 55–58.
- Bradbury, J. (2004). Mitochondrial fusion protein mutated in CMT2A. *Lancet Neurol.* *3*, 326.
- Brand, M.D., Brindle, K.M., Buckingham, J.A., Harper, J.A., Rolfe, D.F., and Stuart, J.A. (1999). The significance and mechanism of mitochondrial proton conductance. *Int. J. Obes. Relat. Metab. Disord. J. Int. Assoc. Study Obes.* *23 Suppl 6*, S4–S11.
- Braschi, E., Zunino, R., and McBride, H.M. (2009). MAPL is a new mitochondrial SUMO E3 ligase that regulates mitochondrial fission. *EMBO Rep.* *10*, 748–754.
- Braschi, E., Goyon, V., Zunino, R., Mohanty, A., Xu, L., and McBride, H.M. (2010). Vps35 mediates vesicle transport between the mitochondria and peroxisomes. *Curr. Biol. CB* *20*, 1310–1315.
- Bravo, R., Gutierrez, T., Paredes, F., Gatica, D., Rodriguez, A.E., Pedrozo, Z., Chiong, M., Parra, V., Quest, A.F.G., Rothermel, B.A., et al. (2012). Endoplasmic reticulum: ER stress regulates mitochondrial bioenergetics. *Int. J. Biochem. Cell Biol.* *44*, 16–20.
- Breckenridge, D.G., Stojanovic, M., Marcellus, R.C., and Shore, G.C. (2003). Caspase cleavage product of BAP31 induces mitochondrial fission through endoplasmic reticulum calcium signals, enhancing cytochrome c release to the cytosol. *J. Cell Biol.* *160*, 1115–1127.
- de Brito, O.M., and Scorrano, L. (2008). Mitofusin 2 tethers endoplasmic reticulum to mitochondria. *Nature* *456*, 605–610.
- Browman, D.T., Resek, M.E., Zajchowski, L.D., and Robbins, S.M. (2006). Erlin-1 and erlin-2 are novel members of the prohibitin family of proteins that define lipid-raft-like domains of the ER. *J. Cell Sci.* *119*, 3149–3160.
- Browne, G.J., Finn, S.G., and Proud, C.G. (2004). Stimulation of the AMP-activated protein kinase leads to activation of eukaryotic elongation factor 2 kinase and to its phosphorylation at a novel site, serine 398. *J. Biol. Chem.* *279*, 12220–12231.
- Buhlman, L., Damiano, M., Bertolin, G., Ferrando-Miguel, R., Lombès, A., Brice, A., and Corti, O. (2014). Functional interplay between Parkin and Drp1 in mitochondrial fission and clearance. *Biochim. Biophys. Acta* *1843*, 2012–2026.
- Burté, F., Carelli, V., Chinnery, P.F., and Yu-Wai-Man, P. (2015). Disturbed mitochondrial dynamics and neurodegenerative disorders. *Nat. Rev. Neurol.* *11*, 11–24.
- Cai, Q., Gerwin, C., and Sheng, Z.-H. (2005). Syntabulin-mediated anterograde transport of mitochondria along neuronal processes. *J. Cell Biol.* *170*, 959–969.
- Calvo, S.E., Clauser, K.R., and Mootha, V.K. (2016). MitoCarta2.0: an updated inventory of mammalian mitochondrial proteins. *Nucleic Acids Res.* *44*, D1251–D1257.
- Cannon, B., and Nedergaard, J. (2004). Brown adipose tissue: function and physiological significance. *Physiol. Rev.* *84*, 277–359.

- Cardoso, S., Correia, S., Carvalho, C., Candeias, E., Plácido, A.I., Duarte, A.I., Seíça, R.M., and Moreira, P.I. (2014). Perspectives on mitochondrial uncoupling proteins-mediated neuroprotection. *J. Bioenerg. Biomembr.* *47*, 119–131.
- Carling, D. (2004). AMPK. *Curr. Biol.* *14*, R220.
- Cassano, A.E., White, J.R., Penraat, K.A., Wilson, C.D., Rasmussen, S., and Karatsoreos, I.N. (2012). Anatomic, hematologic, and biochemical features of C57BL/6NCr mice maintained on chronic oral corticosterone. *Comp. Med.* *62*, 348–360.
- Cassidy-Stone, A., Chipuk, J.E., Ingerman, E., Song, C., Yoo, C., Kuwana, T., Kurth, M.J., Shaw, J.T., Hinshaw, J.E., Green, D.R., et al. (2008). Chemical inhibition of the mitochondrial division dynamin reveals its role in Bax/Bak-dependent mitochondrial outer membrane permeabilization. *Dev. Cell* *14*, 193–204.
- Cereghetti, G., Stangherlin, A., Martins de Brito, O., Chang, C., Blackstone, C., Bernardi, P., and Scorrano, L. (2008). Dephosphorylation by calcineurin regulates translocation of Drp1 to mitochondria. *Proc. Natl. Acad. Sci. U. S. A.* *105*, 15803–15808.
- Chami, M., Oulès, B., Szabadkai, G., Tacine, R., Rizzuto, R., and Paterlini-Bréchet, P. (2008). Role of SERCA1 truncated isoform in the proapoptotic calcium transfer from ER to mitochondria during ER stress. *Mol. Cell* *32*, 641–651.
- Chan, D. (2012). Fusion and fission: interlinked processes critical for mitochondrial health. *Annu. Rev. Genet.* *46*, 265–287.
- Chan, N.C., Salazar, A.M., Pham, A.H., Sweredoski, M.J., Kolawa, N.J., Graham, R.L.J., Hess, S., and Chan, D.C. (2011). Broad activation of the ubiquitin-proteasome system by Parkin is critical for mitophagy. *Hum. Mol. Genet.* *20*, 1726–1737.
- Chang, C.-R., and Blackstone, C. (2007). Drp1 phosphorylation and mitochondrial regulation. *EMBO Rep.* *8*, 1088–1089; author reply 1089–1090.
- Chang, D.T.W., Rintoul, G.L., Pandipati, S., and Reynolds, I.J. (2006). Mutant huntingtin aggregates impair mitochondrial movement and trafficking in cortical neurons. *Neurobiol. Dis.* *22*, 388–400.
- Chen, Y., and Sheng, Z.-H. (2013). Kinesin-1-syntrophin coupling mediates activity-dependent regulation of axonal mitochondrial transport. *J. Cell Biol.* *202*, 351–364.
- Chen, H., Detmer, S.A., Ewald, A.J., Griffin, E.E., Fraser, S.E., and Chan, D.C. (2003). Mitofusins Mfn1 and Mfn2 coordinately regulate mitochondrial fusion and are essential for embryonic development. *J. Cell Biol.* *160*, 189–200.
- Cho, D.-H., Nakamura, T., Fang, J., Cieplak, P., Godzik, A., Gu, Z., and Lipton, S.A. (2009). S-nitrosylation of Drp1 mediates beta-amyloid-related mitochondrial fission and neuronal injury. *Science* *324*, 102–105.
- Cho, D.H., Nakamura, T., and Lipton, S.A. (2010). Mitochondrial dynamics in cell death and neurodegeneration. *Cell Mol Life Sci* *67*, 3435–3447.
- Choi, S.-Y., Huang, P., Jenkins, G.M., Chan, D.C., Schiller, J., and Frohman, M.A. (2006). A common lipid links Mfn-mediated mitochondrial fusion and SNARE-regulated exocytosis. *Nat. Cell Biol.* *8*, 1255–1262.
- Cipolat, S., Rudka, T., Hartmann, D., Costa, V., Serneels, L., Craessaerts, K., Metzger, K., Frezza, C., Annaert, W., D’Adamio, L., et al. (2006). Mitochondrial rhomboid PARL regulates cytochrome c release during apoptosis via OPA1-dependent cristae remodeling. *Cell* *126*, 163–175.
- Civiletto, G., Varanita, T., Cerutti, R., Gorletta, T., Barbaro, S., Marchet, S., Lamperti, C., Viscomi, C., Scorrano, L., and Zeviani, M. (2015). Opa1 overexpression ameliorates the phenotype of two mitochondrial disease mouse models. *Cell Metab.* *21*, 845–854.
- Cogliati, S., Frezza, C., Soriano, M.E., Varanita, T., Quintana-Cabrera, R., Corrado, M., Cipolat, S., Costa, V., Casarin, A., Gomes, L.C., et al. (2013). Mitochondrial cristae shape determines respiratory chain supercomplexes assembly and respiratory efficiency. *Cell* *155*, 160–171.
- Cohen, Y., Klug, Y.A., Dimitrov, L., Erez, Z., Chuartzman, S.G., Elinger, D., Yofe, I., Soliman, K., Gärtner, J., Thoms, S., et al. (2014). Peroxisomes are juxtaposed to strategic sites on mitochondria. *Mol. Biosyst.* *10*, 1742–1748.

- Copeland, D.E., and Dalton, A.J. (1959). An association between mitochondria and the endoplasmic reticulum in cells of the pseudobranch gland of a teleost. *J Biophys Biochem Cytol* 5, 393–396.
- Costa, M., Jagasia, R., and Berninger, B. (2010). Directed Neuronal Differentiation of Embryonic and Adult-Derived Neurosphere Cells. *Protoc. Neural Cell Cult.*
- Cowley, M.A., Smart, J.L., Rubinstein, M., Cerdán, M.G., Diano, S., Horvath, T.L., Cone, R.D., and Low, M.J. (2001). Leptin activates anorexigenic POMC neurons through a neural network in the arcuate nucleus. *Nature* 411, 480–484.
- Cribbs, J.T., and Strack, S. (2007). Reversible phosphorylation of Drp1 by cyclic AMP-dependent protein kinase and calcineurin regulates mitochondrial fission and cell death. *EMBO Rep.* 8, 939–944.
- Crooks, D.R., Natarajan, T.G., Jeong, S.Y., Chen, C., Park, S.Y., Huang, H., Ghosh, M.C., Tong, W.H., Haller, R.G., Wu, C., et al. (2014). Elevated FGF21 secretion, PGC-1 α and ketogenic enzyme expression are hallmarks of iron-sulfur cluster depletion in human skeletal muscle. *Hum Mol Genet* 23, 24–39.
- Csordás, G., Várnai, P., Golenár, T., Roy, S., Purkins, G., Schneider, T.G., Balla, T., and Hajnóczky, G. (2010). Imaging interorganelle contacts and local calcium dynamics at the ER-mitochondrial interface. *Mol. Cell* 39, 121–132.
- Cuevas-Ramos, D., Almeda-Valdés, P., Meza-Arana, C.E., Brito-Córdova, G., Gómez-Pérez, F.J., Mehta, R., Oseguera-Moguel, J., and Aguilar-Salinas, C.A. (2012). Exercise increases serum fibroblast growth factor 21 (FGF21) levels. *PLoS One* 7, e38022.
- Cypess, A.M., Lehman, S., Williams, G., Tal, I., Rodman, D., Goldfine, A.B., Kuo, F.C., Palmer, E.L., Tseng, Y.-H., Doria, A., et al. (2009). Identification and importance of brown adipose tissue in adult humans. *N. Engl. J. Med.* 360, 1509–1517.
- Daniel, E., and Newell-Price, J.D.C. (2015). Therapy of endocrine disease: steroidogenesis enzyme inhibitors in Cushing's syndrome. *Eur. J. Endocrinol. Eur. Fed. Endocr. Soc.* 172, R263–R280.
- Darmanis, S., Sloan, S.A., Zhang, Y., Enge, M., Caneda, C., Shuer, L.M., Hayden Gephart, M.G., Barres, B.A., and Quake, S.R. (2015). A survey of human brain transcriptome diversity at the single cell level. *Proc. Natl. Acad. Sci. U. S. A.* 112, 7285–7290.
- Debattisti, V., Pendin, D., Ziviani, E., Daga, A., and Scorrano, L. (2014). Reduction of endoplasmic reticulum stress attenuates the defects caused by *Drosophila* mitofusin depletion. *J. Cell Biol.* 204, 303–312.
- Degriolamo, C., Sabbà, C., and Moschetta, A. (2016). Therapeutic potential of the endocrine fibroblast growth factors FGF19, FGF21 and FGF23. *Nat. Rev. Drug Discov.* 15, 51–69.
- Demetrius, L.A., Magistretti, P.J., and Pellerin, L. (2014). Alzheimer's disease: the amyloid hypothesis and the Inverse Warburg effect. *Front. Physiol.* 5, 522.
- De Stefani, D., Raffaello, A., Teardo, E., Szabò, I., and Rizzuto, R. (2011). A forty-kilodalton protein of the inner membrane is the mitochondrial calcium uniporter. *Nature* 476, 336–340.
- Detmer, S.A., and Chan, D.C. (2007). Functions and dysfunctions of mitochondrial dynamics. *Nat. Rev. Mol. Cell Biol.* 8, 870–879.
- De Vos, K.J., Chapman, A.L., Tennant, M.E., Manser, C., Tudor, E.L., Lau, K.-F., Brownlee, J., Ackerley, S., Shaw, P.J., McLoughlin, D.M., et al. (2007). Familial amyotrophic lateral sclerosis-linked SOD1 mutants perturb fast axonal transport to reduce axonal mitochondria content. *Hum. Mol. Genet.* 16, 2720–2728.
- Diaz, B., Fuentes-Mera, L., Tovar, A., Montiel, T., Massieu, L., Martínez-Rodríguez, H.G., and Camacho, A. (2015). Saturated lipids decrease mitofusin 2 leading to endoplasmic reticulum stress activation and insulin resistance in hypothalamic cells. *Brain Res.* 1627, 80–89.
- Dickey, A.S., and Strack, S. (2011). PKA/AKAP1 and PP2A/B β 2 regulate neuronal morphogenesis via Drp1 phosphorylation and mitochondrial bioenergetics. *J. Neurosci. Off. J. Soc. Neurosci.* 31, 15716–15726.
- Dietrich, M.O., Liu, Z.-W., and Horvath, T.L. (2013). Mitochondrial dynamics controlled by mitofusins regulate Agrp neuronal activity and diet-induced obesity. *Cell* 155, 188–199.

- Ding, X., Boney-Montoya, J., Owen, B.M., Bookout, A.L., Coate, K.C., Mangelsdorf, D.J., and Kliewer, S.A. (2012). β Klotho is required for fibroblast growth factor 21 effects on growth and metabolism. *Cell Metab.* *16*, 387–393.
- Dogan, S.A., Pujol, C., Maiti, P., Kukat, A., Wang, S., Hermans, S., Senft, K., Wibom, R., Rugarli, E.I., and Trifunovic, A. (2014). Tissue-specific loss of DARS2 activates stress responses independently of respiratory chain deficiency in the heart. *Cell Metab.* *19*, 458–469.
- Donnelly, N., Gorman, A.M., Gupta, S., and Samali, A. (2013). The eIF2 α kinases: their structures and functions. *Cell. Mol. Life Sci. CMLS* *70*, 3493–3511.
- Douris, N., Stevanovic, D.M., Fisher, F.M., Cisu, T.I., Chee, M.J., Nguyen, N.L., Zarebidaki, E., Adams, A.C., Kharitonov, A., Flier, J.S., et al. (2015). Central Fibroblast Growth Factor 21 Browns White Fat via Sympathetic Action in Male Mice. *Endocrinology* *156*, 2470–2481.
- Du, H., Guo, L., Yan, S., Sosunov, A.A., Mckhann, G.M., and Yan, S.S. (2010). Early deficits in synaptic mitochondria in an Alzheimer's disease mouse model. *Proc. Natl. Acad. Sci. U. S. A.* *107*, 18670–18675.
- DuBoff, B., Götz, J., and Feany, M.B. (2012). Tau promotes neurodegeneration via DRP1 mislocalization in vivo. *Neuron* *75*, 618–632.
- Dugail, I. (2014). Lysosome/lipid droplet interplay in metabolic diseases. *Biochimie* *96*, 102–105.
- Dutchak, P.A., Katafuchi, T., Bookout, A.L., Choi, J.H., Yu, R.T., Mangelsdorf, D.J., and Kliewer, S.A. (2012). Fibroblast growth factor-21 regulates PPAR γ activity and the antidiabetic actions of thiazolidinediones. *Cell* *148*, 556–567.
- Ehse, S., Raschke, I., Mancuso, G., Bernacchia, A., Geimer, S., Tondera, D., Martinou, J.-C., Westermann, B., Rugarli, E.I., and Langer, T. (2009). Regulation of OPA1 processing and mitochondrial fusion by m-AAA protease isoenzymes and OMA1. *J. Cell Biol.* *187*, 1023–1036.
- Eiyama, A., and Okamoto, K. (2015). PINK1/Parkin-mediated mitophagy in mammalian cells. *Curr. Opin. Cell Biol.* *33*, 95–101.
- Estaquier, J., and Arnoult, D. (2007). Inhibiting Drp1-mediated mitochondrial fission selectively prevents the release of cytochrome c during apoptosis. *Cell Death Differ.* *14*, 1086–1094.
- Faelber, K., Posor, Y., Gao, S., Held, M., Roske, Y., Schulze, D., Haucke, V., Noé, F., and Daumke, O. (2011). Crystal structure of nucleotide-free dynamin. *Nature* *477*, 556–560.
- Fang, L., Li, J., Flammer, J., and Neutzner, A. (2013). MARCH5 inactivation supports mitochondrial function during neurodegenerative stress. *Front. Cell. Neurosci.* *7*, 176.
- Figuroa-Romero, C., Iñiguez-Lluhí, J.A., Stadler, J., Chang, C.-R., Arnoult, D., Keller, P.J., Hong, Y., Blackstone, C., and Feldman, E.L. (2009). SUMOylation of the mitochondrial fission protein Drp1 occurs at multiple nonconsensus sites within the B domain and is linked to its activity cycle. *FASEB J. Off. Publ. Fed. Am. Soc. Exp. Biol.* *23*, 3917–3927.
- Fisher, F.M., and Maratos-Flier, E. (2015). Understanding the Physiology of FGF21. *Annu. Rev. Physiol.*
- Fisher, F.M., Kleiner, S., Douris, N., Fox, E.C., Mepani, R.J., Verdeguer, F., Wu, J., Kharitonov, A., Flier, J.S., Maratos-Flier, E., et al. (2012). FGF21 regulates PGC-1 α and browning of white adipose tissues in adaptive thermogenesis. *Genes Dev.* *26*, 271–281.
- Ford, M.G.J., Jenni, S., and Nunnari, J. (2011). The crystal structure of dynamin. *Nature* *477*, 561–566.
- Frank, S., Gaume, B., Bergmann-Leitner, E.S., Leitner, W.W., Robert, E.G., Catez, F., Smith, C.L., and Youle, R.J. (2001). The role of dynamin-related protein 1, a mediator of mitochondrial fission, in apoptosis. *Dev. Cell* *1*, 515–525.
- Fransson, S., Ruusala, A., and Aspenström, P. (2006). The atypical Rho GTPases Miro-1 and Miro-2 have essential roles in mitochondrial trafficking. *Biochem. Biophys. Res. Commun.* *344*, 500–510.
- Frezza, C., Cipolat, S., Martins de Brito, O., Micaroni, M., Beznoussenko, G.V., Rudka, T., Bartoli, D., Polishuck, R.S., Danial, N.N., De Strooper, B., et al. (2006). OPA1 controls apoptotic cristae remodeling independently from mitochondrial fusion. *Cell* *126*, 177–189.

- Friedman, J.R., and Nunnari, J. (2014). Mitochondrial form and function. *Nature* 505, 335–343.
- Friedman, J.R., Lackner, L.L., West, M., DiBenedetto, J.R., Nunnari, J., and Voeltz, G.K. (2011). ER tubules mark sites of mitochondrial division. *Science* 334, 358–362.
- de la Fuente, S., Fonteriz, R.I., Montero, M., and Alvarez, J. (2013). Ca²⁺ homeostasis in the endoplasmic reticulum measured with a new low-Ca²⁺-affinity targeted aequorin. *Cell Calcium* 54, 37–45.
- Fujita, T., Maturana, A.D., Ikuta, J., Hamada, J., Walchli, S., Suzuki, T., Sawa, H., Wooten, M.W., Okajima, T., Tatematsu, K., et al. (2007). Axonal guidance protein FEZ1 associates with tubulin and kinesin motor protein to transport mitochondria in neurites of NGF-stimulated PC12 cells. *Biochem. Biophys. Res. Commun.* 361, 605–610.
- Gaich, G., Chien, J.Y., Fu, H., Glass, L.C., Deeg, M.A., Holland, W.L., Kharitonov, A., Bumol, T., Schilske, H.K., and Moller, D.E. (2013). The effects of LY2405319, an FGF21 analog, in obese human subjects with type 2 diabetes. *Cell Metab.* 18, 333–340.
- Galluzzi, L., Pietrocola, F., Levine, B., and Kroemer, G. (2014). Metabolic control of autophagy. *Cell* 159, 1263–1276.
- Gandre-Babbe, S., and van der Blik, A.M. (2008). The novel tail-anchored membrane protein Mff controls mitochondrial and peroxisomal fission in mammalian cells. *Mol. Biol. Cell* 19, 2402–2412.
- Gao, A.W., Cantó, C., and Houtkooper, R.H. (2014). Mitochondrial response to nutrient availability and its role in metabolic disease. *EMBO Mol. Med.* 6, 580–589.
- Giacomello, M., Drago, I., Pizzo, P., and Pozzan, T. (2007). Mitochondrial Ca²⁺ as a key regulator of cell life and death. *Cell Death Differ.* 14, 1267–1274.
- Gomes, L.C., and Scorrano, L. (2008). High levels of Fis1, a pro-fission mitochondrial protein, trigger autophagy. *Biochim. Biophys. Acta* 1777, 860–866.
- Gomes, L.C., Di Benedetto, G., and Scorrano, L. (2011). During autophagy mitochondria elongate, are spared from degradation and sustain cell viability. *Nat. Cell Biol.* 13, 589–598.
- Guardia-Laguarta, C., Area-Gomez, E., Rüb, C., Liu, Y., Magrané, J., Becker, D., Voos, W., Schon, E.A., and Przedborski, S. (2014). α -Synuclein is localized to mitochondria-associated ER membranes. *J. Neurosci. Off. J. Soc. Neurosci.* 34, 249–259.
- Guardia-Laguarta, C., Area-Gomez, E., Schon, E.A., and Przedborski, S. (2015). Novel subcellular localization for α -synuclein: possible functional consequences. *Front. Neuroanat.* 9, 17.
- Guridi, M., Tintignac, L.A., Lin, S., Kupr, B., Castets, P., and Rüegg, M.A. (2015). Activation of mTORC1 in skeletal muscle regulates whole-body metabolism through FGF21. *Sci. Signal.* 8, ra113.
- Guzman, J.N., Sanchez-Padilla, J., Wokosin, D., Kondapalli, J., Ilijic, E., Schumacker, P.T., and Surmeier, D.J. (2010). Oxidant stress evoked by pacemaking in dopaminergic neurons is attenuated by DJ-1. *Nature* 468, 696–700.
- Haegler, P., Grünig, D., Berger, B., Krähenbühl, S., and Bouitbir, J. (2015). Impaired mitochondrial function in HepG2 cells treated with hydroxy-cobalamin[c-lactam]: A cell model for idiosyncratic toxicity. *Toxicology* 336, 48–58.
- Haelterman, N.A., Yoon, W.H., Sandoval, H., Jaiswal, M., Shulman, J.M., and Bellen, H.J. (2014). A mitocentric view of Parkinson's disease. *Annu. Rev. Neurosci.* 37, 137–159.
- Han, J., Back, S.H., Hur, J., Lin, Y.-H., Gildersleeve, R., Shan, J., Yuan, C.L., Krokowski, D., Wang, S., Hatzoglou, M., et al. (2013). ER-stress-induced transcriptional regulation increases protein synthesis leading to cell death. *Nat. Cell Biol.* 15, 481–490.
- Han, X.-J., Lu, Y.-F., Li, S.-A., Kaitsuka, T., Sato, Y., Tomizawa, K., Nairn, A.C., Takei, K., Matsui, H., and Matsushita, M. (2008). CaM kinase I α -induced phosphorylation of Drp1 regulates mitochondrial morphology. *J. Cell Biol.* 182, 573–585.

- Hao, S., Sharp, J.W., Ross-Inta, C.M., McDaniel, B.J., Anthony, T.G., Wek, R.C., Cavener, D.R., McGrath, B.C., Rudell, J.B., Koehnle, T.J., et al. (2005). Uncharged tRNA and sensing of amino acid deficiency in mammalian piriform cortex. *Science* *307*, 1776–1778.
- Harder, Z., Zunino, R., and McBride, H. (2004). Sumo1 conjugates mitochondrial substrates and participates in mitochondrial fission. *Curr. Biol. CB* *14*, 340–345.
- Hardie, D.G., Ross, F.A., and Hawley, S.A. (2012). AMP-activated protein kinase: a target for drugs both ancient and modern. *Chem. Biol.* *19*, 1222–1236.
- Hatch, A.L., Gurel, P.S., and Higgs, H.N. (2014). Novel roles for actin in mitochondrial fission. *J. Cell Sci.* *127*, 4549–4560.
- Head, B., Griparic, L., Amiri, M., Gandre-Babbe, S., and van der Blik, A.M. (2009). Inducible proteolytic inactivation of OPA1 mediated by the OMA1 protease in mammalian cells. *J. Cell Biol.* *187*, 959–966.
- Hemion, C., Flammer, J., and Neutzner, A. (2014). Quality control of oxidatively damaged mitochondrial proteins is mediated by p97 and the proteasome. *Free Radic. Biol. Med.* *75*, 121–128.
- Hetz, C., Chevet, E., and Oakes, S.A. (2015). Proteostasis control by the unfolded protein response. *Nat. Cell Biol.* *17*, 829–838.
- Hirokawa, N., Sato-Yoshitake, R., Kobayashi, N., Pfister, K.K., Bloom, G.S., and Brady, S.T. (1991). Kinesin associates with anterogradely transported membranous organelles in vivo. *J. Cell Biol.* *114*, 295–302.
- Ho, P.W.-L., Chan, D.Y.-L., Kwok, K.H.-H., Chu, A.C.-Y., Ho, J.W.-M., Kung, M.H.-W., Ramsden, D.B., and Ho, S.-L. (2005). Methyl-4-phenylpyridinium ion modulates expression of mitochondrial uncoupling proteins 2, 4, and 5 in catecholaminergic (SK-N-SH) cells. *J. Neurosci. Res.* *81*, 261–268.
- Horvath, T.L., Naftolin, F., and Leranth, C. (1992). GABAergic and catecholaminergic innervation of mediobasal hypothalamic beta-endorphin cells projecting to the medial preoptic area. *Neuroscience* *51*, 391–399.
- Hoyle, J.C., Isfort, M.C., Roggenbuck, J., and Arnold, W.D. (2015). The genetics of Charcot-Marie-Tooth disease: current trends and future implications for diagnosis and management. *Appl. Clin. Genet.* *8*, 235–243.
- Huber, N., Guimaraes, S., Schrader, M., Suter, U., and Niemann, A. (2013). Charcot-Marie-Tooth disease-associated mutants of GDAP1 dissociate its roles in peroxisomal and mitochondrial fission. *EMBO Rep.* *14*, 545–552.
- Inagaki, T., Dutchak, P., Zhao, G., Ding, X., Gautron, L., Parameswara, V., Li, Y., Goetz, R., Mohammadi, M., Esser, V., et al. (2007). Endocrine regulation of the fasting response by PPARalpha-mediated induction of fibroblast growth factor 21. *Cell Metab.* *5*, 415–425.
- Irrcher, I., Aleyasin, H., Seifert, E.L., Hewitt, S.J., Chhabra, S., Phillips, M., Lutz, A.K., Rousseaux, M.W.C., Bevilacqua, L., Jahani-Asl, A., et al. (2010). Loss of the Parkinson's disease-linked gene DJ-1 perturbs mitochondrial dynamics. *Hum. Mol. Genet.* *19*, 3734–3746.
- Ishihara, N., Nomura, M., Jofuku, A., Kato, H., Suzuki, S.O., Masuda, K., Otera, H., Nakanishi, Y., Nonaka, I., Goto, Y.-I., et al. (2009). Mitochondrial fission factor Drp1 is essential for embryonic development and synapse formation in mice. *Nat. Cell Biol.* *11*, 958–966.
- Iwasawa, R., Mahul-Mellier, A.-L., Datler, C., Pazarentzos, E., and Grimm, S. (2011). Fis1 and Bap31 bridge the mitochondria-ER interface to establish a platform for apoptosis induction. *EMBO J.* *30*, 556–568.
- James, D.I., Parone, P.A., Mattenberger, Y., and Martinou, J.-C. (2003). hFis1, a novel component of the mammalian mitochondrial fission machinery. *J. Biol. Chem.* *278*, 36373–36379.
- Johnson, C.L., Weston, J.Y., Chadi, S.A., Fazio, E.N., Huff, M.W., Kharitonov, A., Köester, A., and Pin, C.L. (2009). Fibroblast growth factor 21 reduces the severity of cerulein-induced pancreatitis in mice. *Gastroenterology* *137*, 1795–1804.
- Johnson, M.B., Wang, P.P., Atabay, K.D., Murphy, E.A., Doan, R.N., Hecht, J.L., and Walsh, C.A. (2015). Single-cell analysis reveals transcriptional heterogeneity of neural progenitors in human cortex. *Nat. Neurosci.* *18*, 637–646.

- Jourdain, I., Sontam, D., Johnson, C., Dillies, C., and Hyams, J.S. (2008). Dynamin-dependent biogenesis, cell cycle regulation and mitochondrial association of peroxisomes in fission yeast. *Traffic Cph. Den.* *9*, 353–365.
- Kageyama, Y., Zhang, Z., Roda, R., Fukaya, M., Wakabayashi, J., Wakabayashi, N., Kensler, T.W., Reddy, P.H., Iijima, M., and Sesaki, H. (2012). Mitochondrial division ensures the survival of postmitotic neurons by suppressing oxidative damage. *J. Cell Biol.* *197*, 535–551.
- Kajimura, S., and Saito, M. (2014). A new era in brown adipose tissue biology: molecular control of brown fat development and energy homeostasis. *Annu. Rev. Physiol.* *76*, 225–249.
- Kane, L.A., Lazarou, M., Fogel, A.I., Li, Y., Yamano, K., Sarraf, S.A., Banerjee, S., and Youle, R.J. (2014). PINK1 phosphorylates ubiquitin to activate Parkin E3 ubiquitin ligase activity. *J. Cell Biol.* *205*, 143–153.
- Kasahara, A., Cipolat, S., Chen, Y., Dorn, G.W., and Scorrano, L. (2013). Mitochondrial fusion directs cardiomyocyte differentiation via calcineurin and Notch signaling. *Science* *342*, 734–737.
- Kazlauskaitė, A., Kondapalli, C., Gourlay, R., Campbell, D.G., Ritorto, M.S., Hofmann, K., Alessi, D.R., Knebel, A., Trost, M., and Muqit, M.M.K. (2014). Parkin is activated by PINK1-dependent phosphorylation of ubiquitin at Ser65. *Biochem. J.* *460*, 127–139.
- Keipert, S., Ost, M., Johann, K., Imber, F., Jastroch, M., van Schothorst, E.M., Keijer, J., and Klaus, S. (2014). Skeletal muscle mitochondrial uncoupling drives endocrine cross-talk through the induction of FGF21 as a myokine. *Am. J. Physiol. Endocrinol. Metab.* *306*, E469–E482.
- Kharitonov, A., and DiMarchi, R. (2015). FGF21 Revolutions: Recent Advances Illuminating FGF21 Biology and Medicinal Properties. *Trends Endocrinol. Metab. TEM* *26*, 608–617.
- Kharitonov, A., Shivanova, T.L., Koester, A., Ford, A.M., Micanovic, R., Galbreath, E.J., Sandusky, G.E., Hammond, L.J., Moyers, J.S., Owens, R.A., et al. (2005). FGF-21 as a novel metabolic regulator. *J. Clin. Invest.* *115*, 1627–1635.
- Kharitonov, A., Wroblewski, V.J., Koester, A., Chen, Y.-F., Clutinger, C.K., Tigno, X.T., Hansen, B.C., Shanafelt, A.B., and Etgen, G.J. (2007). The metabolic state of diabetic monkeys is regulated by fibroblast growth factor-21. *Endocrinology* *148*, 774–781.
- Kiernan, M.C., Vucic, S., Cheah, B.C., Turner, M.R., Eisen, A., Hardiman, O., Burrell, J.R., and Zoing, M.C. (2011). Amyotrophic lateral sclerosis. *Lancet Lond. Engl.* *377*, 942–955.
- Kilberg, M.S., Shan, J., and Su, N. (2009). ATF4-dependent transcription mediates signaling of amino acid limitation. *Trends Endocrinol. Metab. TEM* *20*, 436–443.
- Kim, K.H., and Lee, M.-S. (2015). FGF21 as a mediator of adaptive responses to stress and metabolic benefits of anti-diabetic drugs. *J. Endocrinol.* *226*, R1–R16.
- Kim, K.H., Jeong, Y.T., Oh, H., Kim, S.H., Cho, J.M., Kim, Y.-N., Kim, S.S., Kim, D.H., Hur, K.Y., Kim, H.K., et al. (2013). Autophagy deficiency leads to protection from obesity and insulin resistance by inducing Fgf21 as a mitokine. *Nat. Med.* *19*, 83–92.
- Kitada, T., Pisani, A., Porter, D.R., Yamaguchi, H., Tschertner, A., Martella, G., Bonsi, P., Zhang, C., Pothos, E.N., and Shen, J. (2007). Impaired dopamine release and synaptic plasticity in the striatum of PINK1-deficient mice. *Proc. Natl. Acad. Sci. U. S. A.* *104*, 11441–11446.
- Koch, A., Thiemann, M., Grabenbauer, M., Yoon, Y., McNiven, M.A., and Schrader, M. (2003). Dynamin-like protein 1 is involved in peroxisomal fission. *J. Biol. Chem.* *278*, 8597–8605.
- Koch, J., Feichtinger, R.G., Freisinger, P., Pies, M., Schrödl, F., Iuso, A., Sperl, W., Mayr, J.A., Prokisch, H., and Haack, T.B. (2016). Disturbed mitochondrial and peroxisomal dynamics due to loss of MFF causes Leigh-like encephalopathy, optic atrophy and peripheral neuropathy. *J. Med. Genet. jmedgenet* – 2015–103500.
- Koirala, S., Guo, Q., Kalia, R., Bui, H.T., Eckert, D.M., Frost, A., and Shaw, J.M. (2013). Interchangeable adaptors regulate mitochondrial dynamin assembly for membrane scission. *Proc. Natl. Acad. Sci. U. S. A.* *110*, E1342–E1351.
- Kolumam, G., Chen, M.Z., Tong, R., Zavala-Solorio, J., Kates, L., van Bruggen, N., Ross, J., Wyatt, S.K., Gandham, V.D., Carano, R.A.D., et al. (2015). Sustained Brown Fat Stimulation and Insulin Sensitization by a Humanized

- Bispecific Antibody Agonist for Fibroblast Growth Factor Receptor 1/ β Klotho Complex. *EBioMedicine* 2, 730–743.
- Kopeikina, K.J., Carlson, G.A., Pitstick, R., Ludvigson, A.E., Peters, A., Luebke, J.I., Koffie, R.M., Frosch, M.P., Hyman, B.T., and Spires-Jones, T.L. (2011). Tau accumulation causes mitochondrial distribution deficits in neurons in a mouse model of tauopathy and in human Alzheimer's disease brain. *Am. J. Pathol.* 179, 2071–2082.
- Kornmann, B., Currie, E., Collins, S.R., Schuldiner, M., Nunnari, J., Weissman, J.S., and Walter, P. (2009). An ER-mitochondria tethering complex revealed by a synthetic biology screen. *Science* 325, 477–481.
- Korobova, F., Ramabhadran, V., and Higgs, H.N. (2013). An actin-dependent step in mitochondrial fission mediated by the ER-associated formin INF2. *Science* 339, 464–467.
- Korobova, F., Gauvin, T.J., and Higgs, H.N. (2014). A role for myosin II in mammalian mitochondrial fission. *Curr. Biol. CB* 24, 409–414.
- Koutsopoulos, O.S., Laine, D., Osellame, L., Chudakov, D.M., Parton, R.G., Frazier, A.E., and Ryan, M.T. (2010). Human Mitons associate with mitochondria and induce microtubule-dependent remodeling of mitochondrial networks. *Biochim. Biophys. Acta* 1803, 564–574.
- Koyano, F., Okatsu, K., Kosako, H., Tamura, Y., Go, E., Kimura, M., Kimura, Y., Tsuchiya, H., Yoshihara, H., Hirokawa, T., et al. (2014). Ubiquitin is phosphorylated by PINK1 to activate parkin. *Nature* 510, 162–166.
- Krashes, M.J., Koda, S., Ye, C., Rogan, S.C., Adams, A.C., Cusher, D.S., Maratos-Flier, E., Roth, B.L., and Lowell, B.B. (2011). Rapid, reversible activation of AgRP neurons drives feeding behavior in mice. *J. Clin. Invest.* 121, 1424–1428.
- Kroemer, G., Galluzzi, L., Vandenabeele, P., Abrams, J., Alnemri, E.S., Baehrecke, E.H., Blagosklonny, M.V., El-Deiry, W.S., Golstein, P., Green, D.R., et al. (2009). Classification of cell death: recommendations of the Nomenclature Committee on Cell Death 2009. *Cell Death Differ.* 16, 3–11.
- Kwok, K.H.-H., Ho, P.W.-L., Chu, A.C.-Y., Ho, J.W.-M., Liu, H.-F., Yiu, D.C.-W., Chan, K.-H., Kung, M.H.-W., Ramsden, D.B., and Ho, S.-L. (2010). Mitochondrial UCP5 is neuroprotective by preserving mitochondrial membrane potential, ATP levels, and reducing oxidative stress in MPP+ and dopamine toxicity. *Free Radic. Biol. Med.* 49, 1023–1035.
- van der Laan, M., Bohnert, M., Wiedemann, N., and Pfanner, N. (2012). Role of MINOS in mitochondrial membrane architecture and biogenesis. *Trends Cell Biol.* 22, 185–192.
- Labbé, K., Murley, A., and Nunnari, J. (2014). Determinants and functions of mitochondrial behavior. *Annu. Rev. Cell Dev. Biol.* 30, 357–391.
- Labbé, S.M., Caron, A., Lanfray, D., Monge-Rofarello, B., Bartness, T.J., and Richard, D. (2015). Hypothalamic control of brown adipose tissue thermogenesis. *Front. Syst. Neurosci.* 9, 150.
- Labrousse, A.M., Zappaterra, M.D., Rube, D.A., and van der Bliek, A.M. (1999). *C. elegans* dynamin-related protein DRP-1 controls severing of the mitochondrial outer membrane. *Mol. Cell* 4, 815–826.
- Lackner, L.L., Horner, J.S., and Nunnari, J. (2009). Mechanistic analysis of a dynamin effector. *Science* 325, 874–877.
- Lahiri, S., Chao, J.T., Tavassoli, S., Wong, A.K.O., Choudhary, V., Young, B.P., Loewen, C.J.R., and Prinz, W.A. (2014). A conserved endoplasmic reticulum membrane protein complex (EMC) facilitates phospholipid transfer from the ER to mitochondria. *PLoS Biol.* 12, e1001969.
- Langston, J.W., and Ballard, P.A. (1983). Parkinson's disease in a chemist working with 1-methyl-4-phenyl-1,2,5,6-tetrahydropyridine. *N. Engl. J. Med.* 309, 310.
- Langston, J.W., Ballard, P., Tetrud, J.W., and Irwin, I. (1983). Chronic Parkinsonism in humans due to a product of meperidine-analog synthesis. *Science* 219, 979–980.
- Leboucher, G.P., Tsai, Y.C., Yang, M., Shaw, K.C., Zhou, M., Veenstra, T.D., Glickman, M.H., and Weissman, A.M. (2012). Stress-induced phosphorylation and proteasomal degradation of mitofusin 2 facilitates mitochondrial fragmentation and apoptosis. *Mol. Cell* 47, 547–557.

- Lee, M.-S. (2015). Effect of mitochondrial stress on systemic metabolism. *Ann. N. Y. Acad. Sci.* *1350*, 61–65.
- Lee, C., Zeng, J., Drew, B.G., Sallam, T., Martin-Montalvo, A., Wan, J., Kim, S.-J., Mehta, H., Hevener, A.L., de Cabo, R., et al. (2015). The mitochondrial-derived peptide MOTS-c promotes metabolic homeostasis and reduces obesity and insulin resistance. *Cell Metab.* *21*, 443–454.
- Lee, Y., Jeong, S.-Y., Karbowski, M., Smith, C.L., and Youle, R.J. (2004). Roles of the mammalian mitochondrial fission and fusion mediators Fis1, Drp1, and Opa1 in apoptosis. *Mol. Biol. Cell* *15*, 5001–5011.
- Legros, F., Lombès, A., Frachon, P., and Rojo, M. (2002). Mitochondrial fusion in human cells is efficient, requires the inner membrane potential, and is mediated by mitofusins. *Mol. Biol. Cell* *13*, 4343–4354.
- Lewis, M.R., and Lewis, W.H. (1914). MITOCHONDRIA IN TISSUE CULTURE. *Science* *39*, 330–333.
- Li, X., and Gould, S.J. (2003). The dynamin-like GTPase DLP1 is essential for peroxisome division and is recruited to peroxisomes in part by PEX11. *J. Biol. Chem.* *278*, 17012–17020.
- Li, P., Nijhawan, D., Budihardjo, I., Srinivasula, S.M., Ahmad, M., Alnemri, E.S., and Wang, X. (1997). Cytochrome c and dATP-dependent formation of Apaf-1/caspase-9 complex initiates an apoptotic protease cascade. *Cell* *91*, 479–489.
- Li, Y., Wang, P., Wei, J., Fan, R., Zuo, Y., Shi, M., Wu, H., Zhou, M., Lin, J., Wu, M., et al. (2015). Inhibition of Drp1 by Mdivi-1 attenuates cerebral ischemic injury via inhibition of the mitochondria-dependent apoptotic pathway after cardiac arrest. *Neuroscience* *311*, 67–74.
- Liesa, M., and Shirihai, O.S. (2013). Mitochondrial dynamics in the regulation of nutrient utilization and energy expenditure. *Cell Metab.* *17*, 491–506.
- Lill, R., Dutkiewicz, R., Elsässer, H.-P., Hausmann, A., Netz, D.J.A., Pierik, A.J., Stehling, O., Urzica, E., and Mühlhoff, U. (2006). Mechanisms of iron-sulfur protein maturation in mitochondria, cytosol and nucleus of eukaryotes. *Biochim. Biophys. Acta* *1763*, 652–667.
- Lin, M.-Y., and Sheng, Z.-H. (2015). Regulation of mitochondrial transport in neurons. *Exp. Cell Res.* *334*, 35–44.
- Lin, Z., Tian, H., Lam, K.S.L., Lin, S., Hoo, R.C.L., Konishi, M., Itoh, N., Wang, Y., Bornstein, S.R., Xu, A., et al. (2013). Adiponectin mediates the metabolic effects of FGF21 on glucose homeostasis and insulin sensitivity in mice. *Cell Metab.* *17*, 779–789.
- Liu, J.-M., Yi, Z., Liu, S.-Z., Chang, J.-H., Dang, X.-B., Li, Q.-Y., and Zhang, Y.-L. (2015a). The mitochondrial division inhibitor mdivi-1 attenuates spinal cord ischemia-reperfusion injury both in vitro and in vivo: Involvement of BK channels. *Brain Res.* *1619*, 155–165.
- Liu, L., Zhang, K., Sandoval, H., Yamamoto, S., Jaiswal, M., Sanz, E., Li, Z., Hui, J., Graham, B.H., Quintana, A., et al. (2015b). Glial lipid droplets and ROS induced by mitochondrial defects promote neurodegeneration. *Cell* *160*, 177–190.
- Lo, A.C., Callaerts-Vegh, Z., Nunes, A.F., Rodrigues, C.M.P., and D’Hooge, R. (2013). Tauroursodeoxycholic acid (TUDCA) supplementation prevents cognitive impairment and amyloid deposition in APP/PS1 mice. *Neurobiol. Dis.* *50*, 21–29.
- Losón, O.C., Song, Z., Chen, H., and Chan, D.C. (2013). Fis1, Mff, MiD49, and MiD51 mediate Drp1 recruitment in mitochondrial fission. *Mol. Biol. Cell* *24*, 659–667.
- Lustbader, J.W., Cirilli, M., Lin, C., Xu, H.W., Takuma, K., Wang, N., Caspersen, C., Chen, X., Pollak, S., Chaney, M., et al. (2004). ABAD directly links Abeta to mitochondrial toxicity in Alzheimer’s disease. *Science* *304*, 448–452.
- Lutz, A.K., Exner, N., Fett, M.E., Schlehe, J.S., Kloos, K., Lämmermann, K., Brunner, B., Kurz-Drexler, A., Vogel, F., Reichert, A.S., et al. (2009). Loss of parkin or PINK1 function increases Drp1-dependent mitochondrial fragmentation. *J. Biol. Chem.* *284*, 22938–22951.
- Ma, X.M., and Blenis, J. (2009). Molecular mechanisms of mTOR-mediated translational control. *Nat. Rev. Mol. Cell Biol.* *10*, 307–318.
- MacAskill, A.F., and Kittler, J.T. (2010). Control of mitochondrial transport and localization in neurons. *Trends Cell Biol.* *20*, 102–112.

- Magistretti, P.J., and Allaman, I. (2015). A cellular perspective on brain energy metabolism and functional imaging. *Neuron* *86*, 883–901.
- Mäkelä, J., Tselykh, T.V., Maiorana, F., Eriksson, O., Do, H.T., Mudò, G., Korhonen, L.T., Belluardo, N., and Lindholm, D. (2014). Fibroblast growth factor-21 enhances mitochondrial functions and increases the activity of PGC-1 α in human dopaminergic neurons via Sirtuin-1. *SpringerPlus* *3*, 2.
- Manczak, M., Calkins, M.J., and Reddy, P.H. (2011). Impaired mitochondrial dynamics and abnormal interaction of amyloid beta with mitochondrial protein Drp1 in neurons from patients with Alzheimer's disease: implications for neuronal damage. *Hum. Mol. Genet.* *20*, 2495–2509.
- Mao, K., Liu, X., Feng, Y., and Klionsky, D.J. (2014). The progression of peroxisomal degradation through autophagy requires peroxisomal division. *Autophagy* *10*, 652–661.
- Margulis, L. (1975). Symbiotic theory of the origin of eukaryotic organelles; criteria for proof. *Symp. Soc. Exp. Biol.* *21*–38.
- Marsin, A.S., Bertrand, L., Rider, M.H., Deprez, J., Beauloye, C., Vincent, M.F., Van den Berghe, G., Carling, D., and Hue, L. (2000). Phosphorylation and activation of heart PFK-2 by AMPK has a role in the stimulation of glycolysis during ischaemia. *Curr. Biol. CB* *10*, 1247–1255.
- McLelland, G.-L., Soubannier, V., Chen, C.X., McBride, H.M., and Fon, E.A. (2014). Parkin and PINK1 function in a vesicular trafficking pathway regulating mitochondrial quality control. *EMBO J.* *33*, 282–295.
- Millecamps, S., Gentil, B.J., Gros-Louis, F., Rouleau, G., and Julien, J.-P. (2005). Alsin is partially associated with centrosome in human cells. *Biochim. Biophys. Acta* *1745*, 84–100.
- Mizushima, N., and Komatsu, M. (2011). Autophagy: renovation of cells and tissues. *Cell* *147*, 728–741.
- Molina, A.J.A., Wikstrom, J.D., Stiles, L., Las, G., Mohamed, H., Elorza, A., Walzer, G., Twig, G., Katz, S., Corkey, B.E., et al. (2009). Mitochondrial networking protects beta-cells from nutrient-induced apoptosis. *Diabetes* *58*, 2303–2315.
- Montessuit, S., Somasekharan, S.P., Terrones, O., Lucken-Ardjomande, S., Herzig, S., Schwarzenbacher, R., Manstein, D.J., Bossy-Wetzell, E., Basañez, G., Meda, P., et al. (2010). Membrane remodeling induced by the dynamin-related protein Drp1 stimulates Bax oligomerization. *Cell* *142*, 889–901.
- Morais, V.A., Verstreken, P., Roethig, A., Smet, J., Snellinx, A., Vanbrabant, M., Haddad, D., Frezza, C., Mandemakers, W., Vogt-Weisenhorn, D., et al. (2009). Parkinson's disease mutations in PINK1 result in decreased Complex I activity and deficient synaptic function. *EMBO Mol. Med.* *1*, 99–111.
- Moreno, J.A., Halliday, M., Molloy, C., Radford, H., Verity, N., Axten, J.M., Ortori, C.A., Willis, A.E., Fischer, P.M., Barrett, D.A., et al. (2013). Oral treatment targeting the unfolded protein response prevents neurodegeneration and clinical disease in prion-infected mice. *Sci. Transl. Med.* *5*, 206ra138.
- Morton, G.J., Meek, T.H., and Schwartz, M.W. (2014). Neurobiology of food intake in health and disease. *Nat. Rev. Neurosci.* *15*, 367–378.
- Mottis, A., Jovaisaite, V., and Auwerx, J. (2014). The mitochondrial unfolded protein response in mammalian physiology. *Mamm. Genome* *25*, 424–433.
- Muñoz, J.P., Ivanova, S., Sánchez-Wandelmer, J., Martínez-Cristóbal, P., Noguera, E., Sancho, A., Díaz-Ramos, A., Hernández-Alvarez, M.I., Sebastián, D., Mauvezin, C., et al. (2013). Mfn2 modulates the UPR and mitochondrial function via repression of PERK. *EMBO J.* *32*, 2348–2361.
- Münzberg, H., Qualls-Creekmore, E., Berthoud, H.-R., Morrison, C.D., and Yu, S. (2015). Neural Control of Energy Expenditure. *Handb. Exp. Pharmacol.*
- Muroya, S., Yada, T., Shioda, S., and Takigawa, M. (1999). Glucose-sensitive neurons in the rat arcuate nucleus contain neuropeptide Y. *Neurosci. Lett.* *264*, 113–116.
- Nagashima, S., Tokuyama, T., Yonashiro, R., Inatome, R., and Yanagi, S. (2014). Roles of mitochondrial ubiquitin ligase MITOL/MARCH5 in mitochondrial dynamics and diseases. *J. Biochem. (Tokyo)* *155*, 273–279.
- Nasrallah, C.M., and Horvath, T.L. (2014). Mitochondrial dynamics in the central regulation of metabolism. *Nat. Rev. Endocrinol.* *10*, 650–658.

- Naylor, K., Ingerman, E., Okreglak, V., Marino, M., Hinshaw, J.E., and Nunnari, J. (2006). Mdv1 interacts with assembled dnm1 to promote mitochondrial division. *J. Biol. Chem.* *281*, 2177–2183.
- Neuspiel, M., Schauss, A.C., Braschi, E., Zunino, R., Rippstein, P., Rachubinski, R.A., Andrade-Navarro, M.A., and McBride, H.M. (2008). Cargo-selected transport from the mitochondria to peroxisomes is mediated by vesicular carriers. *Curr. Biol. CB* *18*, 102–108.
- Ngoh, G.A., Papanicolaou, K.N., and Walsh, K. (2012). Loss of mitofusin 2 promotes endoplasmic reticulum stress. *J. Biol. Chem.* *287*, 20321–20332.
- Niemann, A., Ruegg, M., La Padula, V., Schenone, A., and Suter, U. (2005). Ganglioside-induced differentiation associated protein 1 is a regulator of the mitochondrial network: new implications for Charcot-Marie-Tooth disease. *J. Cell Biol.* *170*, 1067–1078.
- Nilsson, R., Jain, M., Madhusudhan, N., Sheppard, N.G., Strittmatter, L., Kampf, C., Huang, J., Asplund, A., and Mootha, V.K. (2014). Metabolic enzyme expression highlights a key role for MTHFD2 and the mitochondrial folate pathway in cancer. *Nat. Commun.* *5*, 3128.
- Noda, N.N., and Inagaki, F. (2015). Mechanisms of Autophagy. *Annu. Rev. Biophys.* *44*, 101–122.
- Novikoff, A.B., Beaufay, H., and De Duve, C. (1956). Electron microscopy of lysosomeric fractions from rat liver. *J. Biophys. Biochem. Cytol.* *2*, 179–184.
- Oettinghaus, B., Licci, M., Scorrano, L., and Frank, S. (2012). Less than perfect divorces: dysregulated mitochondrial fission and neurodegeneration. *Acta Neuropathol. (Berl.)* *123*, 189–203.
- Oettinghaus, B., Schulz, J.M., Restelli, L.M., Licci, M., Savoia, C., Schmidt, A., Schmitt, K., Grimm, A., Morè, L., Hench, J., et al. (2016). Synaptic dysfunction, memory deficits and hippocampal atrophy due to ablation of mitochondrial fission in adult forebrain neurons. *Cell Death Differ.* *23*, 18–28.
- Orr, H.T., and Zoghbi, H.Y. (2007). Trinucleotide repeat disorders. *Annu. Rev. Neurosci.* *30*, 575–621.
- Otera, H., Wang, C., Cleland, M.M., Setoguchi, K., Yokota, S., Youle, R.J., and Mihara, K. (2010). Mff is an essential factor for mitochondrial recruitment of Drp1 during mitochondrial fission in mammalian cells. *J. Cell Biol.* *191*, 1141–1158.
- Owen, B.M., Bookout, A.L., Ding, X., Lin, V.Y., Atkin, S.D., Gautron, L., Kliewer, S.A., and Mangelsdorf, D.J. (2013). FGF21 contributes to neuroendocrine control of female reproduction. *Nat. Med.* *19*, 1153–1156.
- Owen, B.M., Ding, X., Morgan, D.A., Coate, K.C., Bookout, A.L., Rahmouni, K., Kliewer, S.A., and Mangelsdorf, D.J. (2014). FGF21 acts centrally to induce sympathetic nerve activity, energy expenditure, and weight loss. *Cell Metab.* *20*, 670–677.
- Owen, B.M., Mangelsdorf, D.J., and Kliewer, S.A. (2015). Tissue-specific actions of the metabolic hormones FGF15/19 and FGF21. *Trends Endocrinol. Metab. TEM* *26*, 22–29.
- Pagani, L., and Eckert, A. (2011). Amyloid-Beta interaction with mitochondria. *Int. J. Alzheimers Dis.* *2011*, 925050.
- Pagliarini, D.J., Calvo, S.E., Chang, B., Sheth, S.A., Vafai, S.B., Ong, S.-E., Walford, G.A., Sugiana, C., Boneh, A., Chen, W.K., et al. (2008). A mitochondrial protein compendium elucidates complex I disease biology. *Cell* *134*, 112–123.
- Palade, G.E. (1953). An electron microscope study of the mitochondrial structure. *J. Histochem. Cytochem. Off. J. Histochem. Soc.* *1*, 188–211.
- Palmer, C.S., Osellame, L.D., Laine, D., Koutsopoulos, O.S., Frazier, A.E., and Ryan, M.T. (2011). MiD49 and MiD51, new components of the mitochondrial fission machinery. *EMBO Rep.* *12*, 565–573.
- Patel, R., Bookout, A.L., Magomedova, L., Owen, B.M., Consiglio, G.P., Shimizu, M., Zhang, Y., Mangelsdorf, D.J., Kliewer, S.A., and Cummins, C.L. (2015). Glucocorticoids regulate the metabolic hormone FGF21 in a feed-forward loop. *Mol. Endocrinol. Baltim. Md* *29*, 213–223.
- Pedrola, L., Espert, A., Wu, X., Claramunt, R., Shy, M.E., and Palau, F. (2005). GDAP1, the protein causing Charcot-Marie-Tooth disease type 4A, is expressed in neurons and is associated with mitochondria. *Hum. Mol. Genet.* *14*, 1087–1094.

- Pernas, L., and Scorrano, L. (2015). Mito-Morphosis: Mitochondrial Fusion, Fission, and Cristae Remodeling as Key Mediators of Cellular Function. *Annu. Rev. Physiol.*
- Pflugger, P.T., Kabra, D.G., Aichler, M., Schriever, S.C., Pfuhlmann, K., García, V.C., Lehti, M., Weber, J., Kutschke, M., Rozman, J., et al. (2015). Calcineurin Links Mitochondrial Elongation with Energy Metabolism. *Cell Metab.* *22*, 838–850.
- Pickrell, A.M., and Youle, R.J. (2015). The roles of PINK1, parkin, and mitochondrial fidelity in Parkinson's disease. *Neuron* *85*, 257–273.
- Pigino, G., Morfini, G., Atagi, Y., Deshpande, A., Yu, C., Jungbauer, L., LaDu, M., Busciglio, J., and Brady, S. (2009). Disruption of fast axonal transport is a pathogenic mechanism for intraneuronal amyloid beta. *Proc. Natl. Acad. Sci. U. S. A.* *106*, 5907–5912.
- Pilling, A.D., Horiuchi, D., Lively, C.M., and Saxton, W.M. (2006). Kinesin-1 and Dynein are the primary motors for fast transport of mitochondria in *Drosophila* motor axons. *Mol. Biol. Cell* *17*, 2057–2068.
- Pitts, K.R., Yoon, Y., Krueger, E.W., and McNiven, M.A. (1999). The dynamin-like protein DLP1 is essential for normal distribution and morphology of the endoplasmic reticulum and mitochondria in mammalian cells. *Mol. Biol. Cell* *10*, 4403–4417.
- Potthoff, M.J., Inagaki, T., Satapati, S., Ding, X., He, T., Goetz, R., Mohammadi, M., Finck, B.N., Mangelsdorf, D.J., Kliewer, S.A., et al. (2009). FGF21 induces PGC-1 α and regulates carbohydrate and fatty acid metabolism during the adaptive starvation response. *Proc. Natl. Acad. Sci. U. S. A.* *106*, 10853–10858.
- Prudent, J., Zunino, R., Sugiura, A., Mattie, S., Shore, G.C., and McBride, H.M. (2015). MAPL SUMOylation of Drp1 Stabilizes an ER/Mitochondrial Platform Required for Cell Death. *Mol. Cell* *59*, 941–955.
- Qi, X., Disatnik, M.-H., Shen, N., Sobel, R.A., and Mochly-Rosen, D. (2011). Aberrant mitochondrial fission in neurons induced by protein kinase C $\{\delta\}$ under oxidative stress conditions in vivo. *Mol. Biol. Cell* *22*, 256–265.
- Qi, X., Qvit, N., Su, Y.-C., and Mochly-Rosen, D. (2013). A novel Drp1 inhibitor diminishes aberrant mitochondrial fission and neurotoxicity. *J. Cell Sci.* *126*, 789–802.
- Qian, W., Wang, J., and Van Houten, B. (2013). The role of dynamin-related protein 1 in cancer growth: a promising therapeutic target? *Expert Opin. Ther. Targets* *17*, 997–1001.
- Qian, W., Wang, J., Roginskaya, V., McDermott, L.A., Edwards, R.P., Stolz, D.B., Llambi, F., Green, D.R., and Houten, B.V. (2014). Novel combination of mitochondrial division inhibitor 1 (mdivi-1) and platinum agents produces synergistic pro-apoptotic effect in drug resistant tumor cells. *Oncotarget* *5*, 4180–4194.
- Radford, H., Moreno, J.A., Verity, N., Halliday, M., and Mallucci, G.R. (2015). PERK inhibition prevents tau-mediated neurodegeneration in a mouse model of frontotemporal dementia. *Acta Neuropathol. (Berl.)* *130*, 633–642.
- Rambold, A.S., Cohen, S., and Lippincott-Schwartz, J. (2015). Fatty acid trafficking in starved cells: regulation by lipid droplet lipolysis, autophagy, and mitochondrial fusion dynamics. *Dev. Cell* *32*, 678–692.
- Ramsden, D.B., Ho, P.W.-L., Ho, J.W.-M., Liu, H.-F., So, D.H.-F., Tse, H.-M., Chan, K.-H., and Ho, S.-L. (2012). Human neuronal uncoupling proteins 4 and 5 (UCP4 and UCP5): structural properties, regulation, and physiological role in protection against oxidative stress and mitochondrial dysfunction. *Brain Behav.* *2*, 468–478.
- Rappold, P.M., Cui, M., Grima, J.C., Fan, R.Z., de Mesy-Bentley, K.L., Chen, L., Zhuang, X., Bowers, W.J., and Tieu, K. (2014). Drp1 inhibition attenuates neurotoxicity and dopamine release deficits in vivo. *Nat. Commun.* *5*, 5244.
- Rath, E., Berger, E., Messlik, A., Nunes, T., Liu, B., Kim, S.C., Hoogenraad, N., Sans, M., Sartor, R.B., and Haller, D. (2012). Induction of dsRNA-activated protein kinase links mitochondrial unfolded protein response to the pathogenesis of intestinal inflammation. *Gut* *61*, 1269–1278.
- Raturi, A., and Simmen, T. (2013). Where the endoplasmic reticulum and the mitochondrion tie the knot: the mitochondria-associated membrane (MAM). *Biochim. Biophys. Acta* *1833*, 213–224.

- Reichert, A.S., and Neupert, W. (2002). Contact sites between the outer and inner membrane of mitochondria: role in protein transport. *Biochim. Biophys. Acta* *1592*, 41–49.
- Richardson, D.R., Lane, D.J.R., Becker, E.M., Huang, M.L.-H., Whitnall, M., Suryo Rahmanto, Y., Sheftel, A.D., and Ponka, P. (2010). Mitochondrial iron trafficking and the integration of iron metabolism between the mitochondrion and cytosol. *Proc. Natl. Acad. Sci. U. S. A.* *107*, 10775–10782.
- Richter, V., Palmer, C.S., Osellame, L.D., Singh, A.P., Elgass, K., Stroud, D.A., Sesaki, H., Kvansakul, M., and Ryan, M.T. (2014). Structural and functional analysis of MiD51, a dynamin receptor required for mitochondrial fission. *J. Cell Biol.* *204*, 477–486.
- Ron, D., and Walter, P. (2007). Signal integration in the endoplasmic reticulum unfolded protein response. *Nat. Rev. Mol. Cell Biol.* *8*, 519–529.
- Rosignol, R., Gilkerson, R., Aggeler, R., Yamagata, K., Remington, S.J., and Capaldi, R.A. (2004). Energy substrate modulates mitochondrial structure and oxidative capacity in cancer cells. *Cancer Res.* *64*, 985–993.
- Rothwell, N.J., and Stock, M.J. (1979). A role for brown adipose tissue in diet-induced thermogenesis. *Nature* *281*, 31–35.
- Rowland, A.A., and Voeltz, G.K. (2012). Endoplasmic reticulum-mitochondria contacts: function of the junction. *Nat. Rev. Mol. Cell Biol.* *13*, 607–625.
- Rutter, G.A. (2001). Nutrient-secretion coupling in the pancreatic islet beta-cell: recent advances. *Mol. Aspects Med.* *22*, 247–284.
- Ryan, B.J., Hoek, S., Fon, E.A., and Wade-Martins, R. (2015). Mitochondrial dysfunction and mitophagy in Parkinson's: from familial to sporadic disease. *Trends Biochem. Sci.* *40*, 200–210.
- Ryu, S.-W., Jeong, H.J., Choi, M., Karbowski, M., and Choi, C. (2010). Optic atrophy 3 as a protein of the mitochondrial outer membrane induces mitochondrial fragmentation. *Cell. Mol. Life Sci. CMLS* *67*, 2839–2850.
- Samms, R.J., Smith, D.P., Cheng, C.C., Antonellis, P.P., Perfield, J.W., Kharitonov, A., Gimeno, R.E., and Adams, A.C. (2015). Discrete Aspects of FGF21 In Vivo Pharmacology Do Not Require UCP1. *Cell Rep.* *11*, 991–999.
- Sancak, Y., Peterson, T.R., Shaul, Y.D., Lindquist, R.A., Thoreen, C.C., Bar-Peled, L., and Sabatini, D.M. (2008). The Rag GTPases bind raptor and mediate amino acid signaling to mTORC1. *Science* *320*, 1496–1501.
- Sandoval, D., Cota, D., and Seeley, R.J. (2008). The integrative role of CNS fuel-sensing mechanisms in energy balance and glucose regulation. *Annu. Rev. Physiol.* *70*, 513–535.
- Santel, A., and Fuller, M.T. (2001). Control of mitochondrial morphology by a human mitofusin. *J. Cell Sci.* *114*, 867–874.
- Santel, A., Frank, S., Gaume, B., Herrler, M., Youle, R.J., and Fuller, M.T. (2003). Mitofusin-1 protein is a generally expressed mediator of mitochondrial fusion in mammalian cells. *J. Cell Sci.* *116*, 2763–2774.
- Saotome, M., Safiulina, D., Szabadkai, G., Das, S., Fransson, A., Aspenstrom, P., Rizzuto, R., and Hajnóczky, G. (2008). Bidirectional Ca²⁺-dependent control of mitochondrial dynamics by the Miro GTPase. *Proc. Natl. Acad. Sci. U. S. A.* *105*, 20728–20733.
- Sarruf, D.A., Thaler, J.P., Morton, G.J., German, J., Fischer, J.D., Ogimoto, K., and Schwartz, M.W. (2010). Fibroblast growth factor 21 action in the brain increases energy expenditure and insulin sensitivity in obese rats. *Diabetes* *59*, 1817–1824.
- Schneeberger, M., Dietrich, M.O., Sebastián, D., Imbernón, M., Castaño, C., Garcia, A., Esteban, Y., Gonzalez-Franquesa, A., Rodríguez, I.C., Bortolozzi, A., et al. (2013). Mitofusin 2 in POMC Neurons Connects ER Stress with Leptin Resistance and Energy Imbalance. *Cell* *155*.
- Schon, E.A., and Przedborski, S. (2011). Mitochondria: the next (neurode)generation. *Neuron* *70*, 1033–1053.
- Schrader, M., Godinho, L.F., Costello, J.L., and Islinger, M. (2015). The different facets of organelle interplay—an overview of organelle interactions. *Front. Cell Dev. Biol.* *3*, 56.

- Scorrano, L., Ashiya, M., Buttle, K., Weiler, S., Oakes, S.A., Mannella, C.A., and Korsmeyer, S.J. (2002). A distinct pathway remodels mitochondrial cristae and mobilizes cytochrome c during apoptosis. *Dev. Cell* 2, 55–67.
- Sebastián, D., Hernández-Alvarez, M.I., Segalés, J., Sorianoello, E., Muñoz, J.P., Sala, D., Waget, A., Liesa, M., Paz, J.C., Gopalacharyulu, P., et al. (2012). Mitofusin 2 (Mfn2) links mitochondrial and endoplasmic reticulum function with insulin signaling and is essential for normal glucose homeostasis. *Proc. Natl. Acad. Sci. U. S. A.* 109, 5523–5528.
- Shahni, R., Cale, C.M., Anderson, G., Osellame, L.D., Hambleton, S., Jacques, T.S., Wedatilake, Y., Taanman, J.-W., Chan, E., Qasim, W., et al. (2015). Signal transducer and activator of transcription 2 deficiency is a novel disorder of mitochondrial fission. *Brain J. Neurol.* 138, 2834–2846.
- Shan, X., Chiang, P.-M., Price, D.L., and Wong, P.C. (2010). Altered distributions of Gemini of coiled bodies and mitochondria in motor neurons of TDP-43 transgenic mice. *Proc. Natl. Acad. Sci. U. S. A.* 107, 16325–16330.
- Shaw, G.C., Cope, J.J., Li, L., Corson, K., Hersey, C., Ackermann, G.E., Gwynn, B., Lambert, A.J., Wingert, R.A., Traver, D., et al. (2006). Mitoferrin is essential for erythroid iron assimilation. *Nature* 440, 96–100.
- Shen, Q., Yamano, K., Head, B.P., Kawajiri, S., Cheung, J.T.M., Wang, C., Cho, J.-H., Hattori, N., Youle, R.J., and van der Bliek, A.M. (2014). Mutations in Fis1 disrupt orderly disposal of defective mitochondria. *Mol. Biol. Cell* 25, 145–159.
- Shi, P., Ström, A.-L., Gal, J., and Zhu, H. (2010). Effects of ALS-related SOD1 mutants on dynein- and KIF5-mediated retrograde and anterograde axonal transport. *Biochim. Biophys. Acta* 1802, 707–716.
- Shiao, Y.J., Lupo, G., and Vance, J.E. (1995). Evidence that phosphatidylserine is imported into mitochondria via a mitochondria-associated membrane and that the majority of mitochondrial phosphatidylethanolamine is derived from decarboxylation of phosphatidylserine. *J. Biol. Chem.* 270, 11190–11198.
- Shields, L.Y., Kim, H., Zhu, L., Haddad, D., Berthet, A., Pathak, D., Lam, M., Ponnusamy, R., Diaz-Ramirez, L.G., Gill, T.M., et al. (2015). Dynamin-related protein 1 is required for normal mitochondrial bioenergetic and synaptic function in CA1 hippocampal neurons. *Cell Death Dis.* 6, e1725.
- Shirendeb, U.P., Calkins, M.J., Manczak, M., Anekonda, V., Dufour, B., McBride, J.L., Mao, P., and Reddy, P.H. (2012). Mutant huntingtin's interaction with mitochondrial protein Drp1 impairs mitochondrial biogenesis and causes defective axonal transport and synaptic degeneration in Huntington's disease. *Hum. Mol. Genet.* 21, 406–420.
- Sidrauski, C., Acosta-Alvear, D., Khoutorsky, A., Vedantham, P., Hearn, B.R., Li, H., Gamache, K., Gallagher, C.M., Ang, K.K.-H., Wilson, C., et al. (2013). Pharmacological brake-release of mRNA translation enhances cognitive memory. *eLife* 2, e00498.
- Smirnova, E., Griparic, L., Shurland, D.-L., and Bliek, A.M. van der (2001). Dynamin-related Protein Drp1 Is Required for Mitochondrial Division in Mammalian Cells. *Mol. Biol. Cell* 12, 2245–2256.
- Smith, J.J., and Aitchison, J.D. (2013). Peroxisomes take shape. *Nat. Rev. Mol. Cell Biol.* 14, 803–817.
- So, E.C., Hsing, C.-H., Liang, C.-H., and Wu, S.-N. (2012). The actions of mdivi-1, an inhibitor of mitochondrial fission, on rapidly activating delayed-rectifier K⁺ current and membrane potential in HL-1 murine atrial cardiomyocytes. *Eur. J. Pharmacol.* 683, 1–9.
- Song, W., Chen, J., Petrilli, A., Liot, G., Klinglmayr, E., Zhou, Y., Poquiz, P., Tjong, J., Pouladi, M.A., Hayden, M.R., et al. (2011). Mutant huntingtin binds the mitochondrial fission GTPase dynamin-related protein-1 and increases its enzymatic activity. *Nat. Med.* 17, 377–382.
- Song, Z., Ghochani, M., McCaffery, J.M., Frey, T.G., and Chan, D.C. (2009). Mitofusins and OPA1 Mediate Sequential Steps in Mitochondrial Membrane Fusion. *Mol. Biol. Cell* 20, 3525–3532.
- Soubannier, V., McLelland, G.-L., Zunino, R., Braschi, E., Rippstein, P., Fon, E.A., and McBride, H.M. (2012). A vesicular transport pathway shuttles cargo from mitochondria to lysosomes. *Curr. Biol. CB* 22, 135–141.
- Spang, A. (2015). A small GTPase involved in mitochondrial morphology and function. *Biochemical Society Transactions* 43, 108–110.

- Stavru, F., Palmer, A.E., Wang, C., Youle, R.J., and Cossart, P. (2013). Atypical mitochondrial fission upon bacterial infection. *Proc. Natl. Acad. Sci. U. S. A.* *110*, 16003–16008.
- Stoica, R., De Vos, K.J., Paillusson, S., Mueller, S., Sancho, R.M., Lau, K.-F., Vizcay-Barrena, G., Lin, W.-L., Xu, Y.-F., Lewis, J., et al. (2014). ER-mitochondria associations are regulated by the VAPB-PTPIP51 interaction and are disrupted by ALS/FTD-associated TDP-43. *Nat. Commun.* *5*, 3996.
- Stokin, G.B., Lillo, C., Falzone, T.L., Brusch, R.G., Rockenstein, E., Mount, S.L., Raman, R., Davies, P., Masliah, E., Williams, D.S., et al. (2005). Axonopathy and transport deficits early in the pathogenesis of Alzheimer's disease. *Science* *307*, 1282–1288.
- Stowers, R.S., Megeath, L.J., Górska-Andrzejak, J., Meinertzhagen, I.A., and Schwarz, T.L. (2002). Axonal transport of mitochondria to synapses depends on Milton, a novel *Drosophila* protein. *Neuron* *36*, 1063–1077.
- Su, Q., Cai, Q., Gerwin, C., Smith, C.L., and Sheng, Z.-H. (2004). Syntabulin is a microtubule-associated protein implicated in syntaxin transport in neurons. *Nat. Cell Biol.* *6*, 941–953.
- Sugiura, A., McLelland, G.-L., Fon, E.A., and McBride, H.M. (2014). A new pathway for mitochondrial quality control: mitochondrial-derived vesicles. *EMBO J.* *33*, 2142–2156.
- Suomalainen, A., Elo, J.M., Pietiläinen, K.H., Hakonen, A.H., Sevastianova, K., Korpela, M., Isohanni, P., Marjavaara, S.K., Tyni, T., Kiuru-Enari, S., et al. (2011). FGF-21 as a biomarker for muscle-manifesting mitochondrial respiratory chain deficiencies: a diagnostic study. *Lancet Neurol.* *10*, 806–818.
- Taguchi, N., Ishihara, N., Jofuku, A., Oka, T., and Mihara, K. (2007). Mitotic phosphorylation of dynamin-related GTPase Drp1 participates in mitochondrial fission. *J. Biol. Chem.* *282*, 11521–11529.
- Tallóczy, Z., Jiang, W., Virgin, H.W., Leib, D.A., Scheuner, D., Kaufman, R.J., Eskelinen, E.-L., and Levine, B. (2002). Regulation of starvation- and virus-induced autophagy by the eIF2alpha kinase signaling pathway. *Proc. Natl. Acad. Sci. U. S. A.* *99*, 190–195.
- Tanaka, A., Cleland, M.M., Xu, S., Narendra, D.P., Suen, D.-F., Karbowski, M., and Youle, R.J. (2010). Proteasome and p97 mediate mitophagy and degradation of mitofusins induced by Parkin. *J. Cell Biol.* *191*, 1367–1380.
- Tang, F.-L., Erion, J.R., Tian, Y., Liu, W., Yin, D.-M., Ye, J., Tang, B., Mei, L., and Xiong, W.-C. (2015). VPS35 in Dopamine Neurons Is Required for Endosome-to-Golgi Retrieval of Lamp2a, a Receptor of Chaperone-Mediated Autophagy That Is Critical for α -Synuclein Degradation and Prevention of Pathogenesis of Parkinson's Disease. *J. Neurosci. Off. J. Soc. Neurosci.* *35*, 10613–10628.
- Tang, T.-S., Tu, H., Chan, E.Y.W., Maximov, A., Wang, Z., Wellington, C.L., Hayden, M.R., and Bezprozvanny, I. (2003). Huntingtin and huntingtin-associated protein 1 influence neuronal calcium signaling mediated by inositol-(1,4,5) triphosphate receptor type 1. *Neuron* *39*, 227–239.
- Tatsuta, T., Scharwey, M., and Langer, T. (2014). Mitochondrial lipid trafficking. *Trends Cell Biol.* *24*, 44–52.
- Thenen, S.W., and Mayer, J. (1976). Hyperinsulinemia and fat cell glycerokinase activity in obese (*ob/ob*) and diabetic (*db/db*) mice. *Horm. Metab. Res. Horm. Stoffwechselforschung Horm. Métabolisme* *8*, 80–81.
- Tondera, D., Grandemange, S., Jourdain, A., Karbowski, M., Mattenberger, Y., Herzig, S., Da Cruz, S., Clerc, P., Raschke, I., Merkwirth, C., et al. (2009). SLP-2 is required for stress-induced mitochondrial hyperfusion. *EMBO J.* *28*, 1589–1600.
- Touvier, T., De Palma, C., Rigamonti, E., Scagliola, A., Incerti, E., Mazelin, L., Thomas, J.-L., D'Antonio, M., Politi, L., Schaeffer, L., et al. (2015). Muscle-specific Drp1 overexpression impairs skeletal muscle growth via translational attenuation. *Cell Death Dis.* *6*, e1663.
- Toyama, E.Q., Herzig, S., Courchet, J., Lewis, T.L., Losón, O.C., Hellberg, K., Young, N.P., Chen, H., Polleux, F., Chan, D.C., et al. (2016). AMP-activated protein kinase mediates mitochondrial fission in response to energy stress. *Science* *351*, 275–281.
- Trushina, E., Dyer, R.B., Badger, J.D., Ure, D., Eide, L., Tran, D.D., Vrieze, B.T., Legendre-Guillemin, V., McPherson, P.S., Mandavilli, B.S., et al. (2004). Mutant huntingtin impairs axonal trafficking in mammalian neurons in vivo and in vitro. *Mol. Cell. Biol.* *24*, 8195–8209.
- Tschöp, M., Smiley, D.L., and Heiman, M.L. (2000). Ghrelin induces adiposity in rodents. *Nature* *407*, 908–913.

- Twig, G., Elorza, A., Molina, A.J.A., Mohamed, H., Wikstrom, J.D., Walzer, G., Stiles, L., Haigh, S.E., Katz, S., Las, G., et al. (2008). Fission and selective fusion govern mitochondrial segregation and elimination by autophagy. *EMBO J.* *27*, 433–446.
- Tynismaa, H., Carroll, C.J., Raimundo, N., Ahola-Erkkilä, S., Wenz, T., Ruhanen, H., Guse, K., Hemminki, A., Peltola-Mjøsund, K.E., Tulkki, V., et al. (2010). Mitochondrial myopathy induces a starvation-like response. *Hum. Mol. Genet.* *19*, 3948–3958.
- Varanita, T., Soriano, M.E., Romanello, V., Zaglia, T., Quintana-Cabrera, R., Semenzato, M., Menabò, R., Costa, V., Civiletto, G., Pesce, P., et al. (2015). The OPA1-dependent mitochondrial cristae remodeling pathway controls atrophic, apoptotic, and ischemic tissue damage. *Cell Metab.* *21*, 834–844.
- Véniant, M.M., Sivits, G., Helmering, J., Komorowski, R., Lee, J., Fan, W., Moyer, C., and Lloyd, D.J. (2015). Pharmacologic Effects of FGF21 Are Independent of the “Browning” of White Adipose Tissue. *Cell Metab.* *21*, 731–738.
- Verstreken, P., Ly, C.V., Venken, K.J.T., Koh, T.-W., Zhou, Y., and Bellen, H.J. (2005). Synaptic mitochondria are critical for mobilization of reserve pool vesicles at *Drosophila* neuromuscular junctions. *Neuron* *47*, 365–378.
- Vilariño-Güell, C., Wider, C., Ross, O.A., Dachsel, J.C., Kachergus, J.M., Lincoln, S.J., Soto-Ortolaza, A.I., Cobb, S.A., Wilhoite, G.J., Bacon, J.A., et al. (2011). VPS35 mutations in Parkinson disease. *Am. J. Hum. Genet.* *89*, 162–167.
- Vinters, H.V. (2015). Emerging concepts in Alzheimer’s disease. *Annu. Rev. Pathol.* *10*, 291–319.
- Volmer, R., van der Ploeg, K., and Ron, D. (2013). Membrane lipid saturation activates endoplasmic reticulum unfolded protein response transducers through their transmembrane domains. *Proc. Natl. Acad. Sci. U. S. A.* *110*, 4628–4633.
- Wai, T., and Langer, T. (2016). Mitochondrial Dynamics and Metabolic Regulation. *Trends Endocrinol. Metab. TEM* *27*, 105–117.
- Wakabayashi, J., Zhang, Z., Wakabayashi, N., Tamura, Y., Fukaya, M., Kensler, T.W., Iijima, M., and Sesaki, H. (2009). The dynamin-related GTPase Drp1 is required for embryonic and brain development in mice. *J. Cell Biol.* *186*, 805–816.
- Walton, P.A., and Pizzitelli, M. (2012). Effects of peroxisomal catalase inhibition on mitochondrial function. *Front. Physiol.* *3*, 108.
- Wang, H., Sreenivasan, U., Sreenevasan, U., Hu, H., Saladino, A., Polster, B.M., Lund, L.M., Gong, D., Stanley, W.C., and Sztalryd, C. (2011a). Perilipin 5, a lipid droplet-associated protein, provides physical and metabolic linkage to mitochondria. *J. Lipid Res.* *52*, 2159–2168.
- Wang, X., Su, B., Lee, H., Li, X., Perry, G., Smith, M.A., and Zhu, X. (2009). Impaired balance of mitochondrial fission and fusion in Alzheimer’s disease. *J. Neurosci. Off. J. Soc. Neurosci.* *29*, 9090–9103.
- Wang, X., Winter, D., Ashrafi, G., Schlehe, J., Wong, Y.L., Selkoe, D., Rice, S., Steen, J., LaVoie, M.J., and Schwarz, T.L. (2011b). PINK1 and Parkin target Miro for phosphorylation and degradation to arrest mitochondrial motility. *Cell* *147*, 893–906.
- Waterham, H.R., Koster, J., van Roermund, C.W.T., Mooyer, P.A.W., Wanders, R.J.A., and Leonard, J.V. (2007). A lethal defect of mitochondrial and peroxisomal fission. *N. Engl. J. Med.* *356*, 1736–1741.
- Wek, R.C., Jiang, H.-Y., and Anthony, T.G. (2006). Coping with stress: eIF2 kinases and translational control. *Biochem. Soc. Trans.* *34*, 7–11.
- Wells, T., Davies, J.R., Guschina, I.A., Ball, D.J., Davies, J.S., Davies, V.J., Evans, B.A.J., and Votruba, M. (2012). Opa3, a novel regulator of mitochondrial function, controls thermogenesis and abdominal fat mass in a mouse model for Costeff syndrome. *Hum. Mol. Genet.* *21*, 4836–4844.
- Wente, W., Efanov, A.M., Brenner, M., Kharitonov, A., Köster, A., Sandusky, G.E., Sewing, S., Treinies, I., Zitzer, H., and Gromada, J. (2006). Fibroblast growth factor-21 improves pancreatic beta-cell function and survival by activation of extracellular signal-regulated kinase 1/2 and Akt signaling pathways. *Diabetes* *55*, 2470–2478.

- Wilson, T.J., Slupe, A.M., and Strack, S. (2013). Cell signaling and mitochondrial dynamics: Implications for neuronal function and neurodegenerative disease. *Neurobiol. Dis.* *51*, 13–26.
- Wong, E.D., Wagner, J.A., Gorsich, S.W., McCaffery, J.M., Shaw, J.M., and Nunnari, J. (2000). The dynamin-related GTPase, Mgm1p, is an intermembrane space protein required for maintenance of fusion competent mitochondria. *J. Cell Biol.* *151*, 341–352.
- Wu, A.-L., Feng, B., Chen, M.Z., Kolumam, G., Zavala-Solorio, J., Wyatt, S.K., Gandham, V.D., Carano, R.A.D., and Sonoda, J. (2013a). Antibody-mediated activation of FGFR1 induces FGF23 production and hypophosphatemia. *PLoS One* *8*, e57322.
- Wu, J., Cohen, P., and Spiegelman, B.M. (2013b). Adaptive thermogenesis in adipocytes: is beige the new brown? *Genes Dev.* *27*, 234–250.
- Xie, N., Wang, C., Lian, Y., Zhang, H., Wu, C., and Zhang, Q. (2013). A selective inhibitor of Drp1, mdivi-1, protects against cell death of hippocampal neurons in pilocarpine-induced seizures in rats. *Neurosci. Lett.* *545*, 64–68.
- Xu, J., Lloyd, D.J., Hale, C., Stanislaus, S., Chen, M., Sivits, G., Vonderfecht, S., Hecht, R., Li, Y.-S., Lindberg, R.A., et al. (2009). Fibroblast growth factor 21 reverses hepatic steatosis, increases energy expenditure, and improves insulin sensitivity in diet-induced obese mice. *Diabetes* *58*, 250–259.
- Xu, S., Cherok, E., Das, S., Li, S., Roelofs, B.A., Ge, S.X., Polster, B.M., Boyman, L., Lederer, W.J., Wang, C., et al. (2016). Mitochondrial E3 ubiquitin ligase MARCH5 controls mitochondrial fission and cell sensitivity to stress-induced apoptosis through regulation of MiD49 protein. *Mol. Biol. Cell* *27*, 349–359.
- Yamano, K., and Youle, R.J. (2013). PINK1 is degraded through the N-end rule pathway. *Autophagy* *9*, 1758–1769.
- Yasuda-Yamahara, M., Kume, S., Yamahara, K., Nakazawa, J., Chin-Kanasaki, M., Araki, H., Araki, S., Koya, D., Haneda, M., Ugi, S., et al. (2015). Lamp-2 deficiency prevents high-fat diet-induced obese diabetes via enhancing energy expenditure. *Biochem. Biophys. Res. Commun.* *465*, 249–255.
- Yoneda, T., Benedetti, C., Urano, F., Clark, S.G., Harding, H.P., and Ron, D. (2004). Compartment-specific perturbation of protein handling activates genes encoding mitochondrial chaperones. *J. Cell Sci.* *117*, 4055–4066.
- Yoon, Y., Pitts, K.R., Dahan, S., and McNiven, M.A. (1998). A novel dynamin-like protein associates with cytoplasmic vesicles and tubules of the endoplasmic reticulum in mammalian cells. *J. Cell Biol.* *140*, 779–793.
- Youle, R.J., and Narendra, D.P. (2011). Mechanisms of mitophagy. *Nat. Rev. Mol. Cell Biol.* *12*, 9–14.
- Yuan, H.-X., Xiong, Y., and Guan, K.-L. (2013). Nutrient sensing, metabolism, and cell growth control. *Mol. Cell* *49*, 379–387.
- Yu-Wai-Man, P., Trenell, M.I., Hollingsworth, K.G., Griffiths, P.G., and Chinnery, P.F. (2011). OPA1 mutations impair mitochondrial function in both pure and complicated dominant optic atrophy. *Brain J. Neurol.* *134*, e164.
- Zhan, C., Zhou, J., Feng, Q., Zhang, J.-E., Lin, S., Bao, J., Wu, P., and Luo, M. (2013). Acute and long-term suppression of feeding behavior by POMC neurons in the brainstem and hypothalamus, respectively. *J. Neurosci. Off. J. Soc. Neurosci.* *33*, 3624–3632.
- Zhang, Y., Lyver, E.R., Knight, S.A.B., Lesuisse, E., and Dancis, A. (2005). Frataxin and mitochondrial carrier proteins, Mrs3p and Mrs4p, cooperate in providing iron for heme synthesis. *J. Biol. Chem.* *280*, 19794–19807.
- Zhang, Y., Xie, Y., Berglund, E.D., Coate, K.C., He, T.T., Katafuchi, T., Xiao, G., Potthoff, M.J., Wei, W., Wan, Y., et al. (2012). The starvation hormone, fibroblast growth factor-21, extends lifespan in mice. *eLife* *1*, e00065.
- Zhao, J., Liu, T., Jin, S., Wang, X., Qu, M., Uhlén, P., Tomilin, N., Shupliakov, O., Lendahl, U., and Nistér, M. (2011). Human MIEF1 recruits Drp1 to mitochondrial outer membranes and promotes mitochondrial fusion rather than fission. *EMBO J.* *30*, 2762–2778.
- Zhao, Q., Wang, J., Levichkin, I.V., Stasinopoulos, S., Ryan, M.T., and Hoogenraad, N.J. (2002). A mitochondrial specific stress response in mammalian cells. *EMBO J.* *21*, 4411–4419.

- Zimprich, A., Benet-Pagès, A., Struhal, W., Graf, E., Eck, S.H., Offman, M.N., Haubenberger, D., Spielberger, S., Schulte, E.C., Lichtner, P., et al. (2011). A mutation in VPS35, encoding a subunit of the retromer complex, causes late-onset Parkinson disease. *Am. J. Hum. Genet.* *89*, 168–175.
- Zingaretti, M.C., Crosta, F., Vitali, A., Guerrieri, M., Frontini, A., Cannon, B., Nedergaard, J., and Cinti, S. (2009). The presence of UCP1 demonstrates that metabolically active adipose tissue in the neck of adult humans truly represents brown adipose tissue. *FASEB J. Off. Publ. Fed. Am. Soc. Exp. Biol.* *23*, 3113–3120.
- Zorzano, A., and Claret, M. (2015). Implications of mitochondrial dynamics on neurodegeneration and on hypothalamic dysfunction. *Front. Aging Neurosci.* *7*, 101.
- Züchner, S. (1993). Charcot-Marie-Tooth Neuropathy Type 2A. In *GeneReviews*(®), R.A. Pagon, M.P. Adam, H.H. Ardinger, S.E. Wallace, A. Amemiya, L.J. Bean, T.D. Bird, C.-T. Fong, H.C. Mefford, R.J. Smith, et al., eds. (Seattle (WA): University of Washington, Seattle),.
- Züchner, S., and Vance, J.M. (1993). Charcot-Marie-Tooth Neuropathy Type 4A. In *GeneReviews*(®), R.A. Pagon, M.P. Adam, H.H. Ardinger, S.E. Wallace, A. Amemiya, L.J. Bean, T.D. Bird, C.-T. Fong, H.C. Mefford, R.J. Smith, et al., eds. (Seattle (WA): University of Washington, Seattle),.
- Zunino, R., Schauss, A., Rippstein, P., Andrade-Navarro, M., and McBride, H.M. (2007). The SUMO protease SENP5 is required to maintain mitochondrial morphology and function. *J. Cell Sci.* *120*, 1178–1188.

8. Abbreviations

Abbreviation	Meaning	Abbreviation	Meaning
4EBP	Eukaryotic initiation factor 4E binding protein	LAMP	Lysosomal-Associated Membrane Protein
α-MSH	α Melanocyte-Stimulating-Hormone	LC3	Microtubule-associated protein 1A/1B-light chain 3
Aβ	Amyloid β	LRRK2	Leucine-rich repeat kinase 2
ACTH	Adrenocorticotrophic Hormone	MAM	Mitochondria-Associated Membrane
AD	Alzheimer's Disease	MAPL	Mitochondria-Associated Protein Ligase
ADOA	Autosomal Dominant Optic Atrophy	MDV	Mitochondria-Derived Vesicle
ADP	Adenosine Di-Phosphate	MFF	Mitochondria Fission Factor
AFG3L2	AFG3-Like AAA ATPase 2	MFN	Mitofusin
AgRP	Agouti-Related Peptide	MICOS	Mitochondrial Contact Site
ALS	Amyotrophic Lateral Sclerosis	MiD(49/51)	Mitochondrial Division
AMP	Adenosine Mono-Phosphate	Miro	Mitochondrial RHO GTPase
AMPK	5' AMP-activated protein kinase	MitoPLD	Mitochondrial PhosphoLipase D
APP	Amyloid Precursor Protein	MPTP	1-methyl-4-phenyl-1,2,3,6-tetrahydropyridine
ARC	Arcuate nucleus	mtDNA	Mitochondrial DNA
ATF(3/4)	Activating Transcription Factor	mTORC	mammalian Target Of Rapamycin Complex
ATG	Autophagy-related Gene	mtUPR	mitochondrial UPR
ATP	Adenosine Tri-Phosphate	NPY	NeuroPeptide Y
BAT	Brown Adipose Tissue	NTS	Nucleus Tractus Solitarii
BBB	Blood-Brain Barrier	OMM	Outer Mitochondrial Membrane
Bip	Binding Immunoglobulin Protein	OMMAD	Outer Mitochondrial Membrane-Associated Degradation
BW	Body Weight	OPA(1/3)	Optic Atrophy
C/EBP	CCAAT/enhancer binding protein	PARL	Presenilins-Associated Rhomboid-Like protein
CaMK	Ca ²⁺ /calmodulin-dependent protein kinase	PC	PhosphatidylCholine
cAMP	cyclic Adenosine Mono-Phosphate	PD	Parkinson's Disease

Abbreviations

CDK1	Cyclin-Dependent Kinase	PERK	Protein kinase RNA-like Endoplasmic Reticulum Kinase
ChIP	Chromatin ImmunoPrecipitation	PGC1α	Peroxisome proliferator-activated receptor γ Coactivator gene
CHOP	CCAAT-enhancer-binding protein homologous protein	PINK1	Phosphatase and Tensin Homolog-Induced putative Kinase
CJ	Cristae Junction	PKA	Protein Kinase A
CL	CardioLipin	PKC	Protein Kinase C
CMT	Charcot-Marie-Tooth	POMC	ProOpioMelanoCortin
CNS	Central Nervous System	PP2A	Protein Phosphatase 2A
CoA	Coenzyme A	PPAR	Peroxisome Proliferator-Activated Receptor
CREB	cAMP response element-binding protein	PS	PhosphatidylSerine
CRH	Corticotropin Releasing Hormone	PTI	Post Tamoxifen Injection
CT	Cycle Threshold	PTPIP51	Protein tyrosine phosphatase interacting protein 51
DARS	Aspartate tRNA ligase	PVN	ParaVentricular Nucleus
DOPA	L-3,4-dihydroxyphenylalanine	qRT-PCR	quantitative Real Time Polymerase Chain Reaction
DRP(1)	Dynamin-Related Protein	R123	Rhodamine 123
EchoMRI	Echo Magnetic Resonance Imaging	rER	rough Endoplasmic Reticulum
EEF	Eukaryotic translation Elongation Factor 2	ROS	Reactive Oxygen Species
eIF(2A/4E)	Eukaryotic translation Initiation Factor	rRNA	ribosomal RNA
ELISA	Enzyme-Linked ImmunoSorbent Assay	S6K1	p70 ribosomal protein S6 Kinase 1
EM	Electron Microscopy	SCN	SupraChiasmatic Nucleus
EMC	Endoplasmic reticulum Membrane protein Complex	SDS PAGE	Sodium Dodecyl Phosphate Poly Acrylamide Gel Electrophoresis
ER	Endoplasmic Reticulum	SenP5	Sentrin-specific Protease 5
ERMES	ER–Mitochondria Encounter Structure	SNARE	SNAP (Soluble NSF Attachment Protein) Receptor
FCCP	Carbonyl cyanide-4-(trifluoromethoxy)phenylhydrazine	SOD1	SuperOxide Dismutase 1
FFPE	Formalin-Fixed Paraffin-Embedded	STAT	Signal Transducer and Activator of Transcription

Abbreviations

FGF	Fibroblast Growth Factor	SUMO	Small Ubiquitin-like Modifier
FRS2α	Fibroblast growth factor receptor substrate 2	TCA	TriCarboxylic Acid
GABA	γ -AminoButyric Acid	TDP43	TAR DNA-binding Protein 43
GADD34	Growth Arrest and DNA Damage-inducible protein 34	TEM	Transmission Electron Microscopy
GCN	General control NonDerepressible	TFAM	Transcription Factor A, Mitochondrial
GDAP1	Ganglioside Induced Differentiation Associated Protein 1	TMRM	Tetramethylrhodamine, methyl ester
GLP1	Glucagon-Like Peptide 1	TRAK	Trafficking Kinesin Protein
GLUT	Glucose Transporter type 4	tRNA	transfer RNA
GRP78	Glucose-Related Protein 78	TSC	Tuberous Sclerosis Complex
H&E	Hematoxylin and Eosin	TUDCA	Tauroursodeoxycholic acid
HRI	Heme-Regulated eIF2 α kinase	TXR	Thyroid X Receptor
HSP	Heat Shock Protein	UBC1	Ubiquitin-conjugating enzyme E2
HTT	Huntingtin	UCP	Uncoupling Protein
IBM	Inner Boundary Membrane	uORF	upstream Open Reading Frame
ICV	IntraCerebroVentricular	UPR	Unfolded Protein Response
IMM	Inner Mitochondrial Membrane	VAPB	VAMP (Vesicle-Associated Membrane Protein)-Associated Protein B
IMS	InterMembrane Space	VLH	VentroLateral Hypothalamus
IP3R	Inositol trisphosphate receptor	VMH	VentroMedial Hypothalamus
IRE	Inositol-Requiring Enzyme	VPS35	Vacuolar Protein Sorting 35
ISR	Integrated Stress Response	WAT	White Adipose Tissue
kFU	kilo Fluorescence Units	XBP1	X-box Binding Protein 1

9. Authors' Contributions

The presented results were obtained through collaborative work performed by the author and Dr. Björn Oettinghaus.

Specifically, the experiments shown in figures 3 to 6 are the result of joint work between the author and Dr. Oettinghaus, with equal contributions as far as sample preparation and processing, as well as experiment planning, are concerned. Data represented in figures 7 and 8, and the sympathectomy model, were the exclusive responsibility of the author, with minor technical help from Dr. Oettinghaus.

Work described in figures 1 and 2 was for the most part performed by Dr. Oettinghaus, with minor technical help from the author.

Measurements of mitochondrial membrane potential were obtained in Prof. Anne Eckert's laboratory by Karen Schmitt and Amandine Grimm (UPKBS, Basel).

The author significantly contributed to project design and manuscript preparation; in addition, the author was solely responsible for obtaining the relevant permissions for animal experiments from the Veterinary Office.

Curriculum Vitae

Personal information

Name **Lisa Michelle Restelli**
Address Bärenfelsenstrasse 11, 4057 Basel, SWITZERLAND
Telephone +41 76 447 6298
E-mail **restelli.lisa@gmail.com**
Nationality Italian
Date of birth December 16th 1988
Gender Female

Education

Degree **PhD**
Dates 10/2012 – 03/2016
Title of qualification awarded **PhD in Neurobiology, Faculty of Natural Sciences**
Thesis: Metabolic consequences of neuronal mitochondrial fission ablation
University Basel University – Basel, Switzerland

Degree 2nd level degree – Master
Dates 2010-2012
Title of qualification awarded **Medical, Molecular And Cellular Biotechnologies** – summa cum laude
Thesis: Iron handling and mis-handling in a cellular model of mitochondrial dysfunction
University Vita-Salute San Raffaele University – Milan, Italy

Degree 1st level degree – Bachelor
Dates 2007-2010
Title of qualification awarded **Medical And Pharmaceutical Biotechnologies** – summa cum laude
Thesis: Iron handling in mitochondria: physiopathological implications in the central nervous system
University Vita-Salute San Raffaele University – Milan, Italy

Research experience

Dates and institution 2012 – present, Institute of Pathology – Basel, Switzerland
Position **PhD candidate**
Project Role of mitochondrial morphology in central nervous system function, and in systemic regulation of energy expenditure. The project relies on both in vivo mouse models and in vitro neurobiology techniques.
Employer Supervisor: Prof. Stephan Frank – stephan.frank@usb.ch

Dates and institution 2011-2012, Vita-Salute San Raffaele University – Milan, Italy
Position **Master student**

Project	Role of mitochondria in the response to iron-induced oxidative stress, in a cellular model of mitochondrial dysfunction.
Employer	Supervisor: Prof. Fabio Grohovaz – grohovaz.fabio@hsr.it
Dates and institution	Sept 2009, Vita-Salute San Raffaele University – Milan, Italy
Position	Undergraduate student volunteer
Project	Analysis of iron and calcium competition for entry pathways in primary neuronal cultures.
Employer	Supervisor: Prof. Fabio Grohovaz – grohovaz.fabio@hsr.it
Languages	
Mother tongue	Italian
Other languages	English (native proficiency) French (fluent) German (basic)
Publications	
	Oettinghaus B, Schulz JM, Restelli LM , Licci M, Savoia C, Schmidt A, Schmitt K, Grimm A, Morè L, Hench J, Tolnay M, Eckert A, D'Adamo P, Franken P, Ishihara N, Mihara K, Bischofberger J, Scorrano L, Frank S. Synaptic dysfunction, memory deficits and hippocampal atrophy due to ablation of mitochondrial fission in adult forebrain neurons. Cell Death Differ. 2016 Jan;23(1):18-28. doi: 10.1038/cdd.2015.39.
	Pfeiffer NV, Dirndorfer D, Lang S, Resenberger UK, Restelli LM , Hemion C, Miesbauer M, Frank S, Neutzner A, Zimmermann R, Winklhofer K and Tatzelt J Structural features within the nascent chain regulate alternative targeting of secretory proteins to mitochondria. EMBO J 2013 Apr 3;32(7):1036-51.doi: 10.1038/emboj.2013.46.
	Oettinghaus B, D'Alonzo D, Barbieri E, Restelli LM , Savoia C, Licci M, Tolnay M, Frank S, Scorrano L DRP1-dependent apoptotic mitochondrial fission occurs independently of BAX, BAK and APAF1 to amplify cell death by BID and oxidative stress. BBA Bioenergetics 2016 Mar 17. doi: 10.1016/j.bbabi.2016.03.016.
Scientific communications	
	Selected short talk: Stressed to death: Drp1 ablation in the adult mouse forebrain Frontiers in Metabolism: From Molecular Physiology to Systems Medicine, EMBL Heidelberg (DE) 17th November 2014
	Selected short talk: Stressed to death: Drp1 ablation in the adult mouse forebrain Italian Association for Cell Biology and Differentiation Annual Meeting, Bologna (IT) 19th September 2015
Awards	
	For all three years of my undergraduate degree I held a merit-based scholarship for placing first at the admission tests.
	I won the student prize at the Keystone Symposium on Mitochondrial Dynamics and Physiology (Santa Fe, NM; February 2014).
	I was a winner of the NatureJobs Career Expo Journalism competition , London 2014.